

# High Dynamic Range Imaging

Rafał K. Mantiuk, Karol Myszkowski and Hans-Peter Seidel

April 18, 2016

## Abstract

High dynamic range (HDR) images and video contain pixels, which can represent much greater range of colors and brightness levels than that offered by existing, standard dynamic range images. Such “better pixels” greatly improve the overall quality of visual content, making it appear much more realistic and appealing to the audience. HDR is one of the key technologies of the future imaging pipeline, which will change the way the digital visual content is represented and manipulated.

This article offers a broad review of the HDR methods and technologies with the introduction on fundamental concepts behind the perception of HDR imagery. It serves both as an introduction to the subject and review of the current state-of-the-art in HDR imaging. It covers the topics related capture of HDR content with cameras and its generation with computer graphics methods; encoding and compression of HDR images and video; tone-mapping for displaying HDR content on standard dynamic range displays; inverse tone-mapping for up-scaling legacy content for presentation on HDR displays; the display technologies offering HDR range; and finally image and video quality metrics suitable for HDR content.

## Contents

<b>1</b>	<b>Introduction</b>	<b>3</b>
1.1	Low vs. high dynamic range imaging . . . . .	3
1.2	Device- and scene-referred image representations . . . . .	5
1.3	HDRI: mature imaging technology . . . . .	5
1.4	HDR imaging pipeline . . . . .	8
<b>2</b>	<b>Fundamental concepts</b>	<b>8</b>
2.1	Dynamic range . . . . .	9
2.2	The difference between LDR and HDR pixel values . . . . .	10
2.3	Display models and gamma correction . . . . .	11
2.4	The logarithmic domain and the sensitivity to light . . . . .	13
<b>3</b>	<b>Image and video acquisition</b>	<b>17</b>
3.1	Computer graphics . . . . .	17
3.2	RAW vs. JPEG images . . . . .	18

3.3	Time sequential multi-exposure techniques . . . . .	19
3.3.1	Deghosting: handling camera and object motion . . . . .	20
3.3.2	Video solutions . . . . .	21
3.4	HDR sensors and cameras . . . . .	21
3.4.1	Spatial exposure change . . . . .	21
3.4.2	Multiple sensors with beam splitters . . . . .	22
3.4.3	Solid state sensors . . . . .	22
<b>4</b>	<b>Storage and compression</b>	<b>23</b>
4.1	HDR pixel formats and color spaces . . . . .	23
4.2	HDR image file formats . . . . .	28
4.3	High bit-depth encoding for HDR . . . . .	29
4.4	Backward-compatible compression . . . . .	30
<b>5</b>	<b>Tone mapping</b>	<b>32</b>
5.1	Intents of tone mapping . . . . .	32
5.2	Algebra of tone mapping . . . . .	33
5.3	Major approaches to tone mapping . . . . .	37
5.3.1	Illumination and reflectance separation . . . . .	37
5.3.2	Forward visual model . . . . .	40
5.3.3	Forward and inverse visual models . . . . .	41
5.3.4	Constrained mapping problem . . . . .	42
5.4	Perceptual effects for the enhancement of tone-mapped images . . . . .	44
<b>6</b>	<b>Inverse tone mapping</b>	<b>47</b>
6.1	Recovering dynamic range . . . . .	48
6.1.1	LDR pixel linearization . . . . .	48
6.1.2	Dynamic range expansion . . . . .	49
6.2	Suppression of contouring and quantization errors . . . . .	52
6.3	Recovering under- and over-saturated textures . . . . .	53
6.4	Exploiting image capturing artifacts for upgrading dynamic range . . . . .	53
<b>7</b>	<b>HDR display technology</b>	<b>55</b>
7.1	Dual modulation . . . . .	56
7.2	HDR displays . . . . .	58
7.3	HDR projectors . . . . .	59
7.4	Light field displays in HDR applications . . . . .	60
<b>8</b>	<b>HDR image quality</b>	<b>61</b>
8.1	Display-referred vs. luminance independent metrics . . . . .	61
8.2	Perceptually-uniform encoding for quality assessment . . . . .	62
8.3	Visual difference predictor for HDR images . . . . .	63
8.4	Tone-mapping metrics . . . . .	64

## 1 Introduction

High dynamic range imaging (HDRI) offers a radically new approach of representing colors in digital images and video. Instead of using the range of colors produced by a given display device, HDRI methods manipulate and store all colors and brightness levels visible to the human eye. Since the visible range of colors is much larger than the range achievable by cameras or displays (see Fig. 1), HDR color space is in principle a superset of all color spaces used in traditional standard dynamic range imaging.

The goal of this article is a systematic survey of all elements of HDRI pipeline from image/video acquisition, then storage and compression, to display and quality evaluation. Before a detailed presentation of underlying technology and algorithmic solutions, at first we discuss basic differences between HDR and standard imaging, which is still predominantly in use (Sec. 1.1). This brings us naturally to the problem of image representation, which in HDRI directly attempts to grasp possibly complete information on depicted scenes, while in standard imaging it is explicitly tailored to display capabilities at all processing stages (Sec. 1.2). Finally, we survey possible application areas of HDRI technology in Sec. 1.3, and we overview the content of this article in Sec. 1.4.

### 1.1 Low vs. high dynamic range imaging

Although tremendous progress can be observed in recent years towards improving the quality of captured and displayed digital images and video, the reproduction of real world appearance, which is seamless and convincingly immersive, is still a farfetched goal. The discretization in spatial and temporal domains can be considered as a conceptually important difference with respect to the inherently continuous real world, however, the pixel resolution in ultra high definition (UHD) imaging pipelines and achievable there framerates are not the key limiting factors. The problem is the restricted color gamut and even more constrained luminance and contrast ranges that are captured by cameras and stored by the majority of image and video formats.

For instance, each pixel value in the JPEG image encoding is represented using three 8-bit integer numbers (0-255) using the  $YC_aC_b$  color space. This color space is able to store only a small part of visible color gamut, as illustrated in Fig. 1-left, and an even smaller part of the luminance range that can be perceived by our eyes, as illustrated in Fig. 1-right. Similar limitations apply to predominantly used profiles of video standards MPEG/H.264.

While the so-called multiple RAW formats with 12–16 bit precision, which is determined by the sensor capabilities, are available on many modern cameras, a common practice is an immediate conversion to JPEG/MPEG at early stages of on-camera processing. This leads to irrecoverable losses of information with respect to the capabilities of human vision, and clearly will be a limiting factor for upcoming image processing, storage, and display technologies. To emphasize these limitations of traditional imaging technology it is often called *low-dynamic range* or simply *LDR*.

High dynamic range imaging overcomes those limitations by imposing pixel colorimetric precision, which enables representing all colors found in real world that can be perceived by the human eye. This in turn enables depiction of a range of perceptual

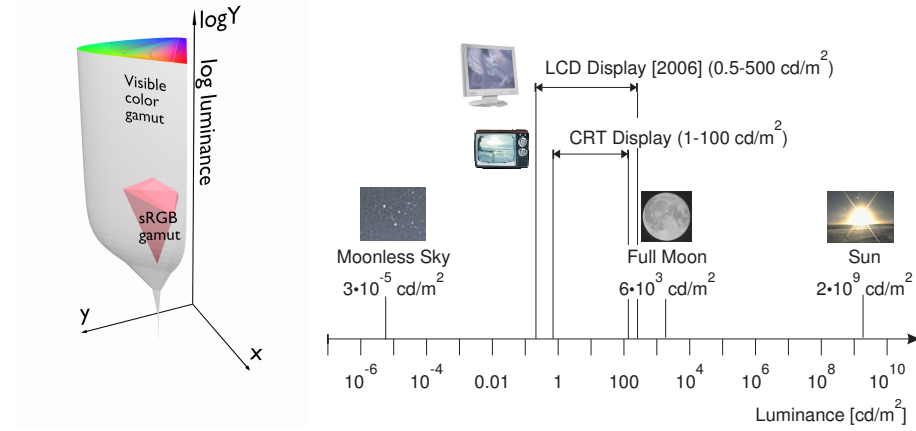


Figure 1: Left: the transparent solid represents the entire color gamut visible to the human eye. The solid tapers towards the bottom as color perception degrades at lower luminance levels. For comparison, the red solid inside represents a standard sRGB (Rec. 709) color gamut, which is produced by a good quality display. Right: real-world luminance values compared with the range of luminance that can be displayed on CRT and LDR monitors. Most digital content is stored in a format that at most preserves the dynamic range of typical displays. (Reproduced with permission from [108] © Morgan & Claypool Publishers.)

cues that are not achievable with traditional imaging. HDRI can represent images of luminance range fully covering the scotopic, mesopic and photopic vision, which leads to different perception of colors, including the loss of color vision in dim conditions. For example, due to the so-called Hunt's effect we tend to regard objects more colorful when they are brightly illuminated. To render enhanced colorfulness properly, digital images must preserve information about the actual level of luminance of the original scene, which is not possible in the case of traditional imaging.

Real-world scenes are not only brighter and more colorful than their digital reproductions, but also contain much higher contrast, both local between neighboring objects, and global between distant objects. The visual system has evolved to cope with such high contrast and its presence in a scene evokes important perceptual cues. Traditional imaging, unlike HDRI, is not able to represent such high-contrast scenes. Similarly, traditional images can hardly represent common visual phenomena, such as self-luminous surfaces (sun, shining lamps) and bright specular highlights. They also do not contain enough information to reproduce visual glare (brightening of the areas surrounding shining objects) and a short-time dazzle due to sudden increase of the brightness of a scene (e.g., when exposed to the sunlight after staying indoors). To faithfully represent, store and then reproduce all these effects, the original scene must be stored and treated using high fidelity HDR techniques.

## 1.2 Device- and scene-referred image representations

To accommodate all discussed requirements imposed on HDRI, a common format of data is required to enable their efficient transfer and processing on the way from HDR acquisition to HDR display devices. This stays in contrast with a plethora of sensor and camera vendor dependent RAW formats. Here again fundamental differences between image formats used in traditional imaging and HDRI arise, which we address in this section.

Commonly used LDR image formats (JPEG, PNG, TIFF, and so on) have been designed to accommodate the capabilities of display devices with little concern on visual information that cannot be displayed on those devices. Therefore those formats can be considered as *device-referred* (also known as *output-referred*), since they are tightly coupled with the capabilities of a particular imaging device. Obviously, such device-referred image representations only vaguely relate to the actual photometric properties of depicted scenes. This makes difficult the high fidelity reproduction of scene appearance across display devices with drastically different contrast ranges, absolute lowest and peak luminance values, and color gamuts.

*Scene-referred* representation of images, which encodes the actual photometric characteristics of depicted scenes, provides an easy solution to this problem. Conversion from such a common representation, which directly corresponds to physical luminance or spectral radiance values, to a format suitable for a particular device is the responsibility of that device. This should guarantee the best possible rendering of the HDR content, since only the device has all the information related to its limitations and sometimes also viewing conditions (e.g. ambient illumination), which is necessary to render the content properly. HDR file formats are examples of scene-referred encoding, as they usually represent either luminance or spectral radiance, rather than gamma corrected and ready to display “pixel values”.

The problem of accuracy of scene-referred image representation arises in terms of tolerable quantization error. For display-referred image formats the pixel precision is directly imposed by the reproduction capabilities of target display devices. For scene-referred image representations the accuracy should not be tailored to any particular imaging technology and, if efficiency of storing data is required, the capabilities of the human visual system should act as the only limiting factor.

To summarize, the difference between HDRI and traditional LDR imaging is that HDRI always operates on device-independent and high-precision data, so that the quality of the content is reduced only at the display stage, and only if a device cannot faithfully reproduce the content. This is contrary to traditional LDR imaging, where the content is usually profiled for particular device and thus stripped from useful information at the acquisition stage or latest at the storage stage. Fig. 2 summarizes these basic conceptual differences between LDR and HDR imaging.

## 1.3 HDRI: mature imaging technology

After over two decades of intensive research and development HDRI has recently gained momentum and is affecting almost all fields of digital imaging. One of the first to adopt HDRI were video game developers together with graphics card vendors. To-



Standard (Low) Dynamic Range	High Dynamic Range
up to 500 cd/m <sup>2</sup>	peak brightness 2000-10 000 cd/m <sup>2</sup>
50 dB	camera dynamic range 120 dB
1:1 000	display contrast 1:1 000 000
from 8 to 16 bit	quantization floating point or variable
display-referred	image representation scene-referred
display-limited	fidelity as good as the eye can see

Figure 2: The advantages of HDR compared to LDR from the application point of view. The quality of the LDR image have been reduced on purpose to illustrate potential differences between the HDR and LDR visual contents as seen on an HDR display. The given numbers serve as an example and are not meant to be a precise reference. For the dynamic range definitions, such as dB, refer to Table 1. Figure adapted from [108].

day virtually all video game engines perform rendering using HDR precision to deliver more believable and appealing virtual reality imagery. Computer generated imagery used in special effect production relies on HDR techniques to achieve the best match between synthetic and real-world scenes, which are often captured with professional video HDR cameras. Advertising in the automotive industry, which is committed to avoid premature release of the car look that still should be presented in an attractive, possibly difficult to access scenography, relies on rendered computer graphics cars. The rendered cars are composited into HDR photographs and videos, while captured at the same spot HDR spherical environment maps enable the realistic simulation of car illumination due to the precise radiometric information. Lower-end HDR cameras are often mounted in cars to improve the safety of driving and parking maneuvers in all lighting conditions. HDR video is also required in all applications in which capturing temporal aspects of changes in the scene is required with high accuracy such as monitoring of some industrial processes including welding, or surveillance systems, to name just a few possible applications.

Consumer-level cameras commonly offer an HDR mode of shooting images, which reduces the problem of under- and over-exposure, where deeply saturated image regions in the LDR photography are now filled with lively textures and other scene details. For more demanding camera users, who do not want to rely on the black box on-camera HDR processing, a number of software tools are available that enable blending of multiple differently exposed images of the same scene into an HDR image with the

full control of this process. The same software tools typically offer a full suite of HDR image editing tools and well as tone mapping solutions to reduce the dynamic range in an HDR image and make it displayable on existing displays. All those developments make the HDR photography really popular as confirmed by over 3 millions uploaded photographs that are tagged as HDR on Flickr.

On the display side, all key vendors experiment with local dimming technology with a grid of LEDs as the backlight device, which significantly enhances the dynamic range offered by those displays. The full-fledged HDR displays with even higher density of high luminous power LEDs, which in some cases requires active liquid-based cooling systems, are available for high-end consumers as well as for professional users. In the latter case dedicated HDR displays can emulate all existing LDR displays due to their superior contrast range and color gamut, which greatly simplifies video material postproduction and color grading, so that the appearance of the final distribution-ready video version looks optimally on all display technologies. Dual-modulation technology is also used in the context of large HDR projection systems in digital cinema applications, and inexpensive pico-projectors enable their local overlap on the screen, which after careful calibration leads to contrast enhancement as well.

Besides its significant impact on existing imaging technologies that we can observe today, HDRI radically changes the methods by which imaging data is processed, displayed and stored in several fields of science. Computer vision algorithms and image-based rendering techniques greatly benefit from the increased precision of HDR images, which do not have over- or under-exposed regions often causing the algorithm failure. Medical imaging has developed image formats (e.g. the DICOM format) that partly cope with the shortcomings of traditional images, however they are supported only by specialized hardware and software. HDRI gives the sufficient precision for medical imaging and therefore its capture, processing and rendering techniques is used also in this field. HDR techniques also find applications in astronomical imaging, remote sensing, industrial design, scientific visualization, forensics at crime spots, artifact digitization and appearance capture in cultural heritage and internet shopping.

The maturity of HDRI technologies is confirmed by ongoing standardization efforts for HDR JPEG and MPEG. The research literature is also immense and summarized in a number of textbooks [10, 57, 101, 108, 128]. Multiple guides for photographers and CG artists have been released as well [18]. An interesting account of historical developments on dynamic range expansion in the art, traditional photography, and electronic imaging has been presented in [97, 101].

All these exciting developments in HDRI may suggest that the transition of LDR imaging pipelines into their full-fledged HDR versions is a revolutionary step that can be compared to the quantum leap from black&white to color imaging [18]. Obviously, during the transition time some elements of imaging pipeline may still rely on traditional LDR technology. This will require backward compatibility of HDR formats to enable their use on LDR output devices such as printers, displays, and projectors. For some of such devices the format extensions to HDR should be transparent, and standard *display-referred* content should be directly accessible. However, more advanced LDR devices may take advantage of HDR information by adjusting *scene-referred* content to their technical capabilities through customized tone reproduction. Finally, the legacy images and video should be upgraded when displayed on HDR devices, so that the

best possible image quality is achieved (the so-called inverse tone mapping). In this work we address all these important issues and we structure our text following the key elements of HDRI pipeline, which we briefly introduce in the following section.

## 1.4 HDR imaging pipeline

This article presents a complete pipeline for HDR image and video processing from acquisition, through compression and quality evaluation, to display (refer to Fig. 3). At the first stage digital images are acquired either with cameras or computer rendering methods (Sec. 3). At the second stage, digital content is efficiently compressed and encoded either for storage or transmission purposes (Sec. 4). Finally, digital video or images are displayed on display devices. Tone mapping is required to accommodate HDR content to LDR devices (Sec. 5), and conversely LDR content upgrading (the so-called inverse tone mapping) is necessary for displaying on HDR devices (Sec. 6). Apart from considering technical capabilities of display devices (Sec. 7), the viewing conditions such as ambient lighting and amount of light reflected by the display play an important role for proper determination of tone mapping parameters. Quality metrics are employed to verify algorithms at all stages of the pipeline (Sec. 8).

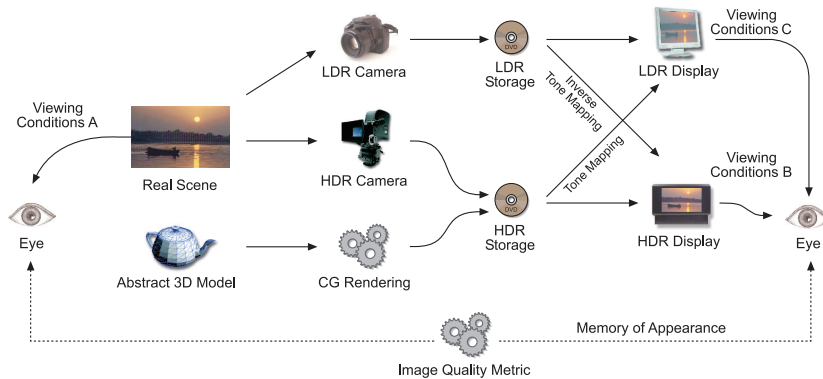


Figure 3: Imaging pipeline and available HDR technologies. (Reproduced with permission from [108] © Morgan & Claypool Publishers.)

Additionally, a short background on contrast sensitivity and brightness perception is given as well as the terminology used for dynamic range measures in digital photography, camera sensors, and displays is discussed (Sec. 2).

## 2 Fundamental concepts

This section introduces some fundamental concepts and definitions commonly used in high dynamic range imaging. When discussing the algorithms and methods in the following sections, we will refer to these concepts. First, several definitions of a dynamic range are reviewed. Then, the differences between LDR and HDR pixels are explained.

name	formula	example	context
contrast ratio	$CR = (Y_{peak}/Y_{noise}) : 1$	500:1	displays
log exposure range	$D = \log_{10}(Y_{peak}) - \log_{10}(Y_{noise})$ $L = \log_2(Y_{peak}) - \log_2(Y_{noise})$	2.7 orders 9 stops	HDR imaging, photography
peak signal to noise ratio	$PSNR = 20 \cdot \log_{10}(Y_{peak}/Y_{noise})$	53 [dB]	digital cameras

Table 1: Measures of dynamic range and their context of application. The example column illustrates the same dynamic range expressed in different units (adapted from [108]).

This is followed by the description of a display model, which explains the relation between LDR pixel values and the light emitted by a display. Finally, the last section describes the relation between luminance in the logarithmic domain and the sensitivity of the human visual system.

## 2.1 Dynamic range

In principle, the term *dynamic range* is used in engineering to define the ratio between the largest and the smallest quantity under consideration. With respect to images, the observed quantity is the luminance level and there are several measures of dynamic range in use depending on the application. They are summarized in Table 1.

The *contrast ratio* is a measure used in display systems and defines the ratio between the luminance of the brightest color it can produce (white) and the darkest (black). In case a display does not emit any light at zero level, as for instance in HDR displays [135], the first controllable level above zero is considered as the darkest to avoid infinity. The ratio is usually normalized so that the second value is always one, for example 1000:1, rather than 100:0.1.

The *log exposure range* is a measure commonly adopted in high dynamic range imaging to measure the dynamic range of scenes. Here the considered range is between the brightest and the darkest luminance in a given scene. The range is calculated as the difference between the logarithm (base 10) of the brightest and the darkest spots. The advantage of using logarithmic values is that they better describe the perceived difference in dynamic range than the contrast ratio. The values are usually rounded to the first decimal fraction.

The *exposure latitude* is defined as the luminance range the film can capture minus the luminance range of the photographed scene and is expressed using logarithm base 2 with precision up to  $1/3$ . The choice of logarithmic base is motivated by the scale of exposure settings, aperture closure (f-stops) and shutter speed (seconds), where one step doubles or halves the amount of captured light. Thus the exposure latitude tells the photographers how large a mistake they can make in setting the exposure parameters while still obtaining a satisfactory image. This measure is mentioned here, because its units, *stop steps* or *stops* in short, are often used in HDR photography to define the luminance range of a photographed scene alone.

The *signal to noise ratio* (SNR) is most often used to express the dynamic range of a digital camera. In this context, it is usually measured as the ratio of the intensity that starts to saturate the image sensor to the minimum intensity that can be observed above the noise level of the sensor. It is expressed in decibels [dB] using 20 times base-10 logarithm.

The physical range of luminance, captured by the above measures, does not necessarily correspond the perceived magnitude of the dynamic range. This is because our contrast sensitivity is significantly reduced for lower luminance levels, such as those we find at night or in a dim cinema. For that reasons, it has been proposed to use the number of just-noticeable contrast differences (JNDs) that a given display is capable of producing as a more relevant measure of the dynamic range [167]. The concept of JNDs will be discussed in more details in Section 2.4.

The actual procedure to measure dynamic range is not well defined and therefore the reported numbers may vary. For instance, display manufacturers often measure the white level and the black level with a separate set of display parameters that are fine-tuned to achieve the highest possible number which is obviously overestimated and no displayed image can show such a contrast. On the other hand, HDR images often have very few light or dark pixels. An image can be low-pass filtered before the actual dynamic range measure is taken to assure reliable estimation. Such filtering averages the minimum luminance thus gives a reliable noise floor, and smoothes single pixels with very high luminance thus gives a reasonable maximum amplitude estimate. Such a measurement is more stable compared to the non-blurred maximum and minimum luminance.

**Perceivable dynamic range** One important and often disputed aspect is the dynamic range that can be perceived by the human eye. The light scattering on the optic of the eye can effectively reduce the maximum luminance contrast that can be projected onto to retina to 2–3 log-10 units [98, 100]. However, since the eye is in fact a highly active sensor, which can rapidly change the gaze and locally adapt, people are believed to be able to perceive simultaneously the scenes of 4 or even more log-10 units of dynamic range [128, Sec. 6.2]. The effective perceivable dynamic range will vary significantly from scene to scene, it is, therefore, impossible to provide a single number. However, it has been shown in multiple studies that people prefer images of the dynamic range higher than 100:1 or 1000:1 when presented on a HDR display [28, 76, 180]. Therefore, it can be stated with high confidence that we can perceive and appreciate the scenes of higher contrast than 1000:1. It must be noted, however, that the actual appreciable dynamic range will depend on the peak brightness of a scene (or a display). For example, OLED displays offer very high dynamic range, but since their peak brightness is limited, most of that range lies in low-luminance range, in which our ability to distinguish colors is severely limited.

## 2.2 The difference between LDR and HDR pixel values

It is important to make distinction between the pixel values that can be found in typical LDR images and those that are stored in HDR images. Pixel values in HDR images

are in general linearly related to *luminance*, which is the photometric quantity that describes the perceived intensity of the light per surface area regardless of its color. The HDR pixel values are hardly ever strictly equal to luminance because the cameras used to capture HDR images have different spectral sensitivity than the luminous efficiency function of the human eye (used in the definition of luminance). However, HDR pixels values are good approximation of photometric quantities. Some sources report the deviation from the photometric measurements in the range from 10% for achromatic surfaces (gray) to 30% for colored objects [177].

If three color channels are considered, each color component in an HDR image is sometimes called *radiance*. This is not strictly correct because the physical definition of radiance assumes that the light is integrated over all wavelengths, while in fact red, green and blue HDR pixel values have their spectral characteristic restricted by the spectral sensitivities of a camera system. HDR pixel values are also not related to *spectral radiance*, which describes a single wavelength of light. The most accurate term describing the quantities that are stored in HDR pixels is *trichromatic color values*. This term is commonly used in color literature.

Pixel values in LDR images are non-linearly related to photometric or colorimetric values. Therefore, the term luminance cannot be used to describe the perceived light intensity in LDR images. Instead, the term *luma* is used to denote the counterpart of luminance in LDR images. In case of displays, the relation between luminance and luma is described by a display model, which is discussed in the next section.

### 2.3 Display models and gamma correction

Most of the low dynamic range image or video formats use so called *gamma correction* to convert luminance or RGB spectral color intensity into integer numbers, which can be later encoded. Gamma correction is usually given in a form of the power function  $\text{intensity} = \text{signal}^\gamma$  (or  $\text{signal} = \text{intensity}^{(1/\gamma)}$  for an inverse gamma correction), where the value of  $\gamma$  is between 1.8 and 2.8. Gamma correction was originally intended to reduce camera noise and to control the current of the electron beam in CRT monitors (for details on gamma correction, see [120]). However, it was found that the gamma function also well corresponds with our lightness (or brightness) perception for a luminance range that is produced by typical displays. The gamma function is a simplification of a more precise display model known as gamma-offset-gain (GOG) [15]. The GOG model describes the relation between LDR pixel values that are sent to the display and the light emitted by the display. In the case of gray-scale images, the relation between LDR luma value and emitted luminance is often modelled as

$$L = (L_{\text{peak}} - L_{\text{black}}) V^\gamma + L_{\text{black}} + L_{\text{refl}}, \quad (1)$$

where  $L$  is luminance and  $V$  is LDR luma, which is expected to be in the range 0–1 (as opposed to 0–255).  $L_{\text{peak}}$  is the peak luminance of the display in a completely dark room,  $L_{\text{black}}$  is the luminance emitted for the black pixels (*black level*), and  $L_{\text{refl}}$  is the ambient light that is reflected from the surface of a display.  $\gamma$  is the gamma-correction parameter that controls non-linearity of a display, which is close to 2.2 for computer monitors, but is often higher for television displays. For LCD displays  $L_{\text{black}}$  varies

in the range from 0.1 to 1 cd/m<sup>2</sup> depending on the display brightness and the contrast of an LCD panel.  $L_{refl}$  depends on the ambient light in an environment and can be approximated in the case of non-glossy screens<sup>1</sup> with:

$$L_{refl} = \frac{k}{2\pi} E_{amb}, \quad (2)$$

where  $E_{amb}$  is the ambient illuminance in lux and  $k$  is the reflectivity for a display panel. The reflectivity is below 1% for modern LCD displays and can be larger for CRT and Plasma displays. The inverse of that model takes the form:

$$V = \left[ \frac{(L - L_{black} - L_{refl})}{L_{peak} - L_{black}} \right]^{(1/\gamma)}, \quad (3)$$

where the square brackets are used to denote clamping values to the range 0–1. Similar display models are used for color images, with the difference that a color-transformation matrix is used to transform from CIE XYZ to linear RGB values of a display.

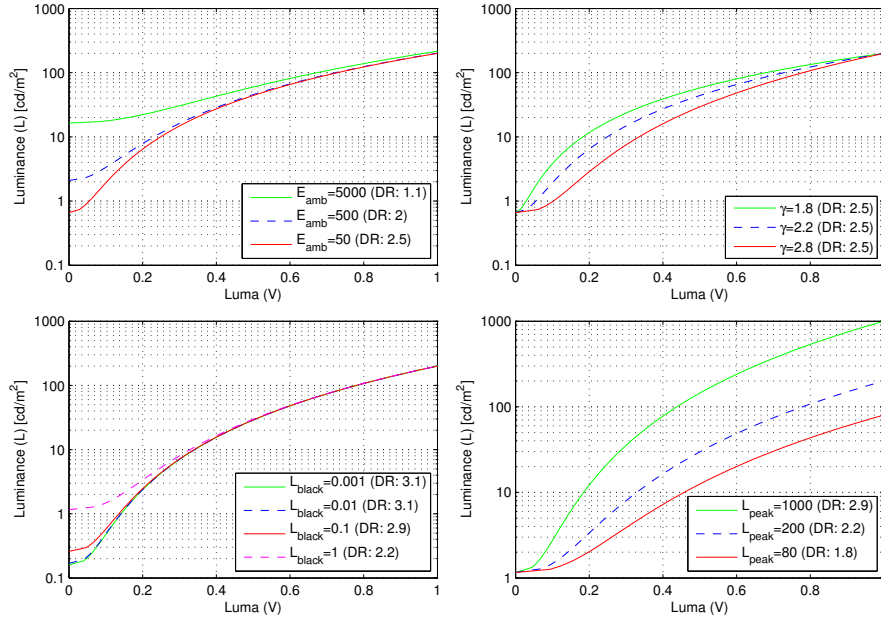


Figure 4: The relation between pixel values ( $V$ ) and emitted light ( $L$ ) for several displays, as predicted by the model from Eq. 1. The corresponding plots show the variation in ambient light, gamma, black level and peak luminance in the row-by-row order. The  $DR$  values in parenthesis is the display dynamic range as log-10 contrast ratio. The parameters not listed in the legend are as follows:  $L_{peak}=200$  cd/m<sup>2</sup>,  $L_{black}=0.5$  cd/m<sup>2</sup>,  $\gamma=2.2$ ,  $E_{amb} = 50$  lux,  $k = 1\%$ .

<sup>1</sup>Note that  $E = \int_0^{2\pi} \int_0^{\pi/2} L(\phi, \omega) \cos\phi d\phi d\omega = 2\pi L$ , for constant  $L(\phi, \omega) = L$ .

Fig. 4 gives several examples of displays modelled by Eq. 1. Note that ambient light can strongly reduce the effective dynamic range of the display (top-left plot). “Gamma” has no impact on the effective dynamic range, but its higher value will increase image contrast and make it appear darker (top-right plot). Lowering the black level increases effective dynamic range to a certain level, then has no effect (bottom-left). This is because the black in most situations will be “polluted” by ambient light reflected from the screen. Brighter display can offer higher dynamic range, provided that the black level of a display remains the same (bottom-right).

The display models above can be used for a basic colorimetric or photometric calibration but they do not account for many other factors that affect the colors of displayed images. For example, the black level of a display is elevated by the luminance of neighboring pixels due to the display’s internal glare. Also, the light emitted by a plasma display varies with image content, so that a small “white” patch shown on a dark surround will have much higher luminance than the same patch shown on a large bright-gray background. The models given above, however, account for most major effects and are relatively accurate for the LCD displays, which is the dominant display technology at the moment.

**sRGB color space** The sRGB is a standard color space used to specify colors shown on computer monitors and many other display devices and it is used widely across the industry. The sRGB specification describes the relation between LDR pixel values and color emitted by the display in terms of luminance and CIE XYZ trichromatic color values. The major difference between the sRGB color space and the display model discussed in the previous section is that the former does not contain black-level components ( $RGB_{black}$  and  $RGB_{refl}$ ), implying that the display luminance can be as low as  $0 \text{ cd/m}^2$ . Obviously, no physical display can prevent light from being reflected from it, and almost all displays emit light even for the darkest pixels. In this sense, the sRGB color space is not a faithful model of a color display for low pixel values. This is especially important in the context of HDR imagery, where the differences between  $0.01$  and  $0.001 \text{ cd/m}^2$  are often perceivable and should be preserved. One advantage of omitting the black level component is that when an image contains pixels equal to  $0$ , this tells the display that the pixel should be as black as possible, regardless of the black level and contrast of the actual device. For LDR devices it is a desirable behavior, however, it can produce contouring artifacts on the displays that support much higher dynamic range.

## 2.4 The logarithmic domain and the sensitivity to light

Many algorithms for HDR images, discussed in the following sections, operate on the logarithms of HDR pixel values rather than on the original HDR pixel values. In fact the easiest way of adapting an existing LDR image processing algorithm to HDR images is to operate on the logarithmic pixel values. The logarithmic domain is more appropriate for processing HDR pixel values because of the way the human visual system is sensitive to light. This section explains how the sensitivity to relative contrast changes is related to the logarithmic function.

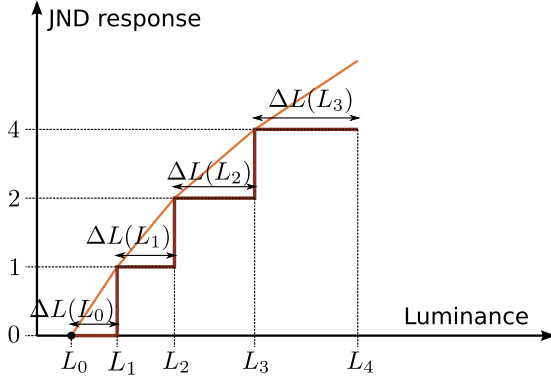


Figure 5: The construction of the mapping from luminance into JND-scaled response. The mapping function (orange line) is formed by joining the nodes.

In the vision research literature the luminance contrast is often defined as

$$C = \frac{\Delta L}{L}, \quad (4)$$

where  $\Delta L$  is the amplitude (modulation) of the sine grating or any other contrast stimulus and  $L$  is the background luminance. A typical example is a sine grating with the amplitude  $\Delta L$  and the mean value  $L$ . Such a contrast definition is used because already over one hundred years ago experimental psychologist found that the smallest luminance difference  $\Delta L$  detectable on a uniform surround is linearly related to the luminance of the surround  $L$ , and the relation is approximately constant, that is

$$\frac{\Delta L}{L} = k, \quad (5)$$

where  $k$  is the Weber fraction. The relation is commonly known as the Weber law after German psychologist Ernst Heinrich Weber. Based on these findings we want to construct a function  $R(L)$  that approximates a hypothetical response of the visual system to light. We assume that the difference in response is equal to 1 when the difference between two luminance levels ( $L$  and  $L + \Delta L$ ) is just noticeable, i.e.

$$R(L + \Delta L) - R(L) = 1 \iff \frac{\Delta L}{L} = k. \quad (6)$$

The equation is intended to scale the response function  $R(L)$  in the units of a *just noticeable difference* (JND), where 1 JND is equivalent to spotting a difference between two luminance levels with 75% probability. After such scaling, adding and subtracting value of 1 in the response space  $R$  will result in introducing a just noticeable difference in luminance. It is possible to derive such a space by an iterative procedure. Starting from some minimum luminance, for example  $L_0 = 0.005$ , the consecutive luminance steps are given by:

$$\begin{aligned} L_t &= L_{t-1} + \Delta L \\ R_t &= t \quad \text{for } t = 1, \dots \end{aligned} \quad (7)$$

After introducing the Weber law from Eq. 5, we get:

$$L_t = L_{t-1} + k L_{t-1} = L_{t-1} (k + 1), \quad \text{for } t = 1, \dots \quad (8)$$

Then, the mapping function is formed by the set of points  $(L_t, R_t)$ , as visually illustrated in Fig. 5. However, the response function can also be derived analytically to give a closed-form solution. Our assumption in Eq. 6 is equivalent to stating that the slope (derivative) of the response function  $R(L)$  is equal to  $1/\Delta L$ , which means that the response increases by one if the luminance increases by  $\Delta L$ :

$$\frac{dR(L)}{dL} = \frac{1}{\Delta L}. \quad (9)$$

Given the derivative, we can find the response function by integration

$$R(L) = \int \frac{1}{\Delta L} dL. \quad (10)$$

If we introduce the Weber fraction from Eq. 5 instead of  $\Delta L$ , we get

$$R(L) = \int \frac{1}{kL} dL = \frac{1}{k} \ln(L) + k_1, \quad (11)$$

where  $k_1$  is an arbitrary offset of the response, which is usually selected so that the response  $R$  for the smallest detectable amount of luminance  $L_{min}$  is equal 0 ( $R(L_{min}) = 0$ ). Even though a natural logarithm was used in this derivation, the base 10 logarithm is more commonly used as it provides more intuitive interpretation of the data and differs from the natural logarithm only by the constant  $k$ .

The important consequence of the above considerations is that luminance values should be always visualized on the logarithmic scale. Linear values of luminance have little relation to visual perception and thus the interpretation of the data is heavily distorted. Therefore, in the remainder of this text, the luminance will be always represented on plots in logarithmic units.

**Weber law revised** The derivation above shows how the logarithmic function is a hypothetical response of the visual system to light given the Weber law. Modern vision research acknowledges the fact that the Weber law in fact does not hold for all conditions and the Weber fraction  $k$  changes with background luminance, spatial frequency of the signal and several other parameters. One simple improvement to that hypothetical response function is to allow the constant  $k$  vary with the background luminance based on the contrast sensitivity models [89, 92]. With varying Weber fraction, the response function is no longer a straight line on the log-linear plot and its slope is strongly reduced for low luminance levels, as shown in Fig. 6 (red, solid line). This is because the eye is much less sensitive at low luminance levels and much higher contrast is needed to detect a just noticeable difference.

The procedure outlined in the previous section is very generic and can be used with any visual model, including threshold versus intensity or contrast sensitivity functions [14]. To get a JND space for an arbitrary visual model, it is sufficient to replace  $\Delta L$

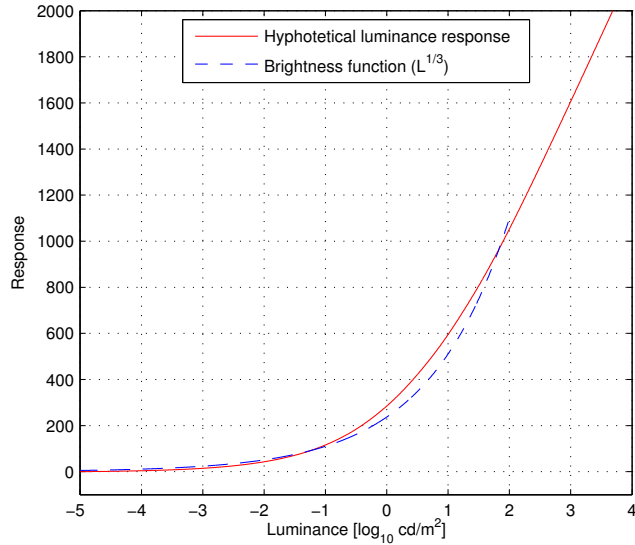


Figure 6: A hypothetical response of the visual system to light derived from the threshold measurements compared with the Stevens' brightness function. The brightness function is arbitrarily scaled for better comparison.

in Eq. 10. The technique is very useful and found many applications, including the DICOM gray-scale function [34] used in medical monitors, quality metrics for HDR [7], and a color space for image and video coding [89, 92, 105]. The latter is discussed in more detail in Sec. 4.1.

**Stevens law and the power function** All the considerations above assume that the measurements of the smallest luminance differences visible to the eye (detection thresholds) have a direct relation to the overall perception of light. This assumption is hard to defend as the thresholds are measured and valid only for very small contrast values, for which the visual system struggles to detect a signal. Such thresholds may be irrelevant for contrast that is much above the detection threshold. As the contrast we see in everyday life is mostly above the detection threshold, the finding for threshold-conditions may not generalize to normal viewing.

In their classical work Stevens and Stevens [147] revisited the problem of finding the relation between the luminance and perceived magnitude (brightness). Instead of Weber's threshold experiments, they used magnitude estimation method in which the observers rated brightness of the stimuli on the numerical scale 0–10. These experiments revealed that the brightness is related to luminance by the power function, with the exponent approximately equal to 1/3 (though the exponent varies with the conditions). This finding was in contrast to the logarithmic response resulting from the Weber law and, therefore, it questioned whether the considerations of the thresholds have any relevance to the luminance perception.

To confront these views, Stevens' brightness function is plotted in Fig. 6 (dashed-blue line) next to the response function derived from the threshold measurements (solid-red line). The brightness function is plotted for luminance levels below  $100 \text{ cd/m}^2$ , which is the most relevant range for the majority of applications. As can be seen on the plot, both curves are very similar and for most practical applications the difference is not significant. This suggests that both approaches achieve the desired result and transform luminance into more perceptually uniform units. However, the power function cannot be used for images of very high dynamic range (more than 3 orders of magnitude). This is because the power function gets too steep for very large luminance range, distorting the relative importance of bright and dark image regions.

### 3 Image and video acquisition

There are two major sources of HDR content: abstract scene modeling using computer graphics tools and real world scenes captured using the photographic approach (refer to Fig. 3). In the former case the most compelling results are achieved by means of realistic image synthesis and global illumination computation, which typically provide with photometrically calibrated pixel values (Sec. 3.1). The photographic approach may rely on traditional cameras (Sec. 3.2) with LDR sensors, where for a mostly static scene multiple exposures are taken in a time-sequential manner, and then merged into an HDR image using computational methods (Sec. 3.3). Specific software solutions are provided to compensate for the photograph misalignment in case of hand-held camera shooting, as well as for removing ghosting due to dynamic aspects in the scene (Sec. 3.3.1). Similar frame alignment techniques can be used in multi-exposure HDR video capturing (Sec. 3.3.2). This problem can be avoided when specialized HDR sensors and cameras are used, which can capture a scene in a single shot (Sec. 3.4).

The HDR content can be created from the legacy LDR content by expanding its dynamic range using a computational approach. This is an ill-posed problem, which typically does not lead to the high quality HDR reconstruction. Such an LDR-to-HDR conversion is addressed separately in Sec. 6.

#### 3.1 Computer graphics

In computer graphics, image rendering has always been one of the major goals, but just in mid-eighties researchers started to combine realistic image synthesis with physically-based lighting simulation [63, 119]. Physically-based lighting simulation requires valid input data expressed in radiometric or photometric units. It is relatively easy to acquire such data describing light sources because manufacturers of lighting equipment measure, and often make available directional emissive characteristics of their luminaires (the so-called goniometric diagrams). It is typically more costly to obtain valid reflectance characteristics of materials (the so-called bi-directional reflectance distribution function - BRDF and bi-directional texture function - BTF), but in many cases they can be approximated by data measured for similar materials, or by analytical reflectance models with a proper parameter setup.



Figure 7: Atrium of the University of Aizu: (left) rendered image, and (right) HDR photograph. Refer also to the accompanying web page <http://www.mpi-inf.mpg.de/resources/atrium/>. (Reproduced with permission from [108] © Morgan & Claypool Publishers.)

Physically-based lighting simulation with the use of physically-valid data, which describe the rendered scenes, result in a good approximation of illumination distribution with respect to the corresponding real-world environments. Also, pixels in rendered images are naturally expressed in terms of radiance or luminance values, which is the distinct characteristic of HDR images. Fig. 7(left) shows a typical example of realistic image rendered using Monte Carlo methods. Fig. 7(right) shows the corresponding HDR image that was captured with a camera in the actual real-world scene.

In recent years graphics processing units (GPU) and major game consoles upgraded their rendering pipelines to the floating point precision, which effectively enabled HDR image rendering in real-time applications. Although physically-based lighting simulation is typically ignored, the resulting images look plausible.

In summary, computer graphics is an important source of HDR content that features virtually arbitrary contrast ranges and negligible quantization errors, which is difficult to achieve using photographic methods mostly due to imperfections of optical systems (Sec.6.4).

### 3.2 RAW vs. JPEG images

Let us now consider standard cameras as a potential source of HDR images. Because of the bandwidth limitations, many cheaper camera modules produce compressed JPEG images as their output. For example inexpensive web-cams transfer video as a series

of JPEG images because sending uncompressed video would exceed the bandwidth offered by the USB-2 interface. Those cameras essentially perform tone-mapping to transform linear response of the CCD or CMOS sensor into gamma-corrected pixel values. Both tone-mapping and JPEG compression introduce distortions and reduce the dynamic range of the captured images.

However, more expensive cameras, in particular DSLR cameras, offer an option to capture so-called RAW images, which contain the snapshot of values registered by a sensor. Such images can be processed (tone-mapped) on a PC rather than in the camera. As such, they typically offer higher dynamic range than one that can be reconstructed from a single JPEG image. The dynamic range gain is especially substantial for larger sensor sizes, which offer higher photon capacity and effectively capture higher dynamic range. In that respect, RAW images can be considered as images of extended (or intermediate) dynamic range.

### 3.3 Time sequential multi-exposure techniques

The simplest method of capturing HDR images involves taking multiple images, each at different exposure settings. While an LDR sensor might capture at once only a limited range of luminance in the scene, its operating range can encompass the full range of luminance through the change of exposure settings. Therefore, each image in a sequence is exposed in a way that a different luminance range is captured (Fig. 8). Afterwards, the images are combined into a single HDR image by weighted averaging of pixel values across the exposures, after accounting for a camera response and normalizing by the exposure change [31, 87, 106, 133]. More detailed discussion on the choice of weighting functions used in pixel irradiance averaging between different exposures is presented by Granados et al. [51]. While, typically such weighting promotes well exposed (non-saturated, close to the center of dynamic range scale) pixels, Granados et al. take into account various sensor noise sources, i.e., temporal (photon and dark current shot noise, readout noise) and spatial (photo-response and dark current non-uniformity) as a function of irradiance reaching the sensor. Reinhard et al. [128, Ch. 5.7] discuss various solutions for deriving the camera response function, whose inverted version enables to recover such irradiance values directly from the corresponding pixel values in each input image. Gallo et al. [48] analyzes the image histogram and adaptively selects a minimal number of exposures to capture the scene with an optimal signal-to-noise-ratio.

Theoretically, the multi-exposure approach allows to capture scenes of arbitrary dynamic range, with an adequate number of exposures per frame, and exploits the full resolution and capture quality of a camera. This technique is available in many consumer products, including mobile phones. This option is usually labeled as “HDR mode”. In contrast to most HDR capture methods discussed in this section, such an “HDR mode” is meant to produce a single JPEG image, which attempts to preserve details from multiple exposures. This is achieved by blending (fusing) several JPEG images taken at different exposures where each blending weight is determined by a measure of quality, such as local contrast, or color distribution [102].

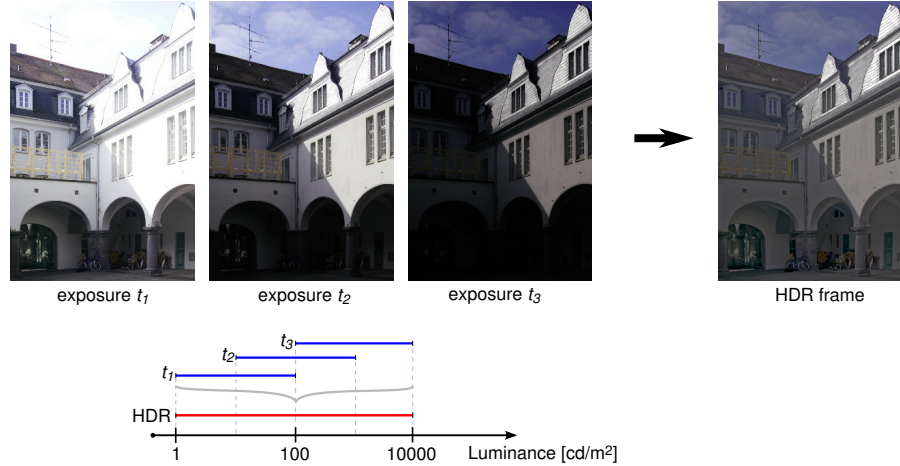


Figure 8: Three consecutive exposures captured at subsequent time steps  $t_1$ ,  $t_2$ ,  $t_3$  register different luminance ranges of a scene. The HDR frame merged from these exposures contains the full range of luminance in this scene. (Images courtesy of Grzegorz Krawczyk. Reproduced with permission from [108] © Morgan & Claypool Publishers.)

### 3.3.1 Deghosting: handling camera and object motion

When merging multiple-exposures taken at different times, some image parts may be misaligned because of movement of the camera or objects in the scene. The former problem is typically solved through an alignment of input image based on a global homography derived using robust statistics such as RANSAC over the corresponding SIFT [154] or SURF [52] features. Such an approach, however, fails when there is a significant parallax in the scene, which cannot be compensated by a global homographic transformation.

To compensate for object motion many techniques rely on the optical flow computation, when after the image alignment some form of color averaging is performed [183], possibly with an explicit rejection of selected exposures in problematic regions [47]. Other approaches rely on local motion detection and weighting of each exposure contribution as a function of the probability of such motion [68]. The HDR image reconstruction and deghosting can be handled in a single processing step as an optimization in which the optimal solution matches a reference exposure in the regions where it is well exposed, and in its poorly exposed regions local similarity to the remaining exposures is maximized by acquiring from them as many details as possible [59, 140]. The patch match algorithm, which exploits self-similarities in images [12, 141], is used in this application to optimize local similarity of the reconstructed HDR image to all input exposures. Granados et al. [52] propose a general purpose technique, which can also handle difficult cases such as cluttered scenes with large object displacements. They estimate the likelihood that a pair of colors in different images are observations of the

same irradiance so that they can use a Markov random field prior to the reconstruction of irradiance from pixels that are likely to correspond to the same static scene object. A recent survey on deghosting algorithms in the context of HDR reconstruction can be found in [145].

### 3.3.2 Video solutions

With the increase of programmability of digital cameras [3] it is possible to alternate exposures between subsequent video frames, which in turn enables the application of multi-exposure techniques for HDR video. The problem of frame alignment to compensate for camera and object motion arises, but then solutions similar to deghosting, as discussed in the previous section, can be readily applied. An additional requirement in video case is temporal coherence between the resulting HDR frames. Two alternating exposure levels are commonly used to achieve real-time HDR video capture at 25 fps [66, 86]. The frame alignment is achieved using optical flow to unidirectionally warp the previous/next frames to a given HDR frame. The distinctive advantages of optical flow [66, 183] and patch-match [140] approaches in the HDR image synthesis can be combined to enforce similarity between adjacent frames and increase this way temporal continuity [59, 65]. Also, a better quality of texture and motion synthesis in fast moving regions can be achieved. An alternative solution that captures a much wider dynamic range of about 140dB, but does not compensate for motion artifacts has been proposed in [157]. Such high dynamic range was possible by using a 200Hz camera with eight exposures per an HDR frame. More recent efforts that also rely on high frame rate cameras but compensate for camera motion have been presented in [21, 54]. However, shorter per-frame capture-time increases requirements on sensor sensitivity, which typically results in increasing noise in low light conditions.

## 3.4 HDR sensors and cameras

As deghosting algorithms might not be reliable in certain scenarios, the best effect can be expected for dedicated single-shot HDR cameras. The popularization of such solutions is somehow limited due to high cost of such devices. The simplest approach, which does not require novel sensor design, relies on introducing variations in pixel sensitivity on a sensor. Such approach trades sensor sensitivity and often spatial resolution for higher dynamic range (Sec. 3.4.1). Alternatively, several standard cameras can be connected through an optical element that splits light onto their sensors with each having a different exposure setting (Sec. 3.4.2). Finally, HDR sensors can be explicitly designed, for example, with a logarithmic response for incoming lighting (Sec. 3.4.3).

### 3.4.1 Spatial exposure change

The spatial exposure change is usually achieved using a mask which has a per pixel variable optical density. The number of different optical densities can be flexibly chosen and they can create a regular or irregular pattern. Nayar and Mitsunaga [109] propose to use a mask with a regular pattern of four different exposures that is placed

directly in front of the sensor chip. As the result of merging those four exposures a dynamic range of about 85dB for an 8-bit sensor can be achieved.

An alternative implementation of spatial exposure change, Adaptive Dynamic Range Imaging (ADRI), utilizes an adaptive optical density mask instead of a fixed pattern element [110, 111]. Such a mask adjusts its optical density per pixel informed by a feedback mechanism from the image sensor. Saturated pixels increase the density of corresponding pixels in the mask, and noisy pixels decrease such density. The feedback, however, introduces a delay which can appear as temporal over- or under-exposure of moving high contrast edges.

### 3.4.2 Multiple sensors with beam splitters

Following the multi-exposure approach to extending dynamic range, one can capture several exposures per video frame at once using beam splitters, which direct light to multiple sensors [4, 5, 73, 152]. This removes completely the problem of motion, but requires high precision in optics design so that images captured at different sensors are aligned. When a single lens system is used, the focal length and aperture control is conveniently simplified. The effective dynamic range is determined by the number of employed sensors, which is typically limited to 3–4. Any additional sensor not only increases the camera cost and complicates the light splitting optics, but also reduces the amount of light per sensor. This imposes additional requirements on the sensor sensitivity, which in turn might increase noise in dark lighting conditions.

### 3.4.3 Solid state sensors

There are currently two major approaches to extend the dynamic range of an imaging sensor. One type of sensor collects charge generated by the photo current. The amount of charge collected per unit of time is linearly related to the irradiance on the chip (similar to a standard CCD chip [62]), the exposure time is however varying per pixel (sometimes called “locally auto-adaptive”) [20, 50, 82]. This can for instance be achieved by sequentially capturing multiple exposures with different exposure time settings or by stopping after some time the exposure of the pixels that would be overexposed during the next time step. A second type of sensor uses the logarithmic response of a component to compute the logarithm of the irradiance in the analog domain [57, 139]. Both types require a suitable analog-digital conversion and generate typically a non-linearly sampled signal encoded using 8–16 bits per pixel value. Several HDR video cameras based on these sensors are already commercially available. Such cameras do not require any exposure time control, which allows for capturing dynamic scenes with strong lighting changes. Also, they typically offer considerably wider dynamic range than multi-exposure video solutions, although their pixel resolution is typically low, and, for the logarithmic sensors, the visible noise in dark scene regions can be an issue.

## 4 Storage and compression

High dynamic range images and video impose huge storage costs when represented in its native floating point format. For example, a 15 mega-pixel image requires between 0.7 MB and 3 MB to store in the popular JPEG format. However, the same resolution image takes 176 MB when stored in a “RAW” HDR format ( $3 \times 32$ -floating point number per pixel). This clearly shows importance of finding a better representation and compression for HDR images and video.

Most of the proposed compression schemes devised for HDR rely on the existing compression standards for LDR images and video. To effectively use those compression standards, the floating point HDR pixel values need to be transformed into more efficient representation, using the lowest number of bits. Such HDR pixel representations are discussed in Sec. 4.1, while the resulting HDR file formats are presented in Sec. 4.2. Then, in Sec. 4.3, several schemes for encoding HDR images and video using existing compression standards are discussed, while Sec. 4.4 focuses on backward-compatible solutions that additionally support standard 8-bit JPEG and MPEG formats.

### 4.1 HDR pixel formats and color spaces

Choice of the color space and the pixel encoding used for image or video compression has a great impact on the compression performance and capabilities of the encoding format. The discussed encoding schemes attempt to minimize the number of required bits while providing sufficient accuracy and capability to encode wide dynamic range. If the bit-depth accuracy is too low, banding (quantization) artefacts become visible. The following sections describe the most popular HDR pixel encodings. Refer to [108, Ch. 5.1] for the discussion of less often used HDR pixel encodings.

**Minifloat: 16-bit floating point numbers** Graphics cards from nVidia and AMD can use a compact representation for floating point numbers, known as *half-precision float*, *fp16* or *S5E10*. The code-name S5E10 indicates that the floating point number consist of one bit of sign, 5-bit exponent, and 10-bit mantissa, as shown in Fig. 9. Such 16-bit floating point representation is used in the OpenEXR image format (see Sec. 4.2).

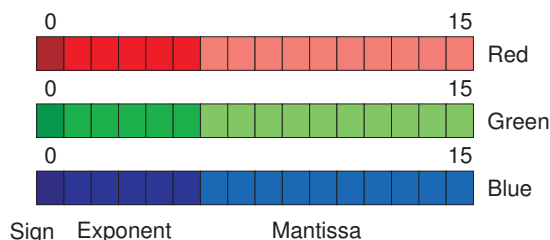


Figure 9: Red-green-blue component encoding using half-precision floating point numbers. (Reproduced with permission from [108] © Morgan & Claypool Publishers.)

The half-precision float offers flexibility of the floating point numbers at the half storage cost of the typical 32-bit floating point format. Floating point numbers are well suited for encoding linear luminance and radiance values, as they can easily encompass large dynamic ranges. One caveat of the half-precision float format is that it can represent numbers up to the maximum value 65,504, which is less than for instance luminance of bright light sources. For this reason, the HDR images containing absolute luminance or radiance units often need to be scaled down by a constant factor before storing them in the half-precision float format.

**RGBE: Common exponent** The *RGBE* pixel encoding is used in the Radiance file format, which will be discussed in Sec. 4.2. The RGBE pixel encoding represents colors using four bytes: the first three bytes encode red, green and blue color channels, and the last byte is a common exponent for all channels (see Fig. 10). RGBE is essentially a custom floating point representation of pixel values, which uses 8 bits to represent exponent and another 8 bits to represent mantissa (8E8). RGBE encoding takes advantage of the fact that all color channels are strongly correlated in the RGB color spaces and their values are at least of the same order of magnitude. Therefore, there is no need to store a separate exponent for each color channel.

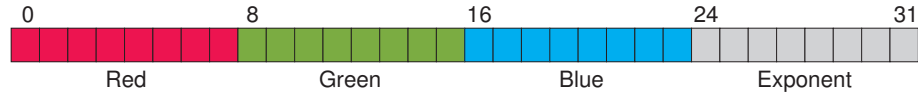


Figure 10: 32-bit per pixel RGBE encoding. (Reproduced with permission from [108] © Morgan & Claypool Publishers.)

The conversion from  $(R, G, B, E)$  bytes to red, green and blue trichromatic color values  $(r, g, b)$  is done using the formulas:

$$(r, g, b) = \begin{cases} \frac{(R, G, B) + 0.5}{256} 2^{E-128} \frac{\text{exposure}}{E_w} & \text{if } E \neq 0 \\ (0, 0, 0) & \text{if } E = 0 \end{cases} \quad (12)$$

where *exposure* parameter (one for the entire image) can be used to adjust absolute values and  $E_w$  is the efficacy of the white constant equal to 179. Both these terms are used in the Radiance file format but are often omitted in other implementations.

The inverse transformation is given by:

$$E = \begin{cases} \lceil \log_2(\max\{r, g, b\}) + 128 \rceil & \text{if } (r, g, b) \neq 0 \\ 0 & \text{if } (r, g, b) = 0 \end{cases} \quad (13)$$

$$(R, G, B) = \left\lfloor \frac{256(r, g, b)}{2^{E-128}} \right\rfloor$$

where  $\lceil \cdot \rceil$  denotes rounding up to the nearest integer and  $\lfloor \cdot \rfloor$  rounding down to the nearest integer.

The limitation of the RGBE encoding is that it cannot represent highly saturated colours outside Rec.709 (sRGB) colour gamut. When such highly saturated colors

are converted to the RGB color space, one or more of their color components become negative. And since RGBE format cannot represent negative values, some color information is lost. As a solution to this problem, the Radiance format can also encode pixels in the CIE XYZ color space using XYZE encoding. Such encoding is analogous to RGBE, except that CIE XYZ color primaries are used.

**LogLuv: Logarithmic encoding** One shortcoming of floating point numbers is that they are not optimal for image compression methods. This is partly because additional bits are required to encode mantissa and exponent separately, instead of a single integer value. Such representation, although flexible, is not necessary for color data. Furthermore, precision error of floating point numbers varies across the full range of possible values and is different than the “precision” of our visual system. Therefore, better compression can be achieved when integer numbers are used to encode HDR pixels.

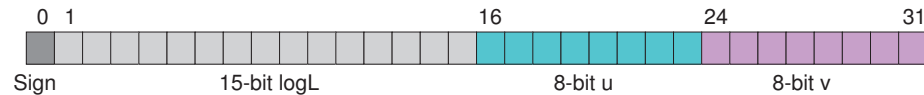


Figure 11: 32-bit per pixel LogLuv encoding. (Reproduced with permission from [108] © Morgan & Claypool Publishers.)

The *LogLuv* pixel encoding [170] requires only integer numbers to encode the full range of luminance and color gamut that is visible to the human eye. It is an optional encoding in the TIFF library. This encoding benefits from the fact that the human eye is not equally sensitive to all luminance levels. In the dark we can see a luminance difference of a fraction of  $1 \text{ cd/m}^2$ , while in the sunlight we need a difference of tens of  $\text{cd/m}^2$  to see a difference. This effect is often called luminance masking. But if, instead of luminance, a logarithm of luminance is considered, the detectable threshold values do not vary so much and a constant value can be a plausible approximation of the visible threshold. Therefore, if a logarithm of luminance is encoded using integer numbers, quantization errors roughly correspond to the visibility thresholds of the human visual system, which is a desirable property for pixel encoding.

The 32-bit LogLuv encoding uses two bytes to encode luminance and another two bytes to represent chrominance (see Fig. 11). Chrominance is encoded using the CIE 1976 Uniform Chromacity Scales  $u'$   $v'$ :

$$u' = \frac{4X}{X+15Y+3Z} \quad v' = \frac{9Y}{X+15Y+3Z} \quad (14)$$

which can be encoded using 8-bits:

$$u_{8bit} = u' \cdot 410 \quad v_{8bit} = v' \cdot 410 \quad (15)$$

Note that the  $u'$  and  $v'$  chromaticities are used rather than  $u^*$  and  $v^*$  of the  $L^*u^*v^*$  color space. Although  $u^*$  and  $v^*$  give better perceptual uniformity and predict loss of color sensitivity at low light, they are strongly correlated with luminance. Such correlation is undesired in image or video compression. Besides, the  $u^*$  and  $v^*$  chromaticities could reach high values for high luminance, which would be difficult to encode using only

eight bits. It is also important to note that the CIE 1976 Uniform Chromacity Scales are only approximately perceptually uniform, and in fact the 8-bit encoding given in Eq. 15 may lead to just visible quantization errors, especially for blue and pink hues. However, such artifacts should be hardly noticeable in complex images.

The LogLuv encoding has a variant which uses only 24 bits per pixel and still offers sufficient precision. However, this format can be ineffective to compress using arithmetic coding, due to discontinuities resulting from encoding two chrominance channels with a single lookup value.

**JND steps: Perceptually uniform encoding** LDR pixel values have a desirable property that their values are approximately linearly related to perceived brightness of that pixels. Because of that, LDR pixel values are also well suited for image encoding since the distortions caused by image compression have the same visual impact across the whole scale of *signal* values. HDR pixel values lack such a property and, therefore, when the same magnitude of distortion is introduced in low-luminance and high-luminance image regions, the artefacts are more visible in the low-luminance regions. The problem is alleviated if the logarithm of luminance is encoded instead of luminance, such as in the LogLuv encoding discussed above. But the logarithmic encoding does not completely solve the problem as the logarithm is not an accurate model of the human visual sensitivity to light (refer to Sec. 2.4). For that reason, several encodings were proposed that employ more accurate models of eye sensitivity to light changes [89, 92, 105].

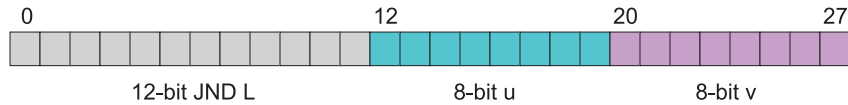


Figure 12: 28-bit per pixel JND encoding. (Reproduced with permission from [108] © Morgan & Claypool Publishers.)

The derivation of such perceptually uniform encoding is essentially the same as the derivation of the response of the visual system to light, described in Sec. 2.4 (Eq. 10). The resulting function maps physical luminance (in  $\text{cd}/\text{m}^2$ ) into the units related to the just-noticeable-differences (JNDs). The first such encoding in the context of HDR compression was proposed in [92], where the threshold vs. intensity function (t.v.i.) was used to determine the smallest noticeable difference in luminance across the luminance range. The paper showed that 10–12 bits are sufficient to encode the range of luminance from  $10^{-4}$  to  $10^8 \text{ cd}/\text{m}^2$ . Similarly as in the LogLuv encoding,  $u'$  and  $v'$  chroma coordinates were used to encode color, resulting in 28-bit per color encoding, as shown in Fig. 12. The follow-up paper [89] replaced the t.v.i. function with a more modern model of the contrast sensitivity (CSF) from the VDP [26]. Recently, a very similar idea was proposed in the context of encoding HDR images to the Society of Motion Picture & Television Engineers [105] using Barten's CSF [13]. The comparison of those recent encodings is shown in Fig. 13. Note that the perceptual encoding curves lies between the logarithmic encoding and the Gamma 2.2 encoding.

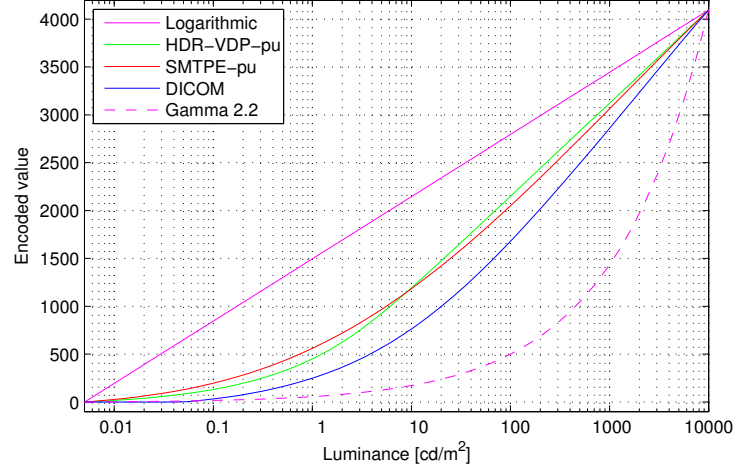


Figure 13: Functions mapping physical luminance into encoded 12-bit luma values. Logarithmic – is the logarithm of luminance; HDR-VDP-pu is the perceptual uniform color space derived from HDR-VDP-2 CSF [91]; SMTPE-pu – is the perceptually uniform encoding derived from Barten’s CSF; DICOM is the DICOM gray-scale function, also derived from Barten’s CSF but using different parameters; “Gamma 2.2” is the typical gamma encoding used for LDR images, but extended to the range 0.005 to 10 000 cd/m<sup>2</sup>.

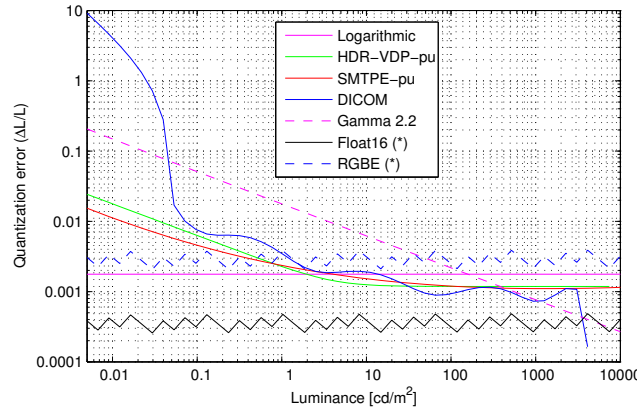


Figure 14: Comparison of the maximum quantization errors for different luminance to luma encodings. The labels are the same as in Fig. 13. The plot also shows the quantization error for two floating point encodings (marked with \*): 16-bit float and RGBC, discussed in Sec. 4.1. Note that more bits are used to encode both floating point formats (16 vs. 12 for other encodings).

One difficulty that arises from the JND luminance encoding is that the luminance must be given in absolute units of  $\text{cd}/\text{m}^2$  of the image that will be eventually shown on a display. This is necessary since the performance of the human visual system (HVS) is affected by the absolute luminance levels and the contrast detection thresholds are significantly higher for low light conditions.

**Quantization errors** All discussed encoding attempt to balance the capability of encoding higher dynamic range with the precision at which such a range is encoded. If the precision is too low, the encoding results in quantization errors, which reveal themselves as banding (contouring) in images, especially in the areas of smooth gradients. The precision of each encoding is best analyzed on the luminance vs. quantization error plot, shown in Fig. 14. Here, the y-axis shows what is the maximum quantization error due to the encoding as a Weber-ratio, which, as discussed Sec. 2.4, is a first-order approximation of the eye-sensitivity to light. Note that the logarithmic and floating point encodings have approximately uniform maximum quantization error across all visible luminance values. The edgy shape of both RGBE and *16-bit half* encodings is caused by rounding of the mantissa. Gamma 2.2 encoding provides very high precision at high luminance levels, but results in excessive errors in low luminance. The DICOM gray-scale function [34], used in medical display applications, relies on the earlier version of the Barten’s CSF model and results in large fluctuations of the error as well as excessive error at very low luminance values. The perceptually uniform encodings (*-pu* in the labels) vary the maximum quantization error across the range to mimic loss of sensitivity in the HVS for low light levels. This not only makes better use of the available range of luma values, but also reduces invisible noise in very dark scenes, which would otherwise be encoded. Such noise reduction can significantly improve image or video compression.

## 4.2 HDR image file formats

There is a number of file formats designed especially for storing HDR images. The following subsections describe the two most popular HDR image formats: Radiance HDR and the OpenEXR format.

**Radiance’s HDR format** One of the first HDR image formats, which gained much popularity, was introduced in 1989 into the Radiance rendering package<sup>2</sup>. Therefore, it is known as the Radiance picture format and can be recognized by the file extensions *.hdr* or *.pic*. The file consist of a short text header, followed by run-length encoded pixels. Pixels are encoded using the XYZE or RGBE pixel formats, discussed in Sec. 4.1. The difference between both formats is that the RGBE uses red, green and blue primaries, while the XYZE uses the CIE 1931 XYZ primaries. As a result, the XYZE format can encode the full visible color gamut, while the RGBE is limited to the chromaticities that lie within the triangle formed by the red, green and blue color primaries

---

<sup>2</sup>Radiance is an open source light simulation and realistic rendering package. Home page: <http://radsite.lbl.gov/radiance/>

of the Rec. 709 color gamut. For more details on this format, the reader should refer to [165] and [128, Sec. 3.3.1].

**OpenEXR** The OpenEXR format or (the EXtended Range format), recognized by the file name extension .exr, was made available with an open source C++ library in 2002 by Industrial Light and Magic (see <http://www.openexr.org/> and [19]). Since then the format has been adapted by many Open Source and commercial applications, and became a de-facto standard for HDR images, in particular, it is commonly used in the special-effect industry. Some features of this format include:

- Support for 16-bit floating-point, 32-bit floating-point, and 32-bit integer pixels.
- Multiple lossless and lossy image compression algorithms. The included codecs can achieve 2:1 lossless compression ratios on images with film grain.
- Extensibility. New compression codecs and image types can easily be added by extending the C++ classes included in the OpenEXR software distribution.

Although the OpenEXR file format offers several data types to encode channels, color data is usually encoded with 16-bit floating point numbers, known as half-precision floating point, discussed in Sec. 4.1.

### 4.3 High bit-depth encoding for HDR

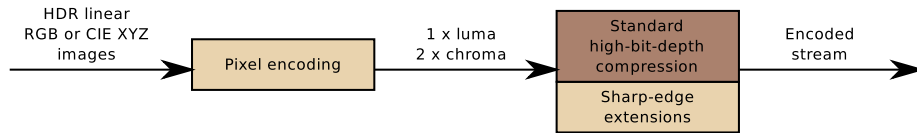


Figure 15: Encoding HDR image or video content using standard high-bit-depth codecs, such as JPEG2000, JPEG XR or selected profiles of H.264. The HDR pixels need to be encoded into one luma and two chroma channels to ensure good decorrelation of color channels and perceptual uniformity of the encoded values. The standard compression can be optionally extended to provide better coding for sharp-contrast edges.

HDR images and video can be stored not only in custom file formats, such as those discussed in Sec. 4.2, but also in any standard compression format that supports higher bit-depths. Many recent image and video compression standards have an optional support for higher bit-depths, making them easy to extend to HDR content. For example, the high-quality content profiles introduced in the MPEG4-AVC/H.264 video coding standard allow to encode up to 14-bits per color channel [149], while JPEG2000 standard supports up to 16 bits. Higher bit-depths of up to 16 or even 32 bits are also supported in the recent JPEG XR image compression standard. Such bit-depths are more than sufficient for HDR applications.

The extension of the existing standards to support HDR is illustrated in Fig. 15. In order to use the existing compression for HDR, pixels need to be first encoded using one of the pixel encodings discussed in Sec. 4.1. This not only reduces the number of required bits, but also improves perceptual uniformity of introduced distortions. Perceptually-uniform encodings provide the best performance [89, 92, 105], but logarithmic [114] and floating point coding is used as well.

One difficulty of encoding HDR images, and in particular images generated by computer graphics methods, is caused by very sharp contrast edges. Since almost all modern compression algorithms employ a frequency transform, such as Discrete Cosine Transform, the sharp contrast edges result in high values of frequency coefficients. When such coefficients are quantized, the decoded images often reveal ringing artefacts near the edges. This can be alleviated by encoding sharp-contrast edges in each  $8 \times 8$  block separately from the rest of the signal. An algorithm for such hybrid encoding can be found in [93].

#### 4.4 Backward-compatible compression

Since the standard low-dynamic range (LDR) file formats for images and video, such as JPEG or MPEG, have become widely adapted standards supported by almost all software and hardware equipment dealing with digital imaging, it cannot be expected that these formats will be immediately replaced with their HDR counterparts. To facilitate transition from the traditional to HDR imaging, there is a need for backward compatible HDR formats, that would be fully compatible with existing LDR formats and at the same time would support enhanced dynamic range and color gamut. Moreover, if such a format is to be successful and adopted, the overhead of HDR information must be low.

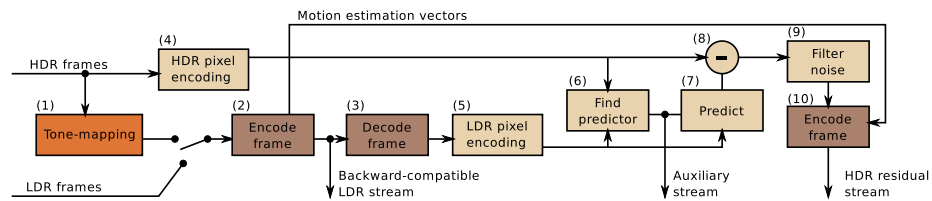


Figure 16: Typical encoding scheme for backward-compatible HDR compression. The darker brown boxes indicate standard (usually 8-bit) image of video codec, such as H.264 or JPEG.

Most backward-compatible compression methods follow similar processing scheme, shown in Fig. 16. The following paragraphs discuss this scheme while referring to concrete solutions and possible variants.

Some backward-compatible compression methods expect both HDR and LDR frames to be supplied separately as input [90]. Other methods provide their own tone-mapping operators (see step 1 in the diagram) and expect only HDR frames as input. The latter approach allow to adjust tone-mapped images to improve compression performance. For example JPEG-HDR method can introduce a “precorrection” step, which

compensates for the resolution reduction introduced at the later stages of the encoding. Mai et al. [83] derived a formula for an optimum tone-curve, which minimizes compression distortions and improves compression performance. The drawback of such compression-driven tone-mapping operators is that they introduce changes to the backward-compatible portion of the video, which is not acceptable in many applications.

The LDR frames are encoded using standard codec, such as JPEG or H.264 (see step 2 in the diagram) to produce a back-ward compatible stream. In order to use this stream for prediction of HDR stream, it is necessary to decode those frames (step 3), which can be done efficiently within the codec itself. Then, both LDR and HDR frames need to be transformed into a color space that would bring LDR and HDR color values into the same domain and make them comparable and easy to decorrelate (steps 4 and 5). Most of the pixel encodings discussed in Sec. 4.1 can be used for that purpose. For example HDR-MPEG method [90] employs perceptually uniform coding. This step, however, may not be sufficient to eliminate all redundancies between LDR and HDR streams, as they could be related in complex and non-linear manner. For that purpose, some encoding schemes find an optimal predictor function (step 6), which can be used to predict HDR pixel values based on LDR pixel values (step 7). Such a predictor could be a single tone-curve provided for the entire image [90, 176] or a simple linear function, but computed separately for each macro-block [138]. In the next step (8), the prediction from such a function is subtracted from the HDR frame to compute a residual that needs to be encoded. Some methods, such as JPEG-HDR [168], use division instead of subtraction. These methods, however, do not encode HDR pixel values (step 4). If the HDR values were encoded in the logarithmic domain, the division would be replaced by subtraction.

The resulting residual image may contain a substantial amount of noise, which is expensive to encode. For that reason, some methods employ a filtering step (9), which could be as simple as low-pass filtering and reducing resolution [168], or as complex as modeling the visibility of the noise in the visual system and removing invisible noise [90]. While reducing residual image resolution greatly reduces noise and improves encoding efficiency, it also removes some sharp contrast details. To prevent such loss, HDR-JPEG method offers two correction methods: enhancing edges in a tone mapped image (so called *pre-correction*) and synthesizing high frequencies in the ratio image during up-sampling (so called *post-correction*) [168, 169]. The residual frame can also be encoded at full resolution but selectively filtered to remove only the noise and the details that are invisible [90]. A visual comparison of both approaches is shown in Fig. 17.

Finally, the filtered frame is encoded to produce an **HDR residual stream** (step 10). Although the encoding of the residual stream is mostly independent from the LDR stream, it is possible to reuse the motion vectors stored in the LDR stream and thus reduce both storage overhead and the computing required to find motion vectors for the residual.

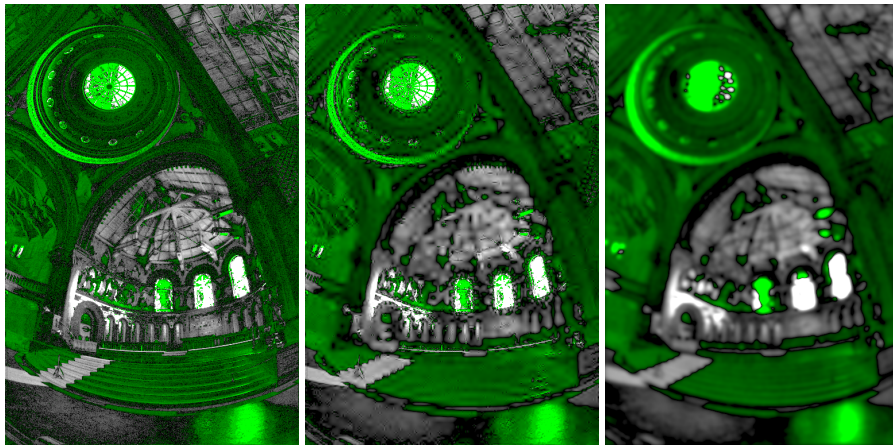


Figure 17: Residual frame before (left) and after (center) filtering invisible noise. Such filtering removes invisible information, while leaving important high frequency details that are lost if ordinary low-pass filtering (downsampling) is used (right). Green color denotes negative and gray positive values. (The *Memorial Church* image courtesy of Paul Debevec. Reproduced with permission from [108] © Morgan & Claypool Publishers.)

## 5 Tone mapping

Tone mapping is the process of rendering scenes of high contrast and potentially wide color gamut on a destination medium of limited contrast and color reproduction. Typically it involves transforming high dynamic range images (or animation frames), representing scene radiance or luminance, into pixel values that can be shown on a computer display. However, there is a huge variety of goals that tone-mapping algorithms try to achieve, methods they employ, and applications they address, which will be discussed in this section.

### 5.1 Intents of tone mapping

The goal of tone-mapping may differ greatly depending on the application and discipline. This variety of goals is the source of much confusion and misconception about tone-mapping, so it is important to clearly identify these goals. We can broadly divide tone-mapping operators depending on their intent into [41]:

- *Visual system simulators (VSS)* — they simulate the limitations and properties of the visual system. For example, a tone mapping operator (TMO) can add glare, simulate the limitations of human night vision, or reduce colorfulness and contrast in dark scene regions. Another example is the adjustment of images for the difference between the adaptation conditions of real-world scenes and the viewing conditions (including chromatic adaptation).

- *Scene reproduction (SRP) operators* — attempt to preserve the original scene appearance, including contrast, sharpness and colors, when an image is shown on a device of reduced color gamut, contrast and peak luminance. Such operators do not try to simulate appearance changes due to perceptual affects, such as loss of acuity and color vision at night. Instead they focus on overcoming the limitation of the output medium and try to achieve the best match given the limited gamut and dynamic range.
- *Best subjective quality (BSQ) operators* — are designed to produce the most preferred images or video in terms of subjective preference or artistic goals. Such operators often include a set of adjustable parameters that can be modified according to artistic goals. A good example of such an operator is photo editing software such as Adobe Photoshop Lightroom.

The intents listed above may not fully cover all possible aspects of tone-mapping and there are applications that do not fit well into any of these categories. However, the intents outline the differences in the fundamental assumptions and expectations for tone-mapping, and partly explain why there is no single “best” tone-mapping. The discussion of intent is especially important in the context of studies comparing operators, which should not juxtapose and benchmark two algorithms that realize two very different goals.

## 5.2 Algebra of tone mapping

In general terms, a tone mapping operator is a mathematical function that transforms HDR scene luminance into the luminance range that can be shown on a display. To fully understand the mechanisms of tone mapping, it is necessary to understand how the shape of the tone-mapping function affects appearance of generated images. In this section we analyze basic mathematical operators used for tone mapping and explain how they affect resulting images.

For simplicity, we restrict our consideration to gray-scale images. The tone mapping function will be denoted by:

$$\hat{L}_p = T(L_p), \quad (16)$$

where  $L$  is the HDR pixel luminance,  $p$  is an index of a pixel, and  $\hat{L}$  is luminance that should be shown on a display. The values of  $\hat{L}$  should be transformed by a display model (refer to Sec. 2.2) to get LDR pixel values that could be sent to a display. This step is often confusingly called *gamma correction*, though it is meant to transform luminance into luma values, as discussed in Sec. 2.2 rather than correct any aspect of an image.

Some tone mapping operators in the literature directly transform HDR values  $L_p$  into LDR pixel values  $V_p$

$$V_p = \tilde{T}(L_p), \quad (17)$$

and disregard the display model. The disadvantage of this approach is that the tone-mapping cannot compensate for the differences between display devices. In the remain-

der of this text we will consider the former formulation of the tone-mapping function from Eq. 16.

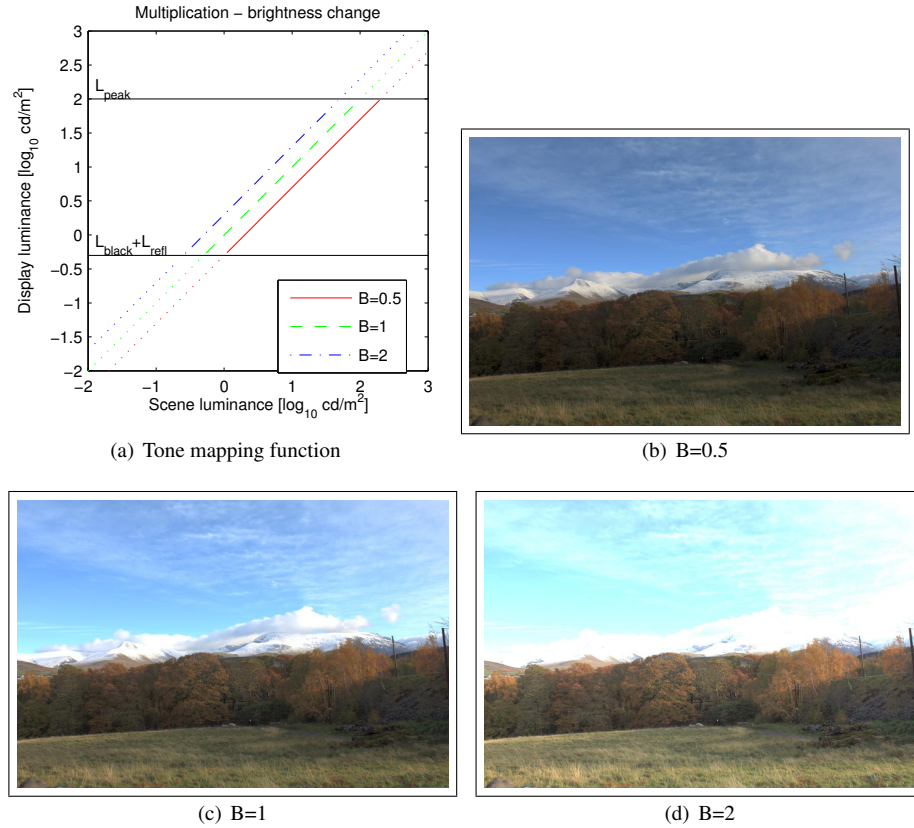


Figure 18: The effect of multiplication on HDR pixel values. The multiplication affects image brightness. The horizontal lines in (a) represent minimum and maximum luminance shown on a display. The luminance values corresponding to the dotted parts of the curves will not be reproduced on a display.

**Multiplication — brightness change** The multiplication performed on luminance values changes image brightness, but it does not affect dynamic range or contrast of an image. Therefore, the tone mapping function

$$T(L_p) = B \cdot L_p, \quad (18)$$

will increase or decrease the overall image brightness by the brightness adjustment parameter  $B$ . The operation is also analogous to exposure change in photographic cameras, so the operation is often called exposure adjustment. An example of this operation is shown in Fig. 18.

In the logarithmic domain (denoted by lower-case symbols) the multiplication becomes addition and the operator becomes

$$t(l_p) = l_p + b, \quad (19)$$

where  $b = \log_{10}(B)$  and  $l_p = \log_{10}(L_p)$ .

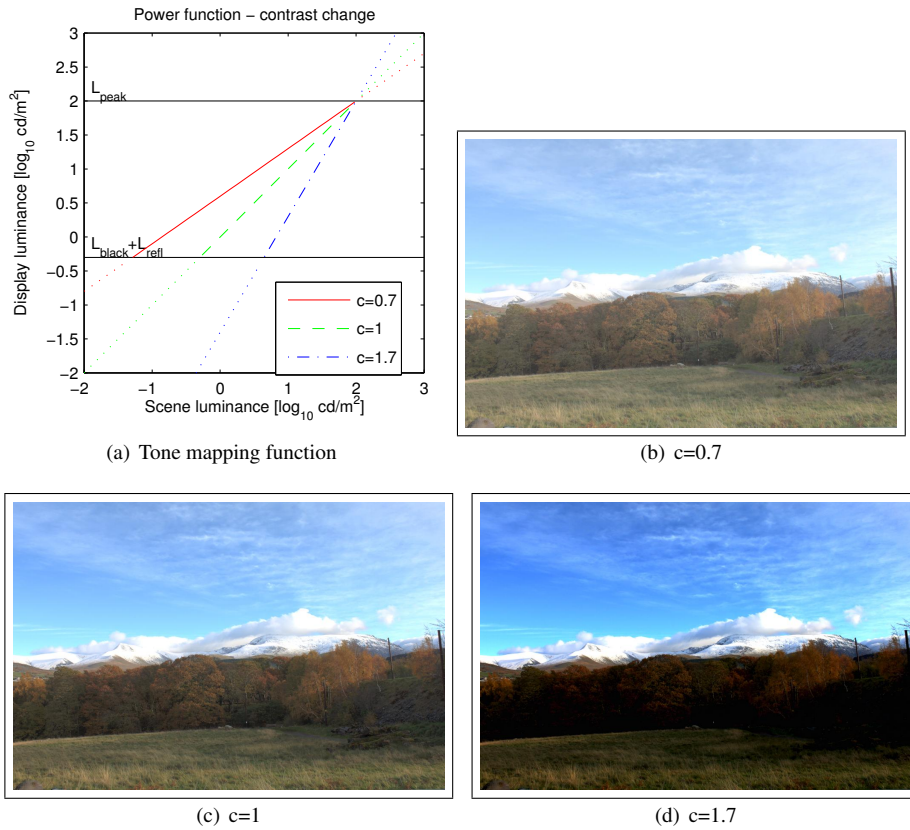


Figure 19: The effect of a power function on HDR pixel values. The operation adjusts image contrast.

**Power function — contrast change** Power function can be used to manipulate the dynamic range of an image. The dynamic range is sometimes used interchangeably with image contrast, as reducing a dynamic range will also reduce an overall image contrast. The contrast adjustment operator is

$$T(L_p) = \left( \frac{L_p}{L_{white}} \right)^c, \quad (20)$$

where  $c$  is the contrast adjustment factor. The change is relative to the luminance of a reference white point  $L_{white}$  so that the contrast will be shrunk or expanded towards or away from that point.  $L_{white}$  is usually assumed to be the scene luminance that is mapped to the peak luminance of a display. An example of this operation is shown in Fig. 19. The operation is sometimes called *gamma correction* in the literature as the formula is similar to the display model with the exponent equal to  $\gamma$ .

In the logarithmic domain the operation becomes multiplication:

$$t(l_p) = c (l_p - l_{white}), \quad (21)$$

where the lower case letters denote logarithmic values.

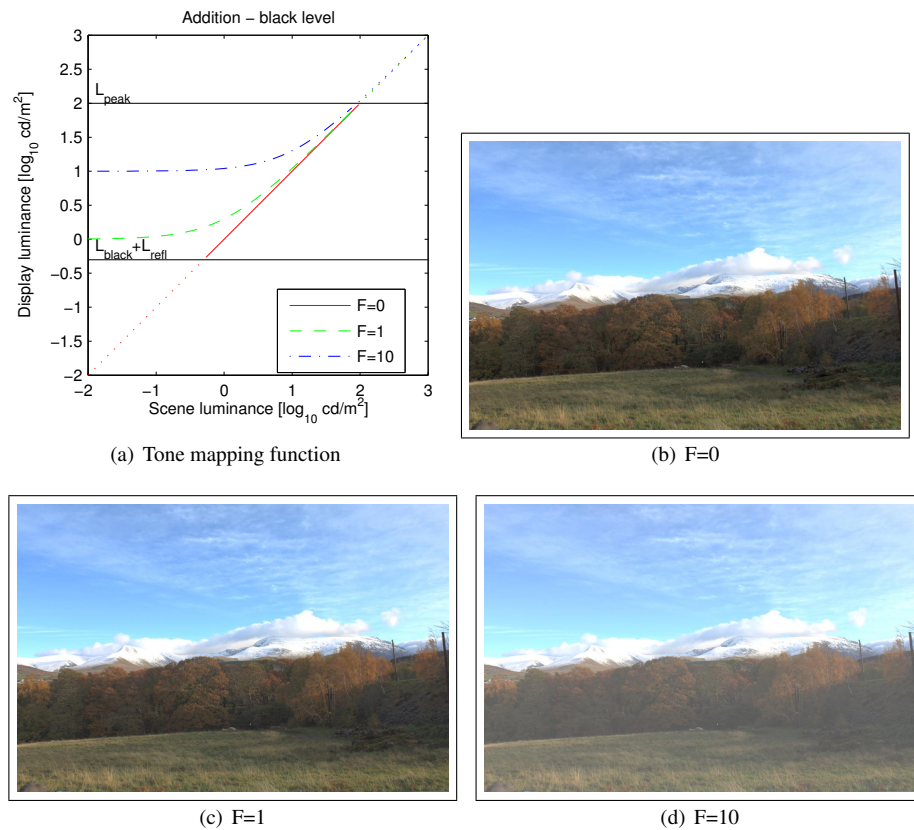


Figure 20: The effect of adding a constant value to the HDR pixel values. The operation elevates black level or introduces fog to an image. It will also affect contrast of the lower tones in an image.

**Addition — black level, flare, fog** As a consequence of the Weber law, adding a constant value to an image, as in the equation

$$T(L_p) = L_p + F, \quad (22)$$

has little impact on the bright image parts, but strongly affects the darker parts of an image. This addition generates an effect of fog or a uniform glare in an image. The operation will affect contrast and brightness of the darker image parts. An example of this operation is shown in Fig. 20. The addition cannot be expressed in the logarithmic domain.

### 5.3 Major approaches to tone mapping

Hundreds of papers on tone mapping have been published in the recent years, giving plenty of alternatives to choose from. Google Scholar lists over 560 papers with “tone-mapping” in the title (as of October 2014). However, many of these operators share very similar assumptions and underlying mechanisms. Instead of reviewing several selected algorithms, we outline the major approaches and give examples of operators which rely on them.

#### 5.3.1 Illumination and reflectance separation

If we consider that the light reaching our eyes is the product of illumination and a surface reflectance, the reflectance is likely to provide more information for the visual system than the illumination. Reflectance delivers information about the shape, texture and color of an object and is mostly invariant to the conditions in which the object is observed. In contrast, illumination can vary greatly depending whether, for example, an object is observed indoors or in the sunlight.

Indeed, there is a strong evidence that several mechanisms in the visual system are meant to discount the effect of illumination, with the chromatic adaptation being a typical example [40,99]. If illumination seems to be less important, it is quite likely that the modifications to the illumination component of an image will be less objectionable than the modifications to reflectance.

Restricting changes to the illumination component is especially attractive for tone-mapping, as the illumination is mostly responsible for the large dynamic range in real-world scenes. The reflectivity of diffuse surfaces varies from about 1% for velvet black to about 90% for high quality white paint. Even if both materials are in the scene, the maximum dynamic range produced by reflectance alone is less than 2 orders of magnitude. However, the dynamic range of the illumination component can easily exceed 4 orders of magnitude in many real-world situations.

For the majority of diffuse objects the pixel values can be regarded as a product of incoming illumination (irradiance) and the surface reflectance:

$$\text{intensity} = \text{reflectance} \times \text{illumination} \quad (23)$$

This is a simplified model, which ignores the geometry and more complex reflectance properties, but is widely used in computer vision and related disciplines. Assuming that

we know how to separate illumination from reflectance, we can create a tone mapping operator that affects only the illumination component without distorting reflectance:

$$\text{intensity}_d = \text{reflectance} \times T(\text{illumination}), \quad (24)$$

where  $\text{intensity}_d$  is the intensity (HDR pixel value) after applying tone mapping function  $T$ . In the simplest case, a tone mapping function can be a plain contrast compression, e.i.

$$T(L_p) = L_p^c, \quad (25)$$

for  $c < 1$ . This approach to the dynamic range compression was originally proposed by Oppenheim et al. [112].

**Low-pass filter decomposition.** The main challenge is finding a way to separate illumination from reflectance. Such problem is heavily under-constrained and finding an accurate solution given an image alone is not possible. However, there exist several approximate methods, which rely on the statistical properties of light in real-world scenes. In contrast to the reflectance, the illumination in a scene usually varies smoothly between pixels. The only sharp discontinuities can be expected at the boundaries of hard shadows and light sources. The easiest way to extract the smoothly changing part of an image is to convolve it with Gaussian filter of a large extent:

$$I_p \approx \sum_{t \in \Omega} f(p-t) L_t \quad (26)$$

where  $I_p$  is the estimate of the illumination component at the pixel location  $p$ ,  $L$  are linear intensity values (or luminance),  $\Omega$  is a local neighborhood of a pixel, and  $f$  is the Gaussian function

$$f(x) = \frac{1}{\sigma_s \sqrt{2\pi}} e^{-\frac{x^2}{2\sigma_s^2}} \quad (27)$$

Although this is only a very rough approximation of the illumination component, it produces satisfactory results in many cases. The tone-mapping based on such separation was proposed by Chiu et al. [24]. They propose a spatially nonuniform mapping function for compressing contrast in HDR images

$$T(L_p) = \frac{L_p}{k I_p}, \quad (28)$$

where  $k$  is a constant that varies from 2 to 8. Note that the constant  $k$  will change the overall image brightness, but not the contrast of the illumination component. More effective contrast compression can be achieved using a power function.

$$T(L_p) = \frac{L_p}{I_p^{1-k}}, \quad (29)$$

where  $k \in (0, 1)$  is the illumination compression factor. The same equation can be expressed in the logarithmic domain using lower case letters to denote logarithmic values

$$t(l_p) = l_p - (1-k) i_p = (l_p - i_p) + k i_p. \quad (30)$$

The Gaussian filter separation is also used in the popular *unsharp masking* algorithm for enhancing image details (refer to Sec. 5.4). Unlike typical tone-mapping that modifies the illumination component, unsharp masking boosts the contrast of the reflectance component of an image, which is equal to  $l - i$ :

$$u(l_p) = c(l_p - i_p) + l_p. \quad (31)$$

Therefore, the simplest case of reflectance-illumination separation TMO can be considered as a generalization of the unsharp masking algorithm for HDR images.

**Bilateral filter decomposition.** The major limitation of the Gaussian filtering as the illumination-separation operator is that it cannot detect sharp illumination changes, which can be found at the boundaries of sharp shadows and light sources. A typical example is a boundary between a sky and a horizon (sky is a source of very strong light). As a result, the illumination component is smoothed out across these boundaries and *halo artifacts* start to appear in an image when strong contrast modification is applied. Fortunately, there is another class of filters that can detect such sharp boundaries and substantially reduce undesirable halos. One example of such edge-preserving operators is the bilateral filter [39, 153], whose smoothing extent is not only limited in the spatial domain, but also in the domain of pixel intensities. The filtered pixel values are computed as

$$I_p \approx \frac{1}{k_s} \sum_{t \in \Omega} f(p-t) g(L_p - L_t) L_t, \quad (32)$$

where  $k_s$  is the normalization term:

$$k_s = \sum_{t \in \Omega} f(p-t) g(L_p - L_t). \quad (33)$$

The function  $g$  is the Gaussian that restricts the range of values in which pixels are averaged. If a pixel  $t$  in the neighborhood of  $p$  has a very different value than  $L_p$ , then the value of the term  $g(L_p - L_t)$  is very low and so is the contribution of the local average. The bilateral filter is one of the most popular methods to separate illumination from reflectance and has found many other applications. Durand and Dorsey [39] provided an insightful analysis of the bilateral filter, proposed a fast implementation of the filter and showed how it can be applied to tone mapping. Their tone mapping function operates on logarithmic luminance values:

$$l_p = \log_{10}(L_p), \quad i_p = \log_{10}(I_p). \quad (34)$$

Then, the contrast of the illumination layer is compressed

$$t(l_p) = c i_p + (l_p - i_p). \quad (35)$$

Although not mentioned in the original publication, the resulting logarithmic values should be presumably converted into the linear domain and an inverse display model needs to be applied (refer to Sec. 2.2).

Since the 2002 publication, several faster algorithms for computing bilateral filter have been proposed [1, 2, 23, 113]. An excellent comparison and analysis of these algorithms can be found in [1].

**Retinex algorithms.** Retinex algorithm was originally proposed by Land and McCann [75] to explain color constancy phenomenon. Retinex was to model the ability of the HVS to extract reliable information from the world we perceive despite changes in illumination. The latter work on the Retinex algorithm formalized the theory mathematically and showed that the problem is equivalent to solving a Poisson equation [58, 60]. The algorithm essentially attempts to separate reflectance from illumination by suppressing small gradients, which are attributed to illumination and in that respect is an effective method of tone-mapping images [103].

**Gradient and contrast based methods.** Instead of separating an image into reflectance and illumination layers, it is possible to enhance the details in an image (reflectance) before compressing image contrast with a gamma function (or linear scaling in the log domain). Such an approach was taken in several operators, which manipulate image gradients or local contrast [43, 45, 94]. The main advantage of performing operations on gradients rather than pixel values is that it allows to radically increase local contrast without introducing objectionable contrast reversals, known as halo artefacts. However, local gradient manipulation [45] may lead to inconsistencies in global image brightness between distant image regions. Therefore, newer operators introduced multi-scale image structures [43, 94] to maintain image contrast at multiple scales.

### 5.3.2 Forward visual model

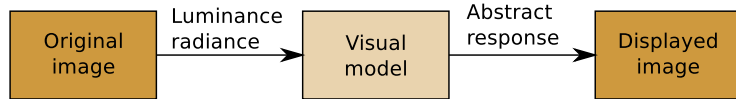


Figure 21: Typical processing pipeline of tone-mapping based on a forward-only visual model. The original image is transformed into abstract representation using a visual model and then sent directly to a display.

Since the neural connection between the retina and visual cortex can transmit only a signal of a limited dynamic range, the visual system needs to employ an effective dynamic range compression in the retina before transmitting the visual information to the brain. Therefore, a possible approach to tone mapping may involve simulating such processing in the visual system in order to reduce the dynamic range of images. By doing so, the physical signal, in terms of luminance or trichromatic color channels, is converted into an abstract internal representation of the visual system, such as response of the photoreceptors [123, 159], lightness [58, 75], or brightness [37, 148]. Then, such a response is mapped to pixel values on a display. These steps are illustrated in Fig. 21.

Although the approach may be effective in reducing the dynamic range, there is clearly one gap in reasoning — the eye expects to see the luminance rather than abstract internal representation on a display. Therefore, such a forward-only approach to tone-mapping can be considered as inspired by a perception, rather than perceptually plausible. It is also difficult to determine the actual intent of such operators, as they do not explicitly attempt to achieve a perceptual match between the original and displayed scene. They can, however, provide pleasing results.

**Photoreceptor models** One particular class of such operators involve modelling the response of a photoreceptor as a sigmoidal S-shaped function [74, 116, 125, 126, 144]. The choice of this function is usually justified by so called Naka-Rushton equation, which explains how the sensitivity of a photoreceptor to flashes of light differs with adapting luminance. It is believed that this function approximates the response of the photoreceptors when adapted to a certain luminance level; when exposed to luminance much exceeding the adaptation luminance, the photoreceptor saturates and cannot differentiate between even larger luminance levels. The challenge of modelling this effect is that the adaptation luminance of the eye is unknown in complex images and tends to vary rapidly from one scene location to another. The ad-hoc approach to the problem usually assumes a certain localized field of adaptation and approximates the adaptation field with a low-pass filtered version of image luminance.

### 5.3.3 Forward and inverse visual models

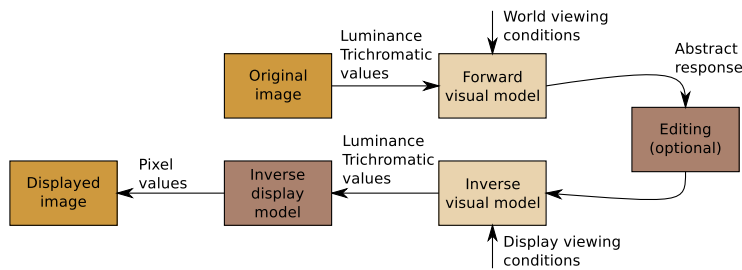


Figure 22: Typical processing pipeline of tone-mapping based on forward and inverse visual models. The original image is transformed into abstract representation using the forward visual model, optionally edited and then transformed back to the physical image domain via an inverse display model.

As discussed in the previous section, forward-only tone-mapping simulates the visual processing that happens when observing the original scenes. They lack, however, the simulation of the visual processing that happens when viewing a tone-mapped image on a display. This gap is addressed by tone-mapping operators, which simulate both forward and inverse visual processing [61, 71, 94, 115, 117, 126, 156, 161]. In such an approach, illustrated in Fig. 22, the original HDR image is first processed by the forward visual model assuming that an observer is adapted to the viewing condition in the original scene. This will usually mean adapting to higher luminance for outdoor scenes and lower luminance for night scenes. Then, the result of the visual model can be optionally edited, for example to reduce the dynamic range or improve the visibility of details [94]. In the next step, the abstract response is converted back to luminance or trichromatic values with an inverse display model while assuming adaptation to a particular display. Finally, the physical luminance or trichromatic values are transformed to pixel values using an inverse display model. This gives “gamma-corrected” RGB values, which can be sent directly to a display.

The approach involving forward-and-inverse visual modelling is physically and

perceptually plausible, unlike the forward-only approach discussed in the previous section. The physical units generated at each step match the input units of the next step. One major advantage of this approach is that it can adjust an image appearance for the difference in viewing conditions between the real-world scene and the display. For example, dark night scenes can be realistically rendered on displays, which are much brighter than the original scene [61, 61, 115, 161]. This is achieved by simulating the night vision (so called scotopic and mesopic vision) in the visual system. Forward-and-inverse visual models can also compensate for color-shift due to chromatic adaptation [25, 126] or simulate a temporal loss of vision due to light or dark adaptation [61, 117].

One of the main shortcomings of forward-and-inverse approach that it makes an assumption that a standard display can reproduce the impression of viewing much brighter or darker scenes. Depending on the visual model employed, the result of the inverse visual model may produce colors that lie outside the color gamut and the dynamic range of the target display. As the result, such operators are often not the most effective at reducing the dynamic range. Another difficulty is that many sophisticated visual models are difficult to invert and cannot be directly used in such forward-and-inverse approach.

The main rendering intent for forward-and-inverse operators is reproducing the appearance or visibility of original scenes, therefore they can be classified as visual system simulators. Such operators are useful in all applications where producing the faithful reproduction of the original scenes is important, such as driving or flight simulators, but also video games. They have been also used to adjust the content for displays, which vary significantly in the luminance range, in which they operate [161].

### 5.3.4 Constrained mapping problem

One of the original goals of the tone mapping problem, as formulated by Tumblin and Rushmeier [156], was to reproduce a scene on a display, so that the brightness sensation of a displayed image is equal or closely matches the real-world brightness sensation. The perfect match between the original and its rendering on a display or in a hard-copy format is almost never possible, as an output medium is hardly ever bright enough, offers insufficient dynamic range (contrast) and color gamut. Therefore, the rendering on an output device is a tradeoff between preserving certain image features at the cost of the others. For example, high contrast and brightness of an image can often be preserved only at the cost of clipping (saturating) certain amount of pixels in bright or in dark regions. The choice of which features are more important should be driven by a particular application, for which an appropriate metric could be designed, possibly involving some aspects of the visual perception. By following these considerations, tone-mapping can be formulated as an optimization problem as illustrated in Fig. 23.

Having an original image as input, which can be in HDR or any scene-referred high quality format, the goal is to generate a display-adapted image that would be the best possible rendering of an original scene. We can assume that this goal is achieved if the response of the HVS for an image shown on the display,  $R_{disp}$ , is as close as possible to the response evoked by the original scene,  $R_{orig}$ . Both responses can almost never be the same as a display can only show limited dynamic range and color gamut. Also the

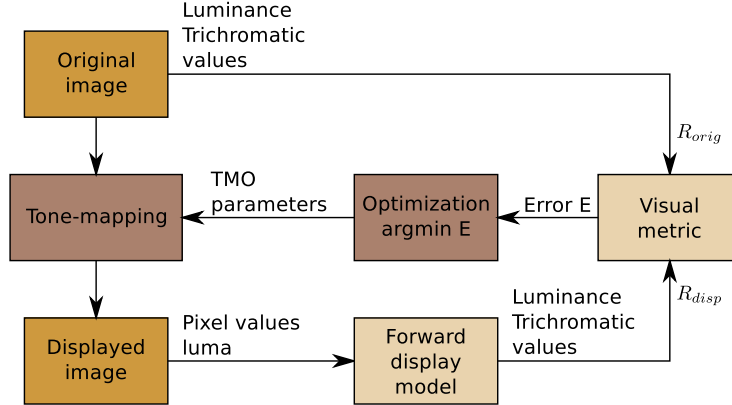


Figure 23: Typical processing pipeline of tone-mapping solving a constrained mapping problem. An image is tone-mapped using a default parameters. Then the displayed image is compared with the original HDR image using a visual metric. The scalar error value from the metric is then used in an iterative optimisation loop to find the best tone-mapping parameters. Note that in practice the solutions are often simplified and formulated as quadratic programming or even have a closed-form solution.

viewing conditions, such as ambient light or luminance adaptation, differ between the original scene and its rendering, making the match even more difficult. The solution of the optimization problem is a set of tone mapping parameters that minimizes the difference between  $R_{orig}$  and  $R_{disp}$ . The display model, shown in Fig. 23, introduces physical constraints on devices' color and luminance reproduction.

The approach shares some similarities with forward and inverse visual models, discussed in the previous section. The difference is that these approaches assume  $R_{disp} = R_{orig}$  and then invert the HVS and display models to compute a tone mapped image. If we follow this approach and compute the desired display luminance that would evoke the same sensation as a real world scene ( $R_{disp} = R_{orig}$ ), we can end up with an image that is too bright or has too much contrast for a given display. In such a situation, if we apply the limitations of a display and clamp luminance values, we get  $R_{disp}$  significantly different from  $R_{orig}$ , which is unlikely the global minimum of our optimization problem. Furthermore, such an optimization problem can be used with arbitrary HVS and display models, while forward-inverse display models require the visual model to be invertible.

The major difficulty with this approach lies in the fact that even simplified models of a display, the HVS and a tone mapping operator lead to a complex non-linear optimization problem, which may exhibit local minima, or be too complex to solve in reasonable time. However, when the problem is skillfully formulated, a solution can be found very efficiently.

Ward et al. [166] proposed a global operator, which preserves the smallest visible contrast, or rather, it ensures that such contrast is not more visible than in the original image. This was achieved by constraining the maximum slope of a tone-curve, which

was computed using the histogram equalisation method. The operator also simulated glare illusion, which is discussed in more detail in Section 5.4.

Mantiuk et al. [88] formulated the visual model in such a way that the constraint mapping problem could be solved using standard optimization techniques, such as quadratic programming. If the visual model is further simplified, it is even possible to find a closed-form solution [83].

This approach mostly addresses the intent of scene reproduction (*SRP*) operators (refer to Sec. 5.1) as it attempts to match appearance given a visual metric, rather than process an image through a visual model. However, the operator of Ward et. al [166] achieves also the goal of the visual system simulator (*VSS*).

#### 5.4 Perceptual effects for the enhancement of tone-mapped images

Existing tone mapping operators are efficient in allocating an available dynamic range to possibly faithfully depict the scene appearance, however, typically deficits in reproduced contrast and brightness still remain apparent. It is unlikely that any further manipulations of physical contrast or luminance relationships can overcome such deficits within a standard tone mapping framework, whose very goal is achieving best possible balance between local details and global contrast reproduction, while at the same time keeping under control the amount of saturated (burned out) pixels. This section reviews two perceptual effects, Cornsweet and glare illusions, which can boost apparent image contrast and brightness without increasing the physical values of contrast or brightness.

**Corn sweet illusion** [70] creates apparent contrast between two patches by introducing a pair of gradient profiles that are gradually darkening and, on the opposite side, lightening towards the common edge (Fig. 24). The lightness levels on both sides of the edge are propagated through some filling-in mechanisms of the HVS, which creates the impression of lightness step. Since away from the edge the luminance levels are the same, effectively apparent contrast impression is created with only modest increase of dynamic range. Traditionally such lightness step is achieved by introducing physical intensity step, which requires dynamic range proportional to the step size. By repeating (cascading) the Cornsweet profiles (Fig. 24-right) even stronger apparent contrast enhancement can be achieved between the most extreme patches, which improves the impression of global contrast in the image, again without using precious and limited dynamic range.

The Cornsweet illusion can be used to enhance perceived contrast by aligning the shading discontinuity in the Cornsweet profile with an existing edge [36], whose contrast magnitude has been excessively compressed, e.g., due to tone mapping. Such procedure has been proposed by Krawczyk et al. [72], where the magnitude of contrast loss in the tone mapped image is measured with respect to its HDR counterpart, and such lost contrast is then restored by locally adaptive Cornsweet profiles (refer to Fig. 25). A multi-resolution procedure is used to measure the contrast loss at a given scale, which decides also upon the spatial extent of introduced Cornsweet profiles. Note that a non-adaptive version of this technique is known as unsharp masking, which is used in photography to sharpen image details, where typically Cornsweet profiles of

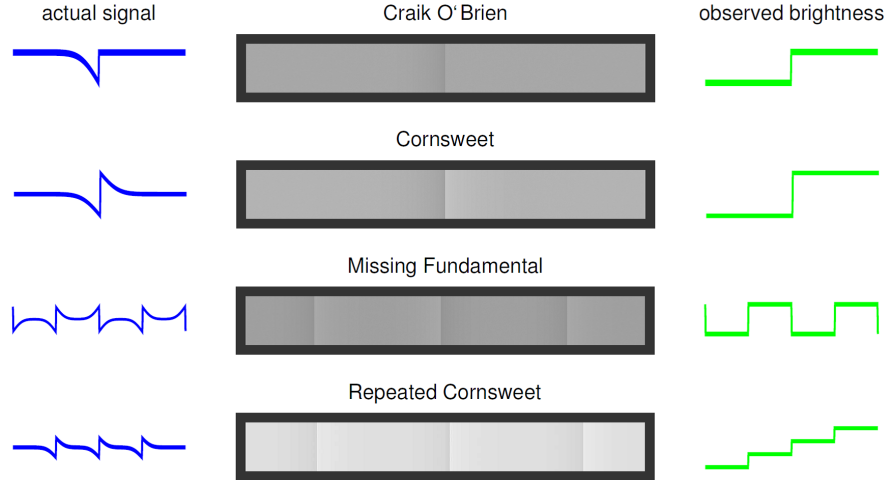


Figure 24: Different luminance profiles, which create the Craik-Cornsweet-O’Brien illusion. (Plots after [70] courtesy of Grzegorz Krawczyk.)

fixed magnitude and spatial extent are employed (refer to Eq. 31). Skillfully inserted Cornsweet profiles affect the image appearance relatively little, as they contribute to a desirable apparent contrast enhancement at the edge, but do not produce additional sharp contrast patterns or ringing, as they gradually vanish. However, when exaggerated such profiles can create undesirable contrast reversals, which are known as the halo artifacts. In Sec. 8.4 a metric that predicts the maximum strength of the enhancement in tone mapping is discussed, while Fig. 40 demonstrates the visual impact of Cornsweet profiles as a function of their spatial extent and magnitude.



Figure 25: Image tone mapped using logarithmic mapping [37] (left), its version with restored global contrast (center), and the corresponding map of Cornsweet profiles (right). The blue profiles darken the image and the red lighten, their intensity corresponds to the profile magnitude. Note that the contrast restoration preserves the particular style of the tone mapping algorithm. (Images courtesy of Grzegorz Krawczyk. Reproduced with permission from [72] © The Eurographics Association 2007.)

Much stronger contrast enhancement has been observed when Cornsweet profiles are consistent with the scene lighting, undergo correct perspective foreshortening, and respect other cues resulting from 3D scene interpretation [121, 131]. This explains the success of employing Cornsweet profiles in the arts [81].

**Glare illusion** Due to imperfections of the eye optics a certain amount of reflected and scattered stray light leads to veiling glare effect in the proximity of bright light sources and highlights (refer to Sec. 6.4 for the discussion of light scattering in the camera lens systems). The resulting contrast loss signals to the HVS the presence of such bright elements in the scene, which is in particular pronounced in the night scenes when scattered light might be dominant in the retina regions around such elements. Since the display cannot natively reproduce this effect due to the brightness deficit, synthetic rendering of plausible veiling glare patterns in the image might be interpreted by the HVS as actually caused by the presence of bright objects, which is called the glare illusion. Zavagano and Caputo [181] show that even the effect of glowing can be obtained by placing smooth gradients around bright objects (Fig. 26). Such gradients have been used by artists to improve the impression of dynamic range in their paintings, and the technique has been used in digital imaging as well.

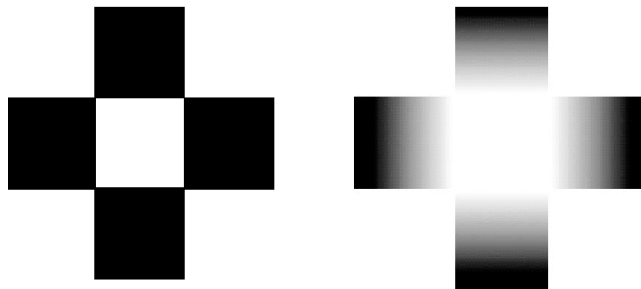


Figure 26: Glare illusion: Painting halo (shading gradients) around objects enhances their brightness and creates an impression of glow without the actual light emission. Redrawn from [181].

In computer games a set of Gaussian filters with different spatial extents are commonly used [67] to introduce smooth gradients as in Fig. 26. Spencer et al. [143] employ a filter based on the point-spread function (PSF), which is measured for the human eye optics [32, 172]. Yoshida et al. [179] shows that by using any of these approaches the apparent image brightness might increase more than 20%. Kakimoto et al. [64], van den Berg et al. [158], and Ritschel et al. [130] investigated the application of wave optics principles to glare rendering. The resulting glare pattern, apart from the familiar veil, features also the ciliary corona (the sharp needles) and lenticular halo as shown in Fig. 27.

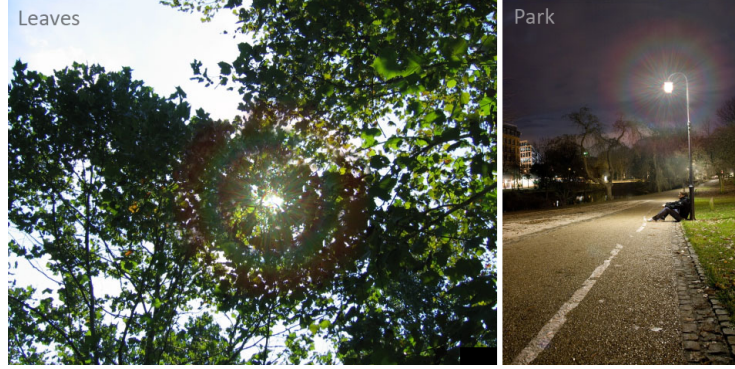


Figure 27: The glare appearance examples due to light scattering in the eye, modelled using the Fresnel diffraction [130]. (Images courtesy of Tobias Ritschel. Reproduced with permission from [130] © The Eurographics Association 2009.)

## 6 Inverse tone mapping

The existing display-referred (Sec. 1.2) image and video formats with 8-bit encoding per color channel do not offer sufficient precision for advanced HDR displays (Sec. 7). For such displays recovering HDR information from legacy LDR images and videos is required. This process is often called inverse tone mapping, although technically speaking the inversion of complete camera response function, which relates the scene luminance values with pixel values encoded in an LDR image, would be desirable. The inverse camera response function should compensate for camera optic imperfections and sensor response non-linearity, as well as image enhancement and tone mapping intentionally performed by camera firmware altogether. Thus, if the inverse camera response function is known, the scene-referred luminance map can be readily reconstructed. The problem of recovering the camera response function based on multiple, differently exposed images of the same mostly static scene is relatively well researched (refer to Sec. 3.3). A challenging question arises how to approximate the response function based on a single image without any knowledge of camera used for capturing, exposition parameters, and the captured scene characteristic? This is a typical situation for legacy images and video.

Since the key component of LDR pixel encoding is gamma-correction like non-linearity (refer to Sec. 2.2), the first step towards the inverting camera response is to compensate for this non-linearity. The resulting pixel values are approximately proportional to the scene luminance values and can be stretched to the dynamic range supported by the HDR display (Sec. 6.1). The problem of banding errors might arise, as perceptually uniform quantization steps in LDR encoding, become highly non-uniform in linearized luminance space with the quantization errors possibly exceeding the visibility thresholds (Sec. 6.2). Another important problem is restoring (inpainting) image details in highlights, light sources, and deep shadows, which are typically clipped in LDR images, but can be readily visible on HDR displays (Sec. 6.3). In some cases

image artifacts such as glare, which arise due to imperfections of camera lens or light streaks around light sources introduced by specialized lens-mounted filters can be used to recover useful HDR information (Sec. 6.4).

In this section we focus mostly on restoring luminance component and we do not cover another important problem of extending color gamut, e.g., extending chromaticity values toward higher saturation, without changing the hue as required for projectors and displays with color primaries based on lasers and LEDs. Such problems are partially discussed in the literature on gamut mapping [107].

## 6.1 Recovering dynamic range

In many practical applications high quality LDR images are available with a small amount of under- and over-exposed pixels and without visible compression and quantization artifacts. For such images the LDR-to-HDR conversion typically relies on:

1. Deriving an inverse gamma correction/tone-mapping function, or whenever possible inverse camera response;
2. Transforming all LDR image pixels using such inverse function to obtain linearized pixel values that are approximately proportional to the luminance in the original scene;
3. Stretching the resulting pixel values to the full dynamic range capabilities of the display device (effectively expanding contrast), subject to the visibility of quantization and compression artifacts, as well as the overall user preference.

A number of solutions presented in the literature adopted such a procedure [6, 11, 35, 95, 104, 129], and they differ mostly in the precision of the inverse function derivation and the actual contrast expansion approach.

### 6.1.1 LDR pixel linearization

**Inverse gamma correction** Instead of using the full-fledged inverse camera response, Rempel et al. [129] and Masia et al. [95] observe that a simple inverse gamma correction with a fixed standard  $\gamma = 2.2$  leads to good artifact-free pixel value linearization. Farid [44] proposes a more principled approach in which the gamma value can be blindly estimated in the absence of any camera calibration information based on the single image (the so-called blind inverse gamma correction). Their methods is based on the observation that gamma correction introduces to the image several new harmonics whose frequencies are correlated to the original harmonics in the image. There is also a strong dependence between the amplitudes of the original and newly created harmonics. It can be shown that such higher order correlations in the frequency domain monotonically increase with increasing non-linearity of gamma correction. Tools from the polyspectral analysis can be used to detect such correlations, and by searching for the inverse gamma, which minimizes such correlations, the actual gamma correction originally applied to the image can be found.

**Inverse tone mapping curve** Banterle et al. [11] investigate non-linear contrast scaling by inverting simple tone mapping operators based on exponential and sigmoid functions. Visually the most compelling results have been obtained by inverting the photographic tone mapping operator [127], but the magnitude of dynamic range expansion is limited due to banding artifacts in particular in bright image regions, in which the sigmoid function strongly compresses contrast.

**Inverse camera response** In practice, the gamma function is only a crude approximation of the camera response, which may affect the accuracy of reconstructed luminance map. Lin et al. [80] show that for a single LDR image the camera response curve can be more precisely reconstructed based on the distribution of color pixels in the proximity of object edges. The most reliable information for such reconstruction is provided by edges separating the scene regions of uniformly distributed and significantly different color (luminance values)  $R_1$  and  $R_2$  (refer to Fig. 28a). For a digitized image of the scene using a camera featuring the linear response, the color  $I_p$  of pixel representing precisely the edge location should be then a linear combination  $I_1$  and  $I_2$  (refer to Fig. 28b). The partial coverage of pixel area by each of the two regions decides about the contribution of  $I_1$  and  $I_2$  values into the pixel color  $I_p$ . However, due to the non-linearity in the camera response the actual measured color  $M_p$  may be significantly different from such a linear combination of measured colors  $M_1$  and  $M_2$  (refer to Fig. 28c), which correspond to  $I_1$  and  $I_2$ . By identifying a number of such  $\langle M_1, M_2, M_p \rangle$  triples and based on the prior knowledge of typical real-world camera responses a Bayesian framework can be used to estimate the camera response function. By applying inverse of this function to each triple  $\langle M_1, M_2, M_p \rangle$ , the corresponding  $\langle I_1, I_2, I_p \rangle$  should be obtained such that  $I_p$  should be a linear combination of  $I_1$  and  $I_2$ . Applying such inverse response function to all image pixels results in reconstruction of the scene luminance map. The authors observe that their method leads to a good accuracy in reconstruction the luminance map. The best accuracy is achieved when the selected edge color  $\langle M_1, M_2, M_p \rangle$  triples cover a broader range of brightness values for each color channel. The method may not be very accurate for images that exhibit a limited range of colors. By using  $\langle M_1, M_2, M_p \rangle$  triples from additional images captured with the same camera, the accuracy of the camera response reconstruction can be further improved.

### 6.1.2 Dynamic range expansion

**Linear contrast stretch** Akyüz et al. [6] and Rempel et al. [129] perform linear stretching of pixel values to the dynamic range of HDR display. Rempel et al. [129] found that the contrast boost to the range 5,000:1 leads a good trade-off between the quality of HDR images and the visibility of artifacts. Interestingly, Akyüz et al. [6] skip completely the LDR pixel linearization step, which works well for considered by them high quality photographs. The inverse gamma correction needs to be applied for the broadcasting quality of LDR video signal, which is expanded to HDR video in [129].

**Locally-varying brightness boost** As found in [11, 136, 180] to achieve good appearance of HDR images, both contrast and brightness of saturated regions should

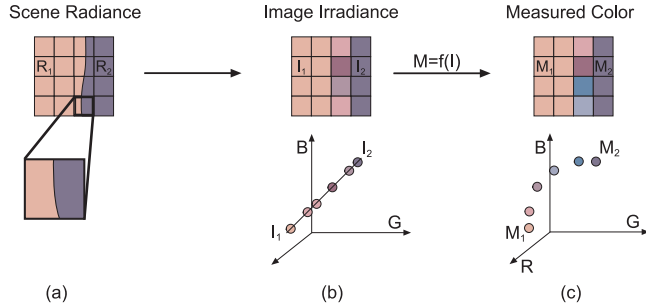


Figure 28: Color distortions in edge regions due to non-linearity in the camera response. (a) Two regions in the scene, which are separated by an object edge, feature distinct spectral luminance  $R_1$  and  $R_2$  values. (b) Hypothetical linear image sensor maps  $R_1$  and  $R_2$  values into  $I_1$  and  $I_2$  values in the RGB color space. Due to the scene radiance digitization by the sensor, the color of each pixel on the edge is a linear combination of  $I_1$  and  $I_2$  with weights proportional to the covered area on the left and right sides of the edge. (c) A non-linear camera response  $f$  warps these colors resulting in their non-linear distribution. Redrawn from [80].

be simultaneously increased. For this reason, Rempel et al. additionally boost the brightness of image regions around pixels with saturation in at least one color channel. The brightness-boosting region is determined by blurring such saturated pixels with a large-kernel Gaussian filter. The cut-off frequency of this low-pass filter (0.5 cycle-per-degree) corresponds to relatively low contrast sensitivity in the human vision, which drops even stronger for lower spatial frequencies, so that the visibility of potential artifacts resulting from such brightness boosting is suppressed. The spatial impact of brightness boosting is limited by an edge-stopping function, that uses strong contrast edges as boundaries.

While the discussed strategies of dynamic range expansion work well for high quality images, Masia et al. [95] observes that this not the case for excessively exposed images. For such images a better effect can be obtained by promoting more details in darker, non-saturated image regions, which is achieved through a gamma contrast expansion. The value of  $\gamma$  increases with the overall LDR image brightness, which is estimated based on a content-dependent statistic that relates the logarithmic pixel intensity average to overall dynamic range in the image as proposed in [124].

**Semantically-driven brightness boost** Other approaches diversify the contrast boost based on semantic differences between scene elements. Meylan et al. [104] employs different linear scaling factors for segmented diffuse scene regions and highlights. In a psychophysical experiment Meylan et al. observe that for outdoor scenes the subjects preferred to allocate a rather small part of the dynamic range to specular highlights to achieve overall brighter image appearance. Conversely, for indoor scenes more preferred results are obtained when more dynamic range is allocated for highlights.

Didyk et al. [35] detect and actively track highlights and light sources in video in

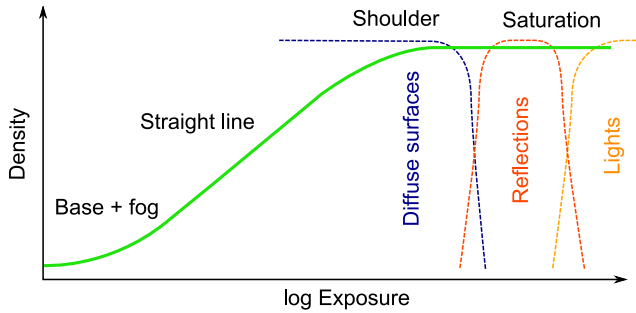


Figure 29: Classification of saturated features into diffuse surfaces, reflections and lights. As the film response curve (green) saturates, the distinction between the three types of features and their brightness disappears. In order to boost brightness of such saturated features, they need to be classified into these three categories, possibly requiring some manual interaction. (Image courtesy of Piotr Didyk. Reproduced with permission from [35] © The Eurographics Association 2008.)

order to boost their brightness and contrast. Highlights and light sources are classified based on a number of predefined features such as luma statistics in the image, the region's similarity to a disk, and its major axis ratio. The classifier is trained in an on-line manner as a human operator marks saturated regions as diffuse surfaces, reflections and light sources (refer to Fig. 29). The saturated features that were manually marked or classified as reflections or lights are then enhanced. This is achieved by computing a tone-curve per each enhanced feature, so that it is steep for pixel intensities corresponding to large gradients. This is because large gradients are unlikely to represent noise, the human visual system is less sensitive to changes of large contrast values (contrast masking) and finally, because large gradients often represent object boundaries, where contrast change is the least objectionable. The tone-curve computation is similar to histogram equalization in [166] but derived for partial derivatives of neighboring pixel intensities.

Fig. 30 shows a comparison of local brightness boost methods when applied to the reference light source and specular highlight with clipped pixel intensities (the left column). Fitting smooth functions or *inpainting* [151] results in flattened profiles, which do not give much brightness boost to the clipped regions. Maintaining temporal coherence is also problematic for these methods. The extrapolation techniques, such as *2D Taylor* series expansion, are not robust because the surrounding pixels used to estimate partial derivatives are often affected by the scene content that is not the part of a clipped region. The resulting reconstruction contains structures in the center of the clipped region, which do not match the appearance of the actual light source or specular highlight. The method of Rempel et al. [129] is strongly affected by the size of clipped region, making larger objects brighter than smaller objects. Linear contrast stretching by Meylan et al. [104] is fast and straightforward but it reveals contouring artifacts and strong noise near the saturation point. The method of Didyk et al. [35]

leads to fewest artifacts as only large gradients are stretched while small gradients are left intact or only moderately enhanced.

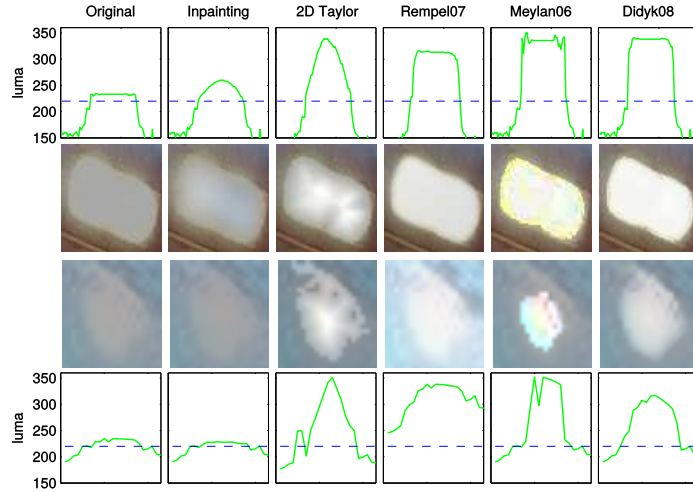


Figure 30: A comparison of local brightness boost methods for a light source (two upper rows) and a specular highlight (two bottom rows). The plots show the luminance distribution across the central scanline of each image. (Image courtesy of Piotr Didyk. Reproduced with permission from [35] © The Eurographics Association 2008.)

## 6.2 Suppression of contouring and quantization errors

Limited bit-depth representation in LDR images and resulting quantization of pixel values inherently leads to the loss of low-contrast details. Limited pixel precision leads also to false contouring (banding artifacts) in smooth gradient regions, which for chromatic channels is often called posterization. All these effects can be strongly aggravated through the dynamic range expansion in the LDR-to-HDR conversion. This is also the case for the sensor noise visibility. For this reason in many LDR-to-HDR techniques various forms of advanced filtering are performed before the contrast and brightness boosting steps.

Bilateral filtering is a natural choice here [35, 95, 129], because it can be specifically tuned to the low amplitude and high spatial frequencies in sensor noise and contouring artifacts [27]. Coring techniques are essentially based on the same principle, but offer more control over high frequency details filtering through multiband image representation [22]. Filtering is applied only to a couple of high frequency bands and its strength is smoothly decreasing towards lower frequency bands. In bilateral filtering and coring methods image details of low amplitude and high frequency may be lost, which may affect the visual image quality. For example, excessive smoothing of the human skin texture may lead to its unnatural plastic appearance, which is highly undesirable effect for any commercial broadcasting and display system.

When the higher precision HDR image is available at certain processing stages, the information loss can be reduced by amplifying (pre-distorting) low amplitudes and high frequencies prior to the dynamic range compression stage (gamma compression, tone mapping), so that they survive the quantization step to the 8-bit LDR image. Such an approach has been proposed in the compander algorithm [79], which can serve as a tone mapping operator that reduces the information loss in the subsequent LDR-to-HDR conversion. However, this can be achieved at the expense of possibly undesirable changes in the appearance of LDR image.

### 6.3 Recovering under- and over-saturated textures

Another problem with legacy images are image under- and over-exposed regions, where texture patterns are mostly saturated and at best contain only sparse information on the scene. Since many scene configurations may lead to the same appearance of an LDR image in such regions, the problem is difficult even for powerful machine learning techniques that should rely on feature vector correspondence between LDR and HDR image pairs. The most promising results have been obtained so far using inpainting and texture synthesis techniques, which are specialized in repairing damaged images or removing unwanted objects. Typically the user interaction is required for the optimal results.

Wang et al. [163] restore image details in clipped regions by transferring textures from well exposed regions. This is a more difficult problem than standard texture synthesis due to diversity of lighting conditions. Since the precise reconstruction of clipped texture is typically not possible, the main goal is to restore a plausible look of resulting HDR image, and for this reason, the authors call their approach “HDR hallucination”. To simplify the problem, illumination and texture reconstruction are considered independently, which is achieved by employing bilateral filtering, similar as in tone mapping solutions discussed in Sec. 5.3.1. Then the smooth illumination component is reconstructed via interpolation from a linear combination of elliptical Gaussian kernels, which are fitted to non-saturated pixels around the over-exposed region. If needed, the fitted illumination function can be further manually adjusted. The high-frequency texture component is reconstructed via constrained texture synthesis [38] based on the source texture and destination location, which are manually indicated by the user. To correct for perspective shortening or properly align texture structure the user draws a pair of strokes in the source texture and destination image regions, and then the source texture is automatically warped to the required size and orientation. Finally, Poisson editing is performed [118] to smooth out transitions between the synthesized textures and the original image. Note that when appropriate textures are missing in the source LDR image, other images can be considered for such texture transfer.

### 6.4 Exploiting image capturing artifacts for upgrading dynamic range

Scattering of light inside the lens can be quite apparent, which defines a limit to the dynamic range that can be acquired with a camera [98]. Such scattering can be modeled with point spread functions (PSF) and removed using deconvolution [146]. However,

precise estimation of the PSF is not trivial especially that its shape is non-uniform across the image. Deconvolution may also lead to high quantization noise in strongly veiled image regions, due to insufficient precision of real scene information. Recently, Talvala et al. [150] have demonstrated that by placing a structured occlusion mask between the scene and the camera, direct and indirect (scattered) light falling on the camera sensor can be separated. For a given position of the mask, the sensor elements, which are occluded by the mask, are illuminated only by scattered light. By jittering the mask position and capturing HDR images for each such position the amount of scattered light can be estimated for each pixel and then removed from the final HDR image. A practical problem with this technique is that the scene must be static, and the mask must be placed near the scene in order to be in camera focus, so that its contribution to the intensity of non-occluded by the mask pixels is reduced. Those problems can be avoided by placing a high frequency mask near the camera sensor to act as a sieve that separates spurious rays in ray-space, which through statistical analysis can be classified as outliers in the angular dimension and removed [122]. This way light scattered in the lens can be significantly reduced, but at the expense of blocking direct light falling on the sensor and reducing its effective resolution.

On the other hand, scattered light in the camera optics may provide some insight concerning bright image regions, which are saturated in the LDR image. The lost information can be partially hidden in the intensity of neighboring non-saturated pixels, which can be strongly polluted by scattered light. Standard image restoration techniques such as blind deconvolution methods that do not rely on the knowledge of the PSF of the camera, may help to predict the amount of energy missing due to the saturation. A practical problem here is quick fall-off of the PSF, which causes that only few nearest pixels with respect to the saturated region may contain easy to discern amount of scattered energy. This means that for saturated regions of wider spatial extents it is difficult to recover any meaningful information concerning the energy distribution in their central parts.

The spatial extent of PSF in the camera lens can be artificially extended using a cross-screen, or star filters that are mounted atop of the lens [134]. This way details of bright image regions such as highlights and light sources are encoded into elongated glare streaks, which are spatially extended across the whole image and optically added to non-saturated image regions. The glare streaks can be separated from the rest of LDR image, and then used to infer the intensity distribution in the saturated image regions. In contrast to the “hallucination” approach [163], the reconstructed this way information is a close approximation of original values.

An additional source of information on bright saturated regions can be found in the image due to the diffraction effect on the aperture boundary, which may also contain higher frequency information. The diffraction pattern becomes more pronounced for smaller camera apertures, and can be meaningfully captured only for cameras of high resolution. Also, chromatic aberration provides additional information on the captured scene, but it is usually well corrected for higher quality lenses and can be easily lost due to on-camera image processing including the JPEG compression.

## 7 HDR display technology

Existing display devices (refer to a recent textbook [55] on this topic) introduce a number of physical constraints, which make real world appearance difficult to realistically reproduce. For example, the continuous nature of spatial and temporal information does not directly fit to the discrete notions of pixels and frames per second. The human visual system (HVS) has its own limitations, which to certain extent reduce the requirements imposed on display devices. For example, the limited density of photoreceptors in the retina as well as imperfections in the eye optics limit the spatial resolution of details that can be perceived to 60–70 cycles per visual degree [162, Fig. 7.21]. In the temporal domain the critical flickering frequency (CFF) limits the ability to discern temporal signals over 60Hz [162, Fig. 7.23]. All such HVS-imposed limitations are taken into account, when designing display devices (e.g., high refresh rate and retinal displays address the problem of flickering and resolution), but still a significant deficit of reproducible contrast and brightness can be observed, which fall short with respect to the HVS capabilities (refer to Sec. 2.1).

Recently, the so-called HDR display devices have been developed whose specification approaches limits imposed by the HVS in terms of reproduced contrast and brightness levels. Two basic approaches can be considered: (1) a direct precise modulation of each pixel over a very wide luminance range and (2) the serial combination of two or more modulators to achieve the same effect.

The first approach is technologically more challenging as 12-16 bit depth precision (refer to Figs. 12–14 in Sec. 4.1) is needed to control each pixel, where zero luminance and a high luminance value (ideally 3,000-6,000 cd/m<sup>2</sup> [136]) should be readily available without causing significant light leaks between neighboring pixels. The Scanning Laser Display Technology developed by JENOPTIK GmbH [33] fulfills these requirements as it directly reproduces bright and dark pixels through modulating the amplitude of RGB laser beams. The flying spot of the laser beam, which is deflected in the horizontal and vertical directions, results in the smooth transition between neighboring pixels without visible pixel boundaries. The full on/full off contrast ratio is higher than 100 000:1, mostly due to the absence of light in black pixels. Another advantage of laser projection technology is expanded color gamut due to more saturated primaries determined by the wavelengths of lasers. With extended contrast offered by the projector this leads to more saturated and vivid colors. Such devices, however, are very rare as extremely expensive high power laser diodes are required [57, Ch. 14.2]. Organic light emitting diodes (OLED) are promising in HDR display applications as well. The zero luminance value can be trivially achieved by switching-off each diode, however, the maximum luminance level is still a limiting factor, and no OLED display with a driver capable of 12–16 bit depth has been presented so far.

The second approach is much more feasible, in particular when only two modulators are considered. Such dual modulation already leads to high quality HDR image display, and it relies on optical multiplication of two independently modulated representations of the same image. Effectively, the resulting image contrast is a product of contrast achieved for each component image, while only standard 8-bit drivers are used to control pixel values in each modulator. The so-called backlight device, directly serves as the first modulator, by actively emitting spatially controllable amount

of light as in the case of a grid of light emitting diodes (LEDs). The backlight device illuminates the second modulator, which is a passive transmissive LCD panel (liquid crystal display) that controls the amount of per-pixel transmitted light. Alternatively a projector can be used as the backlight device, in which case a strong light source is required as the transmitted light is then modulated by two passive layers. Different light modulation technologies could be employed in such projectors such as the transmissive LCDs, the reflective LCDs (known as liquid crystal on silicone - LCoS), and the digital micro-mirror devices (DMD) developed by Texas Instruments (known as digital light processing - DLP). For any projector-based backlight device low luminance levels are achieved through attenuating (LCD, LCoS), or redirecting and discarding light (DMD), which in both cases is highly inefficient in terms of energy. Low luminance values are achieved due to the multiplicative effect, although each modulator separately still might enable to pass some light, e.g., typically at least 1% for LCDs. Close to zero luminance is naturally achieved in case of LED-based backlight device, subject of parasite light from neighboring LEDs that are not switched off.

In the following section we discuss basic principles behind the dual modulation technology, including signal processing that is required to drive each modulation layer (Sec 7.1). Such dual modulation principles are common both for HDR displays (Sec 7.2) and HDR projectors (Sec 7.3), which we discuss next. Finally, we overview more universal light-field display architectures, which typically trade spatial pixel resolution for angular effects, but often offer an HDR display mode with even more than two modulation layers (Sec 7.4).

## 7.1 Dual modulation

In the basic design of a dual-modulation display [135], the input HDR image is decomposed into low-resolution backlight image and high-resolution compensation image as shown in Fig. 31. The requirement of precise alignment of pixels between the two images can be relaxed due the lack of high spatial frequencies in the blurred backlight image. Therefore, as the result of optical multiplication between backlight and compensation images, the achieved global contrast (low spatial frequency) is a product of contrasts in both images, while the local pixel-to-pixel contrast (high spatial frequency) arises only from the compensation image. While this is not a problem for low contrast image patterns, which are successfully reproduced even on traditional single-modulator LDR displays, local pixel-to-pixel contrast reproduction in the proximity of high-contrast edges may not be precise. Fortunately, the veiling glare effect (refer to Sec. 5.4) caused by imperfections of the human eye optics leads to polluting retinal photoreceptors, which represent dark image regions with parasite light coming from bright regions. Thus, the veiling glare reduces the HVS ability to see sharply such local patterns of high contrast, which effectively means that the quality requirements to their reproduction on the display can be relaxed. More recent designs of the backlight device, which are based on modern DLP projectors [46, 132], attempt to project possibly sharp image onto the back side of the front LCD panel, and this way are capable of producing spatial frequencies up to 12 cycles-per-degree (cpd) at luminance contrasts up to 40,000:1. Obviously, even for blurred backlight images high contrast between more distant image regions is faithfully reproduced.

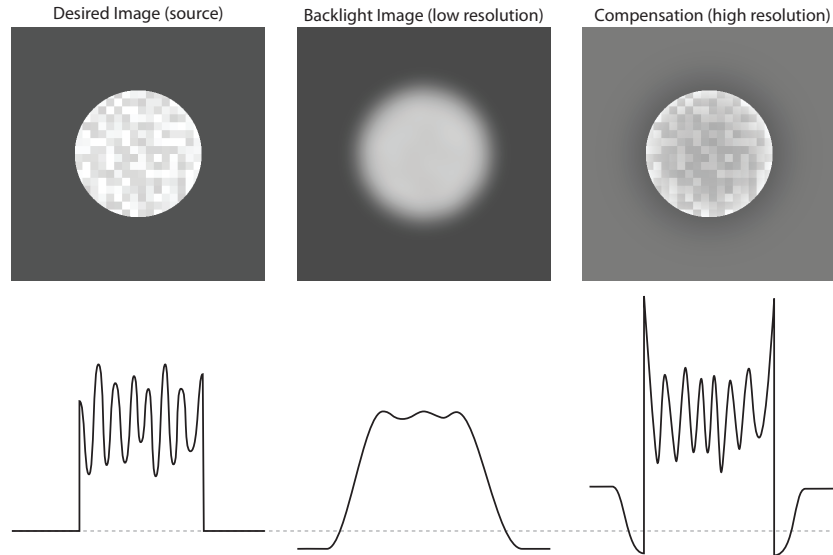


Figure 31: Decomposition of the input HDR image (left) into the downsized backlight image (center), and the compensation image (right). In the bottom row a hypothetical pixel intensity signal along the central scanline is sketched. Note the sharpening effect at the circular patch boundary in the compensation image that counterbalances the loss of high spatial frequencies due to blur in the backlight image.

The backlight and compensation images require special image processing so that their multiplication results in the reconstruction of the original HDR image. The goal of such image processing is to account for different image resolutions and the optical blur in the backlight image. For this purpose, the point-spread function (PSF) characterizing this blur should be modeled for all pixels of the backlight image. The overall flow of image processing in the dual-modulation display architecture is shown in Fig. 32. At first the square-root function is used to compress the luminance contrast in the input HDR image and then the resulting luminance image is downsampled to obtain the low-resolution backlight image (e.g., adjusted to the resolution of LEDs). In the following step, the PSF is modeled for every pixel of the backlight image, which is equivalent to the light field simulation (LFS) that effectively illuminates the high-resolution modulator. By dividing the input HDR image by the LFS the high-resolution compensation image is computed. Since the compensation image is 8-bit encoded, some of its regions may be saturated, which results in undesirable detail loss. Such saturation errors are analyzed and a close-loop control system is used to locally increase the intensity of corresponding pixels in the backlight image to prevent saturation. Fig. 31 shows an example of backlight and compensation images resulting from such image processing.

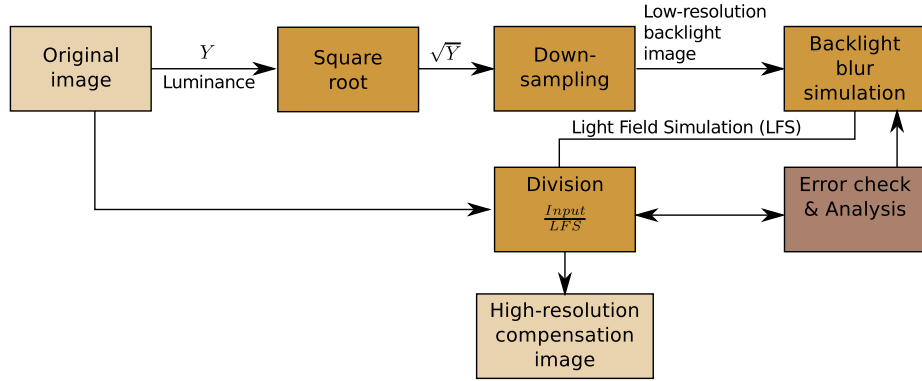


Figure 32: Image processing flow required to drive the low-resolution backlight modulator and the high-resolution front LCD panel in HDR displays [135].

## 7.2 HDR displays

In HDR displays backlight devices are based both on passive and active light modulation principles. Both display design alternatives have been for the first time explored by Seetzen and his collaborators [135, 137].

The first approach as shown Fig. 33a employed a DLP projector producing a modulated backlight that passes through a Fresnel lens, which collimates it, before finally falling on the LCD panel. The diffuser placed in front of the Fresnel lens inhibits the formation of moiré patterns. This design achieves a contrast of 54,000:1 and a peak luminance of 2,700 cd/m<sup>2</sup>. Fig. 33b shows an upgraded version of this design with a modern projector [132], which fivefold improves contrast, and allows for significant blur reduction by focusing the projected image on the back of the LCD panel. This enables reproducing high luminance contrasts across a broad range of spatial frequencies, which is important for depiction of complex luminaires and highly specular materials. Having this particular motivation in mind Ferwerda and Luka [46] used a tiled array of geometrically and colorimetrically corrected inexpensive DLP projectors to match the high resolution of the front LCD panel (2,560 × 1,600). In the limit, the projectors can be eliminated by directly stacking two identical and carefully aligned LCD panels of high resolution [53]. This design leads to sharp images with a remarkable 50,000:1 contrast and a peak luminance of 500 cd/m<sup>2</sup>, and most importantly the need for any image processing stage (Sec. 7.1) is eliminated, as the same image can be used to drive both panels. Guarneri et al. targeted their display for medical applications and only grey-scale images have been considered (color filters have been removed in both LCD panels), so it is not clear whether the alignment precision is sufficient for registering RGB components as well.

In the second pioneering design by Seetzen et al. [135], a hexagonal close-packing matrix of 1,200 independently modulated light emitting diodes (IMLED) is used to produce the backlight for the full HD 1,920 × 1,080 LCD panel. This design features remarkable 200,000:1 global contrast, while the measured ANSI contrast for the

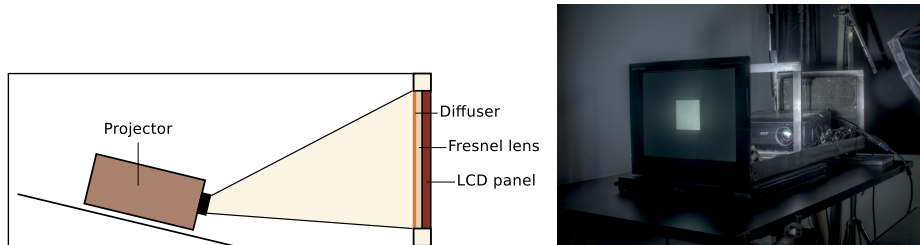


Figure 33: Left: A schematic diagram of a projector-based HDR display — side view. Right: a tone-mapped HDR photograph of the display.

black and white checkerboard pattern reaches 25,000:1 with the peak luminance of 3,000 cd/m<sup>2</sup>. While in the original design white LEDs have been used, later extensions have shown a significant color gamut expansion for integrated RGB LED packages. Interestingly, such IMLED-based backlight device is 3–5 times more power efficient than uniform light employed in conventional LCD displays of similar brightness [57, Ch. 14.2]. Apart from obvious contrast and black level improvements, the power efficiency is one of key factors in promoting the use of IMLED technology in commercial LCD TV sets.

### 7.3 HDR projectors

Modern projectors are based on light modulators such as DMD chips, LCoS or LCD panels, which can produce the contrast ratio between 2,000:1 and 5,000:1 [55, Ch. 8.6.3]. Additional boost of contrast ratio to about 15,000:1 can be achieved through the so-called auto-iris technique, in which the power of light source in the projector is dynamically adjusted based on the overall brightness of image content. Such enhanced contrast ratio can be achieved only between frames, and for a given frame the light modulator technology still remains the limiting factor.

Multi-projector systems with overlapped images from multiple projectors can increase the peak intensity level by summing contributions from all projectors, but also the black level is increased in the same way, which effectively means that the contrast ratio does not improve [30]. The overall perceived image quality still improves on such systems through increased brightness and spatial resolution, which requires careful registration of overlapping images and their colorimetric calibration [85].

Full-fledged HDR effect can be achieved by adding to existing projectors additional light modulators, so that the desired multiplicative effect with the projector native light modulator is achieved. Damberg et al. [29] investigated several variants of such HDR projectors. For example, a standard projection system with three transmissive LCD panels, which modulate chrominance in RGB channels, can be extended to the dual modulation principle by inserting additional passive low-resolution LCD modulators Fig. 34. This way the light emitted by the bulb is spatially modulated before reaching the high-resolution chrominance modulators. Such design enables very faithful color reproduction and does not require any additional optics as the amount of blur

can be directly controlled by changing the distances between each pair of low- and high-resolution LCD panels. Damberg et al. reported that in their projection system they achieved 2,695:1 contrast, which is only by 5% lower than the theoretical product of contrast reproduced by the low (18:1) and high (155:1) resolution modulators. The basic HDR projector architecture as proposed in [29] can be also used for other projection technologies such as LCoS and DLP. Other variants of the basic architecture can be considered by changing the order of low- and high-resolution panels, or using just a single low-resolution luminance modulator, which is placed between the X-Prism and the lens system, i.e., after the recombination of light modulated by the three high-resolution RGB channels.

HDR image depiction can also be achieved using a standard projector that directly illuminates a reflective print. This requires that the original HDR image is decomposed into the projected and printed components, and then by optically aligning both images the multiplicative effect is achieved, which leads to significant dynamic range extension [16]. Zhang and Ferwerda [182] experimented with a similar setup and employed image color appearance models [42] such as iCAM06 [74] to achieve best possible colorimetric reproduction of the original HDR image. They report a remarkable peak luminance of 2,000 cd/m<sup>2</sup> and a dynamic range of 20,000:1. The main limitation of this design is the fact that it can only show static images, unless a controllable reflective surface display, such as the electronic paper is used instead of a print.

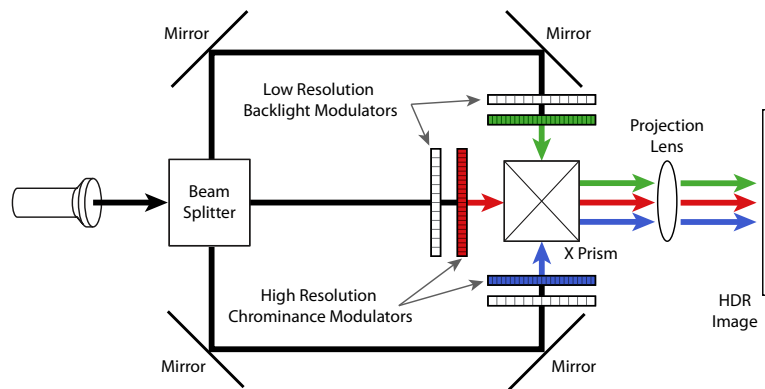


Figure 34: A design variant of HDR projector with three LCD panels for RGB color channels supplemented with three additional low-resolution backlight modulators.

## 7.4 Light field displays in HDR applications

Modern light field displays rely on the co-design of display optics as well as computational processing [96], and here we focus on the design variant that involves a number of light attenuating layers such as stacked LCD panels. In such configuration, each pixel might contribute to multiple directional light paths, so that compressive effect is obtained as the number of pixels in the attenuating layers is significantly smaller

than the number of such paths. By applying tomographic light field decompositions to such a stack of light attenuating layers, apparent image resolution enhancement can be achieved, but as an alternative goal per-pixel attenuation across all layers can be guided towards HDR contrast reproduction [77, 173]. This requires an extension of dual modulation (refer to Sec. 7.1) to handle multiple disjoint attenuators [173]. Moreover, high refresh rate LCD panels can be employed as the attenuation layers, which are capable of displaying optimized patterns beyond the critical flicker frequency in the HVS. The target image is obtained as a result of temporal integration of such quickly changing patterns directly in the HVS [78, 174]. This enables high angular diversification of transmitted light paths, so that binocular disparity, motion parallax and even nearly correct accommodation over wide depth ranges become feasible [84]. Again, by changing the optimization goals to high precision contrast reproduction, HDR display capabilities are achieved at expense of reducing the angular resolution in such compressive light field displays [174] and projection [56] systems.

## 8 HDR image quality

To test and compare imaging algorithms, it is necessary to assess the quality of the resulting images or video. For example, one video compression algorithm can be considered as better than the other, only if it produces smaller bit-stream for the same video quality. A human observer can easily choose which one of the two video clips looks better; yet running an extensive subjective experiments for a number of video clips and algorithm parameter variations is often impractical. Therefore, there is a need for computational metrics that could predict quality of visually significant differences between a test image and its reference, and thus replace tedious experiments.

The majority of image quality metrics consider quality assessment for one particular medium, such as an LCD display or a print. However, the results of physically-accurate computer graphics methods are not tied to any concrete device. They produce images in which pixels contain linear radiometric values (refer to Sec. 3.1), as opposed to the gamma-corrected RGB values of a display device. Furthermore, the radiance values corresponding to real-world scenes can span a very large dynamic range (Fig. 1), which exceeds the contrast range of a typical display device. Hence the problem arises of how to compare the quality of such images, which represent actual scenes, rather than their tone-mapped reproductions.

### 8.1 Display-referred vs. luminance independent metrics

Quality metrics for HDR image and video make a distinction whether the images are given in relative or absolute luminance units.

The display-referred metrics expect that the values in images correspond to the absolute luminance emitted from an HDR or LDR display, on which such images are displayed. They account for the fact that distortions are less visible in darker image parts. Two examples of such metrics are perceptually uniform encoding and HDR-VDP, described in Sec. 8.2 and 8.3 below. Their predictions are likely to be erroneous when used with arbitrary scaled images.

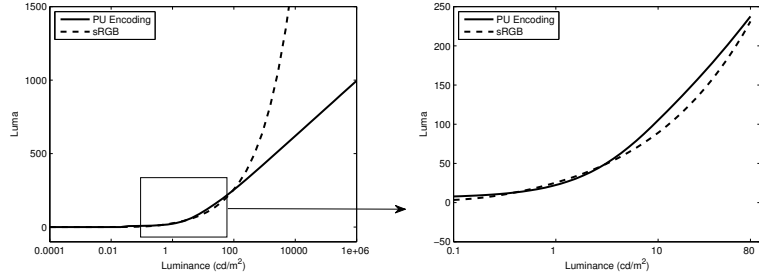


Figure 35: Perceptually uniform (PU) encoding for evaluating quality of HDR images. The absolute luminance values are converted into luma values before they are used with standard image quality metrics, such as MSE, PSNR or SSIM. Note that the PU encoding is designed to give a good fit to the sRGB non-linearity within the range  $0.1 - 80 \text{ cd/m}^2$  so that the results for low dynamic range images are consistent with those performed in the sRGB color space.

Luminance-independent metrics accept any relative HDR pixel values and give identical results when values are multiplied by a constant. They assume that observer's sensitivity to light follows the Weber law, and usually convert HDR pixel values to the logarithmic domain (refer to Sec. 2.4). An example of such a metric is log-PSNR, which follows the standard PSNR formula, with the exception that it is computed for logarithmic values:

$$\log\text{PSNR} = 10 \cdot \log_{10} \frac{\log_{10}(L_{\max})}{MSE} \quad (36)$$

and

$$MSE = \frac{1}{N} \sum_{i=1}^N [\log_{10}(\hat{L}_t(i)) - \log_{10}(\hat{L}_r(i))]^2 \quad (37)$$

where

$$\hat{L}_t(i) = \max(L_t(i), L_{\min}) \quad \text{and} \quad \hat{L}_r(i) = \max(L_r(i), L_{\min}), \quad (38)$$

$L_t(i)$  is the luminance of the pixel  $i$  in the test image, and  $L_r(i, c)$  is its counterpart in the reference image.  $L_{\min}$  is the minimum luminance considered to be above the noise level. Without such clamping of the lowest values, the metric introduces very large error for dark and noisy pixels.  $N$  is the total number of pixels in an image, and  $L_{\max}$  is an arbitrary selected peak luminance value. The typical selection of  $L_{\max}$  is 10 000, as few HDR displays exceed this peak luminance level. The value of  $L_{\max}$  must not be selected as the maximum pixel value in an image, as that would make such a metric image-dependent.

## 8.2 Perceptually-uniform encoding for quality assessment

Aydin et al. [7] proposed a simple luminance encoding that makes it possible to use PSNR and SSIM [164] metrics with HDR images. The encoding transforms physical

luminance values (represented in  $cd/m^2$ ) into an approximately perceptually uniform representation (refer to Fig. 35). The transformation is derived from luminance detection data using the threshold-integration method, similar to the one used for contrast transducer functions [175]. The transformation is further constrained so that the luminance values produced by a typical CRT display (in the range  $0.1\text{--}80\,cd/m^2$ ) are mapped to 0–255 range to mimic the sRGB non-linearity. This way, the quality predictions for typical low-dynamic range images are comparable to those calculated using pixel values. However, the metric can also operate in a much greater range of luminance.

The pixel encoding of Aydin et al. accounts for luminance masking, but it does not account for other luminance-dependent effects, such as intraocular light scattering or the frequency shift of the CSF peak with luminance. Those effects were modeled in the visual difference predictor for high dynamic range images (HDR-VDP) [89]. The HDR-VDP extends Daly’s visual difference predictor (VDP) [26] to predict differences in high dynamic range images. In 2011 the metric was superseded with an improved and thoroughly redesigned metric HDR-VDP-2 [91], which is discussed below.

### 8.3 Visual difference predictor for HDR images

HDR-VDP-2 is the visibility (discrimination) and quality metric capable of detecting differences in achromatic images spanning a wide range of absolute luminance values [91]. Although the metric originates from the classical Visual Difference Predictor [26], and its extension — HDR-VDP [89], the visual models are very different from those used in those earlier metrics. The metric is also an effort to design a comprehensive model of the contrast visibility for a very wide range of illumination conditions.

As shown in Fig. 36, the metric takes two HDR luminance or radiance maps as input and predicts the probability of detecting a difference between the pair of images ( $P_{map}$  and  $P_{det}$ ) as well as the quality ( $Q$  and  $Q_{MOS}$ ), which is defined as the perceived level of distortion.

One of the major factors limiting the contrast perception in high contrast (HDR) scenes is the scattering of the light in the optics of the eye and on the retina [98]. The HDR-VDP-2 models it as a frequency-space filter, which was fitted to an appropriate data set (*inter-ocular light scatter* block in Fig. 36). The contrast perception deteriorates at lower luminance levels, where the vision is mediated mostly by night-vision photoreceptors — rods. This is especially manifested for small contrasts, which are close to the detection threshold. This effect is modeled as a hypothetical response of the photoreceptor (in steady state) to light (*luminance masking* block in Fig. 36). Such response reduces the magnitude of image difference for low luminance according to the contrast detection measurements. The masking model (*neural noise* block in Fig. 36) operates on the image decomposed into multiple orientation-and-frequency-selective bands to predict the threshold elevation due to contrast masking. Such masking is induced both by the contrast within the same band (intra-channel masking) and within neighboring bands (inter-channel masking). The same masking model incorporates also the effect of neural CSF, which is the contrast sensitivity function without the sensitivity reduction due to interocular light scatter. Combining neural CSF with masking model is necessary to account for contrast constancy, which results in “flattening” of

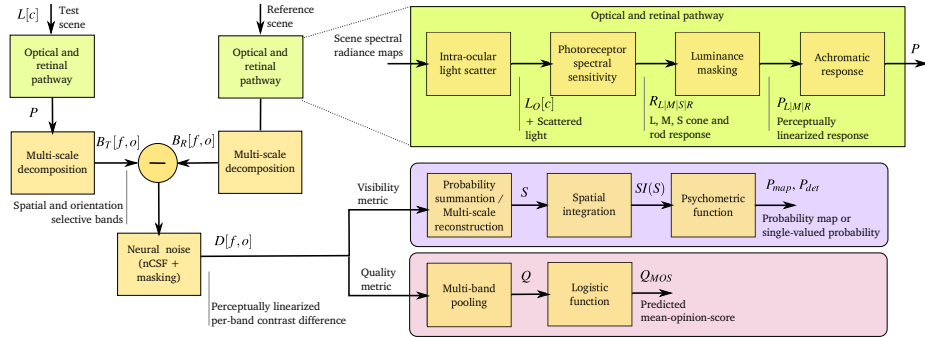


Figure 36: The processing stages of the HDR-VDP-2 metric. Test and reference images undergo similar stages of visual modeling before they are compared at the level of individual spatial-and-orientation selective bands ( $B_T$  and  $B_R$ ). The difference is used to predict both visibility (probability of detection) or quality (the perceived magnitude of distortion).

the CSF at the super-threshold contrast levels [49].

Fig. 37 demonstrates the metric prediction for blur and noise. The model has been shown to predict numerous discrimination data sets, such as ModelFest [171], historical Blackwell's t.v.i. measurements [17], and newly measured CSF [69]. The source code of the metric is freely available for download from <http://hdrvdp.sourceforge.net>. It is also possible to run the metric using an on-line web service at <http://driiqm.mpi-inf.mpg.de/>.

## 8.4 Tone-mapping metrics

Tone mapping is the process of transforming an image represented in approximately physically accurate units, such as radiance and luminance, into pixel values that can be displayed on a screen of a limited dynamic range. Tone-mapping is a part of an image processing stack of any digital camera. ‘‘RAW’’ images captured by a digital sensor would produce unacceptable results if they were mapped directly to pixel values without any tone-mapping. But similar process is also necessary for all computer graphics methods that produce images represented in physical units. Therefore, the problem of tone-mapping and the quality assessment of tone-mapping results have been extensively studied in graphics.

Tone-mapping inherently produces images that are different from the original high dynamic range reference. In order to fit the resulting image within available color gamut and dynamic range of a display, tone-mapping often needs to compress contrast and adjust brightness. Tone-mapped image may lose some quality as compared to the original seen on a high dynamic range display, yet the images look often very similar and the degradation of quality is poorly predicted by most quality metrics. Smith et al. [142] proposed the first metric intended for predicting loss of quality due to local and global contrast distortion introduced by tone-mapping. However, the metric was

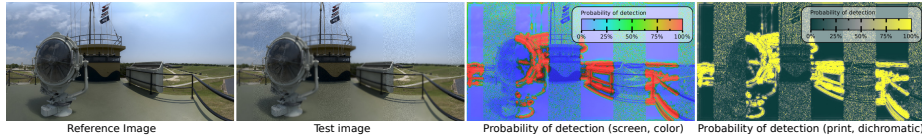


Figure 37: Predicted visibility differences between the test and reference images. The test image contains interleaved vertical stripes of blur and white noise. The images are tone-mapped versions of an HDR input. The two color-coded maps on the right represent the probability that an average observer will notice a difference between the image pair. Both maps represent the same values, but use different color maps, optimized either for screen viewing or for gray-scale/color printing. The probability of detection drops with lower luminance (luminance sensitivity) and higher texture activity (contrast masking). Image courtesy of HDR-VFX, LLC 2008. (Reproduced with permission from [91] © 2011 ACM, Inc.)

only used in the context of controlling counter-shading algorithm and was not validated against experimental data. Aydin et al. [8] proposed a metric for comparing HDR and tone-mapped images that is robust to contrast changes. The metric was later extended to video [9]. Both metrics are invariant to the change of contrast magnitude as long as that change does not distort contrast (inverse its polarity) or affect its visibility. The metric classifies distortions into three types: loss of visible contrast, amplification of invisible contrast and contrast reversal. All three cases are illustrated in Fig. 38 on an example of a simple 2D Gabor patch. These three cases are believed to affect the quality of tone-mapped images. Fig. 38 shows the metric predictions for three tone-mapped images. The main weakness of this metric is that produced distortion maps are suitable mostly for visual inspection and qualitative evaluation. The metric does not produce a single-valued quality estimate and its correlation with subjective quality assessment has not been verified. The metric can be conveniently executed from a web-based service available at <http://drim.mpi-sb.mpg.de/>.

Yeganeh and Wang [178] proposed a metric for tone mapping, which was designed to predict overall quality of a tone-mapped image with respect to an HDR reference. The first component of the metric is the modification of the SSIM [164], which includes the contrast and structure components, but does not include the luminance component. The contrast component is further modified to detect only the cases in which invisible contrast becomes visible and visible contrast becomes invisible, in a similar spirit as in the dynamic range independent metric [8], described above. This is achieved by mapping local standard deviation values used in the contrast component into detection probabilities using a visual model, which consists of a psychometric function and a contrast sensitivity function (CSF). The second component of the metric describes “naturalness”. The naturalness is captured by the measure of similarity between the histogram of a tone-mapped image and the distribution of histograms from the database of 3000 low-dynamic range images. The histogram is approximated by the Gaussian distribution. Then, its mean and standard deviation is compared against the database of histograms. When both values are likely to be found in the database, the image is considered natural and is assigned a higher quality. The metric was tested

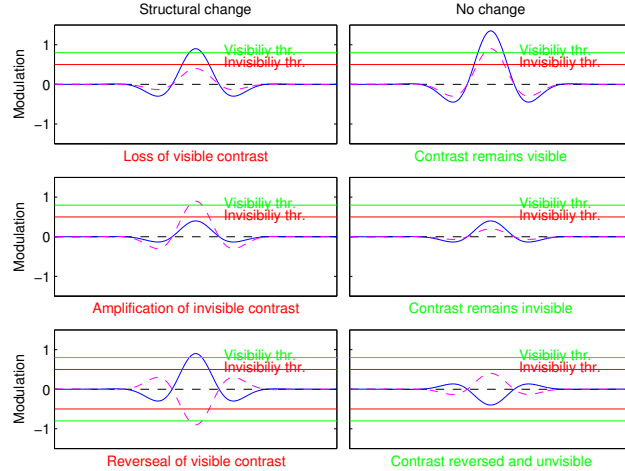


Figure 38: The dynamic range independent metric distinguished between the change of contrast that does and does not result in structural change. Blue continuous line shows a reference signal (from a band-pass pyramid) and magenta dashed line the test signal. When contrast remains visible or invisible after tone-mapping, no distortion is signalized (top and middle right). However, when the change of contrast alters the visibility of details, making visible details becoming invisible (top-left), it is signalized as a distortion. (Reproduced with permission from [8] © 2008 ACM, Inc.)

and cross-validated using three databases, including one from [160] and authors' own measurements. The Spearman rank-order correlation coefficient between the metric predictions and the subjective data was reported to be approximately 0.8. Such value is close to the performance of a random observer, which is estimated as the correlation between the mean and random observer's quality assessment.

Some visible distortions are desirable as long as they are not objectionable. An example of that is contrast enhancement through unsharp masking (high spatial frequencies) or countershading (low spatial frequencies) [72], commonly used in tone-mapping (refer to Sec. 5.4). In both cases, smooth gradients are introduced at both sides of an edge in order to enhance the contrast of that edge (Fig. 24). This is also demonstrated in Fig. 40 where the base contrast shown in the bottom row is enhanced by adding countershading profiles. Note that the brightness of the central part of each patch remains the same across all rows. The region marked with the blue dashed line denotes the range of the Cornsweet illusion, where the gradient remains invisible while the edge is still enhanced. Above that line the Cornsweet illusion breaks and the gradients become visible. In practice, when countershading is added to tone-mapped images, it is actually desirable to introduce such visible gradients. Otherwise, the contrast enhancement is too small and does not improve image quality. But too strong gradient results in visible contrast reversal, also known as “halo” artifact, which is disturbing and objectionable. Trentacoste et al. [155] measured the threshold when countershading profiles become objectionable in complex images. They found that the permissible strength of

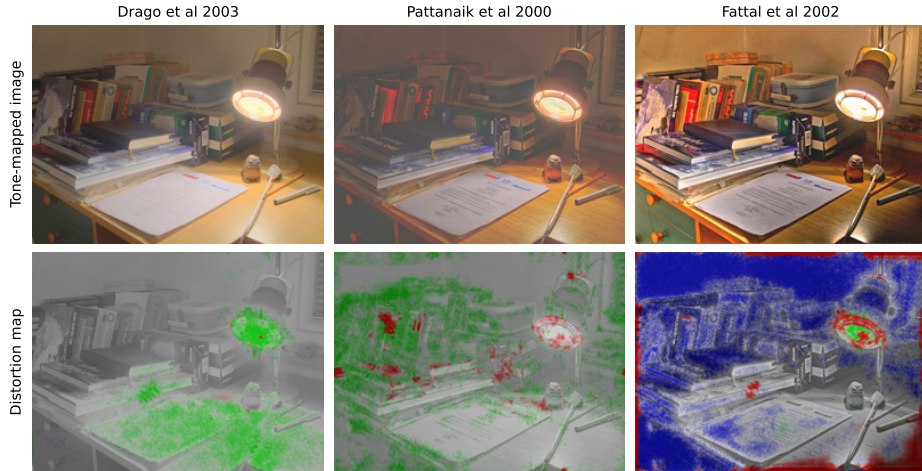


Figure 39: Prediction of the dynamic range independent metric [8] (top) for tone-mapped images (bottom). The green color denotes the loss of visible contrast, the blue color the amplification of invisible contrast and the red color is contrast reversal - refer to Fig. 38. (Reproduced with permission from [8] © 2008 ACM, Inc.)

the countershading depends on the width of the gradient profile, which in turn depends on the size of an image. They proposed a metric predicting the maximum strength of the enhancement and demonstrated its application to tone-mapping. The metric is an example of a problem where it is more important to predict when an artifact becomes objectionable rather than just visible.

## References

- [1] A. Adams, J. Baek, and M.A. Davis. Fast High-Dimensional Filtering Using the Permutohedral Lattice. *Computer Graphics Forum*, 29(2):753–762, 2010.
- [2] A. Adams, N. Gelfand, J. Dolson, and M. Levoy. Gaussian kd-trees for fast high-dimensional filtering. *ACM Transactions on Graphics (TOG)*, 28(3):1–12, 2009.
- [3] Andrew Adams, David E. Jacobs, Jennifer Dolson, Marius Tico, Kari Pulli, Eino-Ville Talvala, Boris Ajdin, Daniel Vaquero, Hendrik P. A. Lensch, Mark Horowitz, Sung Hee Park, Natasha Gelfand, Jongmin Baek, Wojciech Matusik, and Marc Levoy. The frankencamera: An experimental platform for computational photography. *Commun. ACM*, 55(11):90–98, 2012.
- [4] Manoj Aggarwal and Narendra Ahuja. Split aperture imaging for high dynamic range. *Proc. of International Conference on Computer Vision (ICCV)*, 2:10–17, 2001.

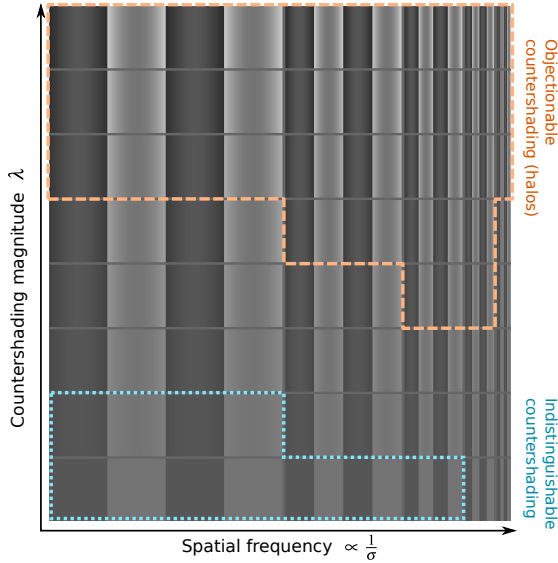


Figure 40: Contrast enhancement by countershading. The figure shows the square-wave pattern with a reduced amplitude of the fundamental frequency, resulting in countershading profiles. The regions of indistinguishable (from a step edge) and objectionable countershading are marked with dotted and dashed lines of different color. The higher magnitude of countershading produces higher contrast edges. But if it is too high, the result appears objectionable. The marked regions are approximate and for illustration and actual regions will depend on the angular resolution of the figure. (Reproduced with permission from [155] © The Eurographics Association 2012.)

- [5] Manoj Aggarwal and Narendra Ahuja. Split aperture imaging for high dynamic range. *Int. J. Comput. Vision*, 58(1):7–17, 2004.
- [6] Ahmet Ouz Akyüz, Erik Reinhard, Roland Fleming, Berhard E. Riecke, and Heinrich H. Bültlhoff. Do HDR displays support LDR content? a psychophysical evaluation. *ACM Transactions on Graphics (Proc. SIGGRAPH)*, 26(3), 2007.
- [7] Tunç O. Aydin, Rafał Mantiuk, and Hans-Peter Seidel. Extending quality metrics to full luminance range images. In *Proc. of Human Vision and Electronic Imaging*, pages 68060B–10, 2008.
- [8] Tunç Ozan Aydin, Rafał Mantiuk, Karol Myszkowski, and Hans-Peter Seidel. Dynamic range independent image quality assessment. *ACM Transactions on Graphics (Proc. of SIGGRAPH)*, 27(3):69, 2008.
- [9] Tunç Ozan Aydin, Martin Čadík, Karol Myszkowski, and Hans-Peter Seidel. Video quality assessment for computer graphics applications. *ACM Transactions on Graphics (Proc. SIGGRAPH Asia)*, 29(6):1, 2010.

- [10] Francesco Banterle, Alessandro Artusi, Kurt Debattista, and Alan Chalmers. *Advanced High Dynamic Range Imaging: Theory and Practice*. AK Peters (CRC Press), Natick, MA, USA, 2011.
- [11] Francesco Banterle, Patrick Ledda, Kurt Debattista, and Alan Chalmers. Inverse tone mapping. In *18th Eurographics Symposium on Rendering*, pages 321–326, 2006.
- [12] Connelly Barnes, Eli Shechtman, Adam Finkelstein, and Dan B Goldman. PatchMatch: A randomized correspondence algorithm for structural image editing. *ACM Transactions on Graphics (Proc. SIGGRAPH)*, 28(3), 2009.
- [13] Peter G. J. Barten. Formula for the contrast sensitivity of the human eye. In Yoichi Miyake and D. Rene Rasmussen, editors, *Proc. SPIE 5294, Image Quality and System Performance*, pages 231–238, 2004.
- [14] Peter G.J. Barten. *Contrast sensitivity of the human eye and its effects on image quality*. SPIE – The International Society for Optical Engineering, 1999.
- [15] Roy S Berns. Methods for characterizing crt displays. *Displays*, 16(4):173–182, 1996.
- [16] Oliver Bimber and Daisuke Iwai. Superimposing dynamic range. *ACM Transactions on Graphics (Proc. SIGGRAPH Asia)*, 27(5):150:1–150:8, 2008.
- [17] H.R. Blackwell. Contrast thresholds of the human eye. *Journal of the Optical Society of America*, 36(11):624–632, 1946.
- [18] Christian Bloch. *The HDRI Handbook 2.0: High Dynamic Range Imaging for Photographers and CG Artists*. rockynook, 2014.
- [19] R. Bogart, F. Kainz, and D. Hess. OpenEXR image file format. In *ACM SIGGRAPH 2003, Sketches & Applications*, 2003.
- [20] V. Brajovic, R. Miyagawa, and T. Kanade. Temporal photoreception for adaptive dynamic range image sensing and encoding. *Neural Networks*, 11(7-8):1149–1158, October 1998.
- [21] M. Buerker, C. Roessing, and H. P. A. Lensch. Exposure control for HDR video. In *Proc. SPIE, vol. 9138*, pages 913805–913805–12, 2014.
- [22] Curtis R. Carlson, Edward H. Adelson, and Charles H. Anderson. System for coring an image-representing signal. In *US Patent 4,523,230*. United States Patent and Trademark Office, 1985.
- [23] J. Chen, S. Paris, and F. Durand. Real-time edge-aware image processing with the bilateral grid. *ACM Transactions on Graphics (TOG)*, 26(3):103, 2007.
- [24] K. Chiu, M. Herf, P. Shirley, S. Swamy, C. Wang, and K. Zimmerman. Spatially nonuniform scaling functions for high contrast images. In *Graphics Interface*, pages 245–253. Citeseer, 1993.

- [25] CIE. *A Colour Appearance Model for Colour Management Systems: CIECAM02*, volume CIE 159:2004. International Commision on Illumination, 2002.
- [26] Scott Daly. The visible differences predictor: An algorithm for the assessment of image fidelity. In Andrew B. Watson, editor, *Digital Images and Human Vision*, pages 179–206. MIT Press, 1993.
- [27] Scott Daly and Xiaofan Feng. Decontouring: Prevention and removal of false contour artifacts. In *Proc. of Human Vision and Electronic Imaging IX*, SPIE, vol. 5292, pages 130–149, 2004.
- [28] Scott Daly, Timo Kunkel, Xing Sun, Suzanne Farrell, and Poppy Crum. 41.1: Distinguished Paper : Viewer Preferences for Shadow, Diffuse, Specular, and Emissive Luminance Limits of High Dynamic Range Displays. *SID Symposium Digest of Technical Papers*, 44(1):563–566, 2013.
- [29] Gerwin Damberg, Helge Seetzen, Greg Ward, Wolfgang Heidrich, and Lorne Whitehead. 3.2: High dynamic range projection systems. *SID Symposium Digest of Technical Papers*, 38(1):4–7, 2007.
- [30] Niranjan Damera-Venkata and Nelson L. Chang. Display supersampling. *ACM Transactions on Graphics*, 28(1):9:1–9:19, 2009.
- [31] Paul E. Debevec and Jitendra Malik. Recovering high dynamic range radiance maps from photographs. In *Proceedings of SIGGRAPH 97*, Computer Graphics Proceedings, Annual Conference Series, pages 369–378, 1997.
- [32] R.J. Deeley, N. Drasdo, and W.N. Charman. A simple parametric model of the human ocular modulation transfer function. *Ophthalmic and Physiological Optics*, 11(1):91–93, 1991.
- [33] Christhard Deter and Wolfram Biehlig. Scanning laser projection display and the possibilities of an extended color space. In *CGIV 2004 – Second European Conference on Color in Graphics, Imaging and Vision*, pages 531–535. Springer-Verlag Berlin Heidelberg New York, 2004.
- [34] DICOM PS 3-2004. Part 14: Grayscale standard display function. In *Digital Imaging and Communications in Medicine (DICOM)*. National Electrical Manufacturers Association, 2004.
- [35] Piotr Didyk, Rafał Mantiuk, Matthias Hein, and Hans-Peter Seidel. Enhancement of bright video features for HDR displays. In *EGSR’08*, pages 1265–1274, 2008.
- [36] R. P. Dooley and M. I. Greenfield. Measurements of edge-induced visual contrast and a spatial-frequency interaction of the cornsweet illusion. *Journal of the Optical Society of America*, 67, 1977.

- [37] Frédéric Drago, William L. Martens, Karol Myszkowski, and Hans-Peter Seidel. Perceptual evaluation of tone mapping operators with regard to similarity and preference. Technical Report MPI-I-2002-4-002, Max-Planck-Institut für Informatik, Im Stadtwald 66123 Saarbrücken, Germany, 2002.
- [38] Iddo Drori, Daniel Cohen-Or, and Hezy Yeshurun. Fragment-based image completion. *ACM Transactions on Graphics (Proc. SIGGRAPH)*, 22(3):303–312, 2003.
- [39] Frédo Durand and Julie Dorsey. Fast bilateral filtering for the display of high-dynamic-range images. *ACM Transactions on Graphics (Proc. SIGGRAPH)*, 21(3):257–266, 2002.
- [40] M. D’Zmura and P. Lennie. Mechanisms of color constancy. *Journal of the Optical Society of America A*, 3(10):1662–1672, 1986.
- [41] Gabriel Eilertsen, Robert Wanat, Rafał Mantiuk, and Jonas Unger. Evaluation of Tone Mapping Operators for HDR-Video. *Computer Graphics Forum*, 32(7):275–284, 2013.
- [42] Mark D. Fairchild. *Color Appearance Models*. Addison-Wesley, 1998. ISBN 0-201-63464-3.
- [43] Zeev Farbman, Raanan Fattal, Dani Lischinski, and Richard Szeliski. Edge-preserving decompositions for multi-scale tone and detail manipulation. *ACM Transactions on Graphics (Proc. SIGGRAPH)*, 27(3):no. 67, 2008.
- [44] Hany Farid. Blind inverse gamma correction. *IEEE Transactions on Image Processing*, pages 1428–1433, 2001.
- [45] Raanan Fattal, Dani Lischinski, and Michael Werman. Gradient domain high dynamic range compression. *ACM Transactions on Graphics (Proc. SIGGRAPH)*, 21(3):249–256, 2002.
- [46] James Ferwerda and Stefan Luka. A high resolution, high dynamic range display for vision research. *Journal of Vision*, 9(8):346, 2009.
- [47] O. Gallo, N. Gelfand, Wei-Chao Chen, M. Tico, and K. Pulli. Artifact-free high dynamic range imaging. In *Computational Photography (ICCP), 2009 IEEE International Conference on*, pages 1–7, 2009.
- [48] O. Gallo, M. Tico, R. Manduchi, N. Gelfand, and K. Pulli. Metering for exposure stacks. *Computer Graphics Forum (Proceedings of Eurographics)*, 31:479–488, 2012.
- [49] M.A. Georgeson and G.D. Sullivan. Contrast constancy: Deblurring in human vision by spatial frequency channels. *Journal of Physiology*, 252:627–656, 1975.
- [50] R. Ginosar and A. Gnusin. A wide dynamic range CMOS image sensor. *IEEE Workshop on CCD and Advanced Image Sensors*, June 1997.

- [51] Miguel Granados, Boris Ajdin, Michael Wand, Christian Theobalt, Hans-Peter Seidel, and Hendrik P. A. Lensch. Optimal HDR reconstruction with linear digital cameras. In *IEEE Conference on Computer Vision and Pattern Recognition*, pages 215–222, 2010.
- [52] Miguel Granados, Kwang In Kim, James Tompkin, and Christian Theobalt. Automatic noise modeling for ghost-free HDR reconstruction. *ACM Transactions on Graphics (Proc. SIGGRAPH Asia)*, 32(6):201:1–201:10, 2013.
- [53] Gabriele Guarneri, Luigi Albani, and Giovanni Ramponi. Image-splitting techniques for a dual-layer high dynamic range lcd display. *Journal of Electronic Imaging*, 17(4):043009:1–9, 2008.
- [54] Benjamin Guthier, Stephan Kopf, and Wolfgang Effelsberg. A real-time system for capturing HDR videos. In *Proceedings of the 20th ACM International Conference on Multimedia*, pages 1473–1476, 2012.
- [55] Rolf Hainich and Oliver Bimber. *Displays: Fundamentals and Applications*. A K Peters, CRC Press, 2011.
- [56] M. Hirsch, G. Wetzstein, and R. Raskar. A compressive light field projection system. *ACM Transactions on Graphics (Proc. SIGGRAPH)*, 33(4):1–12, 2014.
- [57] Bernd Höefflinger, editor. *High-Dynamic-Range (HDR) Vision*, volume 26 of *Springer Series in Advanced Microelectronics*. Springer, 2007.
- [58] Berthold K.P. Horn. Determining lightness from an image. *Computer Graphics and Image Processing*, 3(4):277–299, 1974.
- [59] Jun Hu, O. Gallo, K. Pulli, and Xiaobai Sun. Hdr deghosting: How to deal with saturation? In *Computer Vision and Pattern Recognition (CVPR)*, pages 1163–1170, 2013.
- [60] Anya Hurlbert. Formal connections between lightness algorithms. *Journal of the Optical Society of America A*, 3(10):1684, 1986.
- [61] Piti Irawan, James A. Ferwerda, and Stephen R. Marschner. Perceptually based tone mapping of high dynamic range image streams. In *16th Eurographics Symposium on Rendering*, pages 231–242, 2005.
- [62] James R. Janesick. *Scientific Charge-Coupled Devices*. SPIE, 2001.
- [63] James T. Kajiya. The rendering equation. In *Computer Graphics (Proceedings of SIGGRAPH 86)*, pages 143–150, 1986.
- [64] Masanori Kakimoto, Kaoru Matsuoka, Tomoyuki Nishita, Takeshi Naemura, and Hiroshi Harashima. Glare generation based on wave optics. *Computer Graphics Forum*, 24(2):185–193, 2005.

- [65] Nima Khademi Kalantari, Eli Shechtman, Connelly Barnes, Soheil Darabi, Dan B. Goldman, and Pradeep Sen. Patch-based high dynamic range video. *ACM Transactions on Graphics (Proc. SIGGRAPH Asia)*, 32(6):202:1–202:8, 2013.
- [66] S.B. Kang, M. Uyttendaele, S. Winder, and R. Szeliski. High dynamic range video. *ACM Transactions on Graphics (Proc. SIGGRAPH)*, 22(3):319–325, 2003.
- [67] Masaki Kawase. Practical implementation of high dynamic range rendering. In *Game Developers Conference*, 2005.
- [68] E.A. Khan, A.O. Akyiiz, and E. Reinhard. Ghost removal in high dynamic range images. In *IEEE International Conference on Image Processing*, pages 2005–2008, 2006.
- [69] Kil Joong Kim, Rafał Mantiuk, and Kyoung Ho Lee. Measurements of achromatic and chromatic contrast sensitivity functions for an extended range of adaptation luminance. In Bernice E. Rogowitz, Thrasyvoulos N. Pappas, and Huib de Ridder, editors, *Human Vision and Electronic Imaging*, page 86511A, 2013.
- [70] F. Kingdom and B. Moulden. Border effects on brightness: a review of findings, models and issues. *Spatial Vision*, 3(4):225–262, 1988.
- [71] Adam G. Kirk and James F. O’Brien. Perceptually based tone mapping for low-light conditions. *ACM Transactions on Graphics (Proc. SIGGRAPH)*, 30(4):42, 2011.
- [72] Grzegorz Krawczyk, Karol Myszkowski, and Hans-Peter Seidel. Contrast Restoration by Adaptive Countershading. *Computer Graphics Forum*, 26(3):581–590, 2007.
- [73] J. Kronander, S. Gustavson, G. Bonnet, and J. Unger. Unified HDR reconstruction from raw cfa data. In *Computational Photography (ICCP), 2013 IEEE International Conference on*, pages 1–9, 2013.
- [74] Jiangtao Kuang, Garrett M. Johnson, and Mark D. Fairchild. icam06: A refined image appearance model for HDR image rendering. *Journal of Visual Communication and Image Representation*, 18(5):406–414, 2007.
- [75] E.H. Land and J.J. McCann. Lightness and retinex theory. *Journal of the Optical Society of America*, 61(1):1–11, 1971.
- [76] EHA Langendijk and M Hammer. Contrast requirements for OLEDs and LCDs based on human eye glare. *SID Symp. Dig. Tech. Papers*, pages 192–194, 2010.
- [77] D. Lanman, G. Wetzstein, M. Hirsch, W. Heidrich, and R. Raskar. Polarization fields: Dynamic light field display using multi-layer LCDs. *ACM Transactions on Graphics (Proc. SIGGRAPH Asia)*, 30(6), 2011.

- [78] Douglas Lanman, Matthew Hirsch, Yunhee Kim, and Ramesh Raskar. Content-adaptive parallax barriers: optimizing dual-layer 3d displays using low-rank light field factorization. *ACM Transactions on Graphics (Proc. SIGGRAPH Asia)*, 29(6):163:1–163:10, 2010.
- [79] Yuanzhen Li, Lavanya Sharan, and Edward H. Adelson. Compressing and companding high dynamic range images with subband architectures. *ACM Transactions on Graphics (Proc. SIGGRAPH)*, 24(3):836–844, 2005.
- [80] Stephen Lin, Jinwei Gu, Shuntaro Yamazaki, and Heung-Yeung Shum. Radiometric calibration from a single image. *Conference on Computer Vision and Pattern Recognition (CVPR'04)*, 02:938–945, 2004.
- [81] Margaret Livingstone. *Vision and Art: The Biology of Seeing*. Harry N. Abrams, 2002.
- [82] T. Lulé, H. Keller, M. Wagner, and M. Böhm. LARS II - a high dynamic range image sensor with a-Si:H photo conversion layer. In *1999 IEEE Workshop on Charge-Coupled Devices and Advanced Image Sensors*, Nagano, Japan, 1999.
- [83] Zicong Mai, Hassan Mansour, Rafał Mantiuk, Panos Nasiopoulos, Rabab Ward, and Wolfgang Heidrich. Optimizing a tone curve for backward-compatible high dynamic range image and video compression. *IEEE Transactions on Image Processing*, 20(6):1558 – 1571, 2011.
- [84] A. Maimone, G. Wetzstein, D. Lanman, M. Hirsch, R. Raskar, and H. Fuchs. Focus 3D: Compressive accommodation display. *ACM Transactions on Graphics*, 32(5):1–13, 2013.
- [85] Aditi Majumder and Michael S. Brown. *Practical Multi-Projector Display Design*. A.K. Peters, 2007.
- [86] S. Mangiat and J. Gibson. Spatially adaptive filtering for registration artifact removal in HDR video. In *IEEE International Conference on Image Processing (ICIP)*, pages 1317–1320, 2011.
- [87] Steve Mann and Rosalind W. Picard. On being ‘undigital’ with digital cameras: extending dynamic range by combining differently exposed pictures. In *IS&T’s 48th Annual Conference*, pages 422–428, Washington D.C., 1995. Society for Imaging Science and Technology.
- [88] R. Mantiuk, S. Daly, and L. Kerofsky. Display adaptive tone mapping. *ACM Transactions on Graphics (Proc. SIGGRAPH)*, 27(3):68, 2008.
- [89] Rafał Mantiuk, Scott Daly, Karol Myszkowski, and Hans-Peter Seidel. Predicting visible differences in high dynamic range images: model and its calibration. *Proc. SPIE*, 2005.
- [90] Rafał Mantiuk, Alexander Efremov, Karol Myszkowski, and Hans-Peter Seidel. Backward compatible high dynamic range mpeg video compression. *ACM Transactions on Graphics (Proc. SIGGRAPH)*, 25(3), 2006.

- [91] Rafał Mantiuk, Kil Joong Kim, Allan G. Rempel, and Wolfgang Heidrich. HDR-VDP-2: a calibrated visual metric for visibility and quality predictions in all luminance conditions. *ACM Transactions on Graphics (Proc. SIGGRAPH)*, 30(4):1, 2011.
- [92] Rafał Mantiuk, Grzegorz Krawczyk, Karol Myszkowski, and Hans-Peter Seidel. Perception-motivated high dynamic range video encoding. *ACM Transactions on Graphics (Proc. of SIGGRAPH)*, 23(3):733, 2004.
- [93] Rafał Mantiuk, Grzegorz Krawczyk, Karol Myszkowski, and Hans-Peter Seidel. Perception-motivated high dynamic range video encoding. *ACM Transactions on Graphics (Proc. SIGGRAPH)*, 23(3):730–738, 2004.
- [94] Rafał Mantiuk, Karol Myszkowski, and Hans-Peter Seidel. A perceptual framework for contrast processing of high dynamic range images. *ACM Transactions on Applied Perception*, 3:286–308, 2006.
- [95] Belen Masia, Sandra Agustin, Roland W. Fleming, Olga Sorkine, and Diego Gutierrez. Evaluation of reverse tone mapping through varying exposure conditions. *ACM Transactions on Graphics (Proc. SIGGRAPH Asia)*, 28(5):160:1–160:8, 2009.
- [96] Belen Masia, Gordon Wetzstein, Piotr Didyk, and Diego Gutierrez. A survey on computational displays: Pushing the boundaries of optics, computation, and perception. *Computers & Graphics*, 37(8):1012 – 1038, 2013.
- [97] John McCann. Perceptual rendering of HDR in painting and photography. In *Human Vision and Electronic Imaging XIII*, SPIE, volume 6806. SPIE, 2005. Article 30.
- [98] John McCann and Alessandro Rizzi. Veiling glare: the dynamic range limit of HDR images. In *Human Vision and Electronic Imaging XII*, SPIE, volume 6492, 2007.
- [99] John J. McCann. Do humans discount the illuminant? In *Proceedings of SPIE*, volume 5666, pages 5666–9. SPIE, 2005.
- [100] John J. McCann and Alessandro Rizzi. Camera and visual veiling glare in HDR images. *Journal of the Society for Information Display*, 15(9):721, 2007.
- [101] John J. McCann and Alessandro Rizzi. *The Art and Science of HDR Imaging*. Wiley, 2011.
- [102] T. Mertens, J. Kautz, and F. Van Reeth. Exposure Fusion: A Simple and Practical Alternative to High Dynamic Range Photography. *Computer Graphics Forum*, 28(1):161–171, 2009.
- [103] L. Meylan and S. Susstrunk. High dynamic range image rendering with a retinex-based adaptive filter. *IEEE Transactions on Image Processing*, 15(9):2820–2830, 2006.

- [104] Laurence Meylan, Scott Daly, and Sabine Susstrunk. The reproduction of specular highlights on high dynamic range displays. In *Proc. of the 14th Color Imaging Conference*, 2006.
- [105] S. Miller, M. Nezamabadi, and S. Daly. Perceptual Signal Coding for More Efficient Usage of Bit Codes. *SMPTE Motion Imaging Journal*, 122(4):52–59, 2013.
- [106] Tomoo Mitsunaga and Shree K. Nayar. Radiometric self calibration. In *Proc. of IEEE Conference on Computer Vision and Pattern Recognition*, pages 374–380, 1999.
- [107] Ján Morovič. *Color Gamut Mapping*. John Wiley & Sons, 2008.
- [108] Karol Myszkowski, Rafał Mantiuk, and Grzegorz Krawczyk. *High Dynamic Range Video*. Synthesis Digital Library of Engineering and Computer Science. Morgan & Claypool Publishers, San Rafael, USA, 2008.
- [109] Shree K. Nayar and Tomoo Mitsunaga. High dynamic range imaging: spatially varying pixel exposures. In *Proc. of IEEE Conference on Computer Vision and Pattern Recognition*, 2000.
- [110] S.K. Nayar and V. Branzoi. Adaptive dynamic range imaging: Optical control of pixel exposures over space and time. In *Proc. of IEEE International Conference on Computer Vision (ICCV 2003)*, pages 1168–1175, 2003.
- [111] S.K. Nayar, V. Branzoi, and T.E. Boult. Programmable imaging using a digital micromirror array. In *CVPR04*, pages I: 436–443, 2004.
- [112] AV Oppenheim, R.W. Schafer, and T.G. Stockham. Nonlinear filtering of multiplied and convolved signals. *Proceedings of the IEEE*, 56(8):1264–1291, 1968.
- [113] S. Paris and F. Durand. A fast approximation of the bilateral filter using a signal processing approach. *International journal of computer vision*, 81(1):24–52, 2009.
- [114] S.N. Pattanaik and C.E. Hughes. High-Dynamic-Range Still-Image Encoding in JPEG 2000. *IEEE Computer Graphics and Applications*, 25(6):57–64, 2005.
- [115] Sumanta N. Pattanaik, James A. Ferwerda, Mark D. Fairchild, and Donald P. Greenberg. A multiscale model of adaptation and spatial vision for realistic image display. In *Siggraph 1998, Computer Graphics Proceedings*, pages 287–298, 1998.
- [116] Sumanta N. Pattanaik, Jack Tumblin, Hector Yee, and Donald P. Greenberg. Time-dependent visual adaptation for fast realistic image display. In *Proc. of SIGGRAPH 2000*, pages 47–54, New York, New York, USA, 2000. ACM Press.
- [117] Sumanta N. Pattanaik, Jack E. Tumblin, Hector Yee, and Donald P. Greenberg. Time-dependent visual adaptation for fast realistic image display. In *Proc. of ACM SIGGRAPH 2000*, pages 47–54, 2000. ISBN 1-58113-208-5.

- [118] Patrick Perez, Michel Gangnet, and Andrew Blake. Poisson image editing. *ACM Transactions on Graphics (Proc. SIGGRAPH)*, 22(3):313–318, 2003.
- [119] M. Pharr and G. Humphreys. *Physically Based Rendering from Theory to Implementation*. Morgan Kaufmann, 2010.
- [120] Charles A. Poynton. *A Technical Introduction to Digital Video*. John Wiley & Sons, New York, 1996.
- [121] D. Purves, A. Shimp, and R.B. Lotto. An empirical explanation of the Cornsweet effect. *The Journal of Neuroscience*, 19(19):8542–8551, 1999.
- [122] Ramesh Raskar, Amit Agrawal, Cyrus A. Wilson, and Ashok Veeraraghavan. Glare aware photography: 4d ray sampling for reducing glare effects of camera lenses. *ACM Transactions on Graphics (Proc. SIGGRAPH)*, 27(3):56:1–56:10, 2008.
- [123] E. Reinhard and K. Devlin. Dynamic range reduction inspired by photoreceptor physiology. *IEEE Transactions on Visualization and Computer Graphics*, 11(1):13–24, 2005.
- [124] Erik Reinhard. Parameter estimation for photographic tone reproduction. *Journal of Graphics Tools*, 7(1):45–51, 2003.
- [125] Erik Reinhard and Kate Devlin. Dynamic range reduction inspired by photoreceptor physiology. *IEEE Transactions on Visualization and Computer Graphics*, 11(1):13–24, 2005.
- [126] Erik Reinhard, Tania Pouli, Timo Kunkel, Ben Long, Anders Ballestad, and Gerwin Damberg. Calibrated image appearance reproduction. *ACM Transactions on Graphics*, 31(6):1, 2012.
- [127] Erik Reinhard, Michael Stark, Peter Shirley, and Jim Ferwerda. Photographic tone reproduction for digital images. *ACM Transactions on Graphics (Proc. SIGGRAPH)*, 21(3):267–276, 2002.
- [128] Erik Reinhard, Greg Ward, Paul Debevec, Sumanta Pattanaik, Wolfgang Heidrich, and Karol Myszkowski. *High Dynamic Range Imaging*. Morgan Kaufmann Publishers, 2nd edition, 2010.
- [129] Allan G. Rempel, Matthew Trentacoste, Helge Seetzen, H. David Young, Wolfgang Heidrich, Lorne Whitehead, and Greg Ward. Ldr2Hdr: On-the-fly reverse tone mapping of legacy video and photographs. *ACM Transactions on Graphics (Proc. SIGGRAPH)*, 26(3), 2007. Article 39.
- [130] Tobias Ritschel, Matthias Ihrke, Jeppe Revall Frisvad, Joris Coppens, Karol Myszkowski, and Hans-Peter Seidel. Temporal glare: Real-time dynamic simulation of the scattering in the human eye. *Computer Graphics Forum (Proc. EUROGRAPHICS 2009)*, 28(3):183–192, March 2009.

- [131] Tobias Ritschel, Kaleigh Smith, Matthias Ihrke, Thorsten Grosch, Karol Myszkowski, and Hans-Peter Seidel. 3D unsharp masking for scene coherent enhancement. *ACM Transactions on Graphics (Proc. SIGGRAPH)*, 27:90:1–90:8, 2008.
- [132] Wanat Robert, Josselin Petit, and Rafal Mantiuk. Physical and perceptual limitations of a projector-based high dynamic range display. In *Theory and Practice in Computer Graphics*, 2012.
- [133] Mark A. Robertson, Sean Borman, and Robert L. Stevenson. Estimation-theoretic approach to dynamic range enhancement using multiple exposures. *Journal of Electronic Imaging*, 12(2):219–228, 2003.
- [134] Mushfiqur Rouf, Rafał Mantiuk, Wolfgang Heidrich, Matthew Trentacoste, and Cheryl Lau. Glare encoding of high dynamic range images. In *Computer Vision and Pattern Recognition (CVPR)*, 2011.
- [135] H. Seetzen, W. Heidrich, W. Stuerzlinger, G. Ward, L. Whitehead, M. Trentacoste, A. Ghosh, and A. Vorozcova. High dynamic range display systems. *ACM Transactions on Graphics (Proc. SIGGRAPH)*, 23(3):757–765, 2004.
- [136] H. Seetzen, H. Li, L. Ye, W. Heidrich, L. Whitehead, and G. Ward. 25.3: Observations of luminance, contrast and amplitude resolution of displays. In *SID 06 Digest*, pages 1229–1233, 2006.
- [137] H. Seetzen, L. Whitehead, and G. Ward. High dynamic range display using low and high resolution modulators. In *The Society for Information Display International Symposium*, 2003.
- [138] Andrew Segall. Scalable Coding of High Dynamic Range Video. In *2007 IEEE International Conference on Image Processing*, volume 1, pages I – 1–I – 4, 2007.
- [139] U. Seger, U. Apel, and B. Höefflinger. HDR for natural visual perception. In *Handbook of Computer Vision and Application*, volume 1, pages 223–235. Academic Press, 1999.
- [140] Pradeep Sen, Nima Khademi Kalantari, Maziar Yaeoubi, Soheil Darabi, Dan B. Goldman, and Eli Shechtman. Robust patch-based HDR reconstruction of dynamic scenes. *ACM Transactions on Graphics (Proceedings of SIGGRAPH Asia 2012)*, 31(6):203:1–203:11, 2012.
- [141] Denis Simakov, Yaron Caspi, Eli Shechtman, and Michal Irani. Summarizing visual data using bidirectional similarity. In *CVPR’08*, 2008.
- [142] K Smith, G Krawczyk, and K Myszkowski. Beyond tone mapping: Enhanced depiction of tone mapped HDR images. *Computer Graphics Forum*, 25(3):427–438, 2006.

- [143] Greg Spencer, Peter Shirley, Kurt Zimmerman, and Donald P. Greenberg. Physically-based glare effects for digital images. In *Proceedings of the 22nd Annual Conference on Computer Graphics and Interactive Techniques*, pages 325–334, 1995.
- [144] H. Spitzer, Y. Karasik, and S. Einav. Biological Gain control for High Dynamic Range Compression. In *Proceedings SID Eleventh Color Imaging Conference*, pages 42–50, 2003.
- [145] Abhilash Srikantha and Désiré Sidibé. Ghost detection and removal for high dynamic range images: Recent advances. *Image Commun.*, 27(6):650–662, 2012.
- [146] J. Starck, E. Pantin, and F. Murtagh. Deconvolution in astronomy: A review. *Publications of the Astronomical Society of the Pacific*, 114:1051–1069, 2002.
- [147] JC Stevens and SS Stevens. Brightness function: Effects of adaptation. *JOSA*, 1963.
- [148] TG Stockham Jr. Image processing in the context of a visual model. *Proceedings of the IEEE*, 60(7):828–842, 1972.
- [149] G.J. Sullivan, H. Yu, S. Sekiguchi, H. Sun, T. Wedi, S. Wittmann, Y. Lee, A. Segall, and T. Suzuki. New standardized extensions of MPEG4-AVC/H. 264 for professional-quality video applications. In *Proceedings of ICIP'07*, 2007.
- [150] Eino-Ville Talvala, Andrew Adams, Mark Horowitz, and Marc Levoy. Veiling glare in high-dynamic-range imaging. *ACM Transactions on Graphics (Proc. SIGGRAPH)*, 26(3), 2007.
- [151] P. Tan, S. Lin, L. Quan, and H. Shum. Highlight removal by illumination-constrained inpainting. In *Proc. of International Conference on Computer Vision (ICCV)*, page 164, 2003.
- [152] Michael D. Tocci, Chris Kiser, Nora Tocci, and Pradeep Sen. A versatile HDR video production system. *ACM Transactions on Graphics*, 30(4):41:1–41:10, 2011.
- [153] C. Tomasi and R. Manduchi. Bilateral filtering for gray and color images. In *International Conference on Computer Vision*, pages 839–846. Narosa Publishing House, 1998.
- [154] Anna Tomaszewska and Radosław Mantiuk. Image registration for multi-exposure high dynamic range image acquisition. In *Intl. Conference in Central Europe on Computer Graphics, Visualization and Computer Vision (WSCG)*, 2007.
- [155] Matthew Trentacoste, Ratal Mantiuk, Wolfgang Heidrich, and Florian Dufrot. Unsharp Masking, Countershading and Halos: Enhancements or Artifacts? *Computer Graphics Forum*, 31(2pt3):555–564, 2012.

- [156] Jack Tumblin and Holly E. Rushmeier. Tone reproduction for realistic images. *IEEE Computer Graphics and Applications*, 13(6):42–48, 1993.
- [157] Jonas Unger and Stefan Gustavson. High dynamic range video for photometric measurement of illumination. In *Human Vision and Electronic Imaging XII*, SPIE, volume 6501. SPIE, 2007.
- [158] Thomas J. T. P. van den Berg, Michiel P. J. Hagenouw, and Joris E. Coppens. The ciliary corona: Physical model and simulation of the fine needles radiating from point light sources. *Investigative Ophthalmology and Visual Science*, 46:2627–2632, 2005.
- [159] J. H. Van Hateren. Encoding of high dynamic range video with a model of human cones. *ACM Transactions on Graphics*, 25(4):1380–1399, 2006.
- [160] Martin Čadík, Michael Wimmer, Laszlo Neumann, and Alessandro Artusi. Evaluation of HDR tone mapping methods using essential perceptual attributes. *Computers & Graphics*, 32(3):330–349, 2008.
- [161] Robert Wanat and Rafał Mantiuk. Simulating and compensating changes in appearance between day and night vision. *Transactions on Graphics (Proc. of SIGGRAPH)*, 33(4):147, 2014.
- [162] B. A. Wandell. *Foundations of Vision*. Sinauer Associates, Sunderland, Massachusetts, 1995.
- [163] Lvdi Wang, Liyi Wei, Kun Zhou, Baining Guo, and Heung-Yeung Shum. High dynamic range image hallucination. In *18th Eurographics Symposium on Rendering*, pages 321–326, 2007.
- [164] Zhou Wang, A.C. Bovik, H.R. Sheikh, and E.P. Simoncelli. Image quality assessment: From error visibility to structural similarity. *IEEE Transactions on Image Processing*, 13(4):600–612, 2004.
- [165] G. Ward. Real pixels. In J. Arvo, editor, *Graphics Gems II*, pages 80–83. Academic Press, 1991.
- [166] G. Ward, H. Rushmeier, and C. Piatko. A visibility matching tone reproduction operator for high dynamic range scenes. *IEEE Transactions on Visualization and Computer Graphics*, 3(4):291–306, 1997.
- [167] Greg Ward. 59.2: Defining Dynamic Range. *SID Symposium Digest of Technical Papers*, 39(1):900, 2008.
- [168] Greg Ward and Maryann Simmons. Subband encoding of high dynamic range imagery. In *APGV '04: 1st Symposium on Applied Perception in Graphics and Visualization*, pages 83–90, 2004.
- [169] Greg Ward and Maryann Simmons. JPEG-HDR: A backwards-compatible, high dynamic range extension to JPEG. In *Proceedings of the 13th Color Imaging Conference*, pages 283–290, 2005.

- [170] G. Ward Larson. LogLuv encoding for full-gamut, high-dynamic range images. *Journal of Graphics Tools*, 3(1):815–30, 1998.
- [171] A.B. Watson and A.J. Ahumada Jr. A standard model for foveal detection of spatial contrast. *Journal of Vision*, 5(9):717–740, 2005.
- [172] G. Westheimer. The eye as an optical instrument. In K.R. Boff, L. Kaufman, and J.P. Thomas, editors, *Handbook of Perception and Human Performance: I. Sensory Processes and Perception*, pages 4.1–4.20. Wiley, New York, 1986.
- [173] G. Wetzstein, D. Lanman, W. Heidrich, and R. Raskar. Layered 3D: tomographic image synthesis for attenuation-based light field and high dynamic range displays. *ACM Transactions on Graphics (Proc. SIGGRAPH)*, 30(4), 2011.
- [174] G. Wetzstein, D. Lanman, M. Hirsch, and R. Raskar. Tensor displays: Compressive light field synthesis using multilayer displays with directional backlighting. *ACM Transactions on Graphics (Proc. SIGGRAPH)*, 31(4):1–11, 2012.
- [175] Hugh R. Wilson. A transducer function for threshold and suprathreshold human vision. *Biological Cybernetics*, 38(3):171–178, 1980.
- [176] Martin Winken, Detlev Marpe, Heiko Schwarz, and Thomas Wiegand. Bit-Depth Scalable Video Coding. In *2007 IEEE International Conference on Image Processing*, volume 1, pages I – 5–I – 8. IEEE, 2007.
- [177] Dietmar Wüller and Helke Gabele. The usage of digital cameras as luminance meters. In *Proceedings of SPIE*, volume 6502, pages 65020U–65020U–11. SPIE, 2007.
- [178] Hojatollah Yeganeh and Zhou Wang. Objective quality assessment of tone-mapped images. *IEEE Transactions on Image Processing*, 22(2):657–67, 2013.
- [179] Akiko Yoshida, Matthias Ihrke, Rafał Mantiuk, and Hans-Peter Seidel. Brightness of the glare illusion. In *Proceedings of the ACM Symposium on Applied Perception in Graphics and Visualization*, pages 83–90, 2008.
- [180] Akiko Yoshida, Rafał Mantiuk, Karol Myszkowski, and Hans-Peter Seidel. Analysis of reproducing real-world appearance on displays of varying dynamic range. *Computer Graphics Forum (Proc. of EUROGRAPHICS)*, 25(3):415–426, 2006.
- [181] Daniele Zavagno and Giovanni Caputo. The glare effect and the perception of luminosity. *Perception*, 30(2):209–222, 2001.
- [182] Dan Zhang and James Ferwerda. A low-cost, color-calibrated reflective high dynamic range display. *Journal of Vision*, 10(7):397, 2010.
- [183] Henning Zimmer, Andres Bruhn, and Joachim Weickert. Freehand HDR imaging of moving scenes with simultaneous resolution enhancement. *Computer Graphics Forum*, 30(2):405–414, 2011.